JOHANNES GUTENBERG UNIVERSITÄT MAINZ

Synthesis, radiolabeling and *in vitro* and *in vivo* evaluation of different chelator systems with ^{44}Sc, ^{64}Cu, ^{68}Ga and ^{177}Lu

Dissertation

zur Erlangung des Grades eines
„Doktor rerum naturalium (Dr. rer. nat.)“
im Promotionsfach Chemie

am Fachbereich Chemie, Pharmazie und Geowissenschaften
der Johannes Gutenberg-Universität Mainz
vorgelegt von

Lukas Nikolaus Greifenstein

geboren in Koblenz, Deutschland

Mainz, Mai 2019

Abstract

Prostate cancer is the third most common deadly disease and the most common cancer in industrialized countries. Since prostate cancer is a slow-growing tumor, early diagnosis can significantly increase life expectancy. However, late stage diagnosis is often fatal as it typically affects other organs. There are several methods available for early diagnosis, the most important of which is the determination of the PSA level. Nevertheless, nuclear medicine concepts have been further developed in recent years. For example, prostate cancer can be reliably diagnosed by positron-emisson tomography. So-called tracers labeled with a radioactive nuclide are used for this purpose. The most important representatives for the visualization of prostate carcinomas are [^{68}Ga]Ga-PSMA-11 and [^{68}Ga]Ga-PSMA-617. In addition, PSMA-617 can also be used therapeutically.

Even though these derivatives are already clinically established and routinely used, they have some disadvantages such as high accumulations in other organs or complex syntheses. Therefore, the demand for molecules that are more flexible and offer a better biodistribution is still high. In this context, squaric acid coupled KuE derivatives have proven to be promising. They show an improved biodistribution as the accumulations of gallium complexes in liver and kidney is significantly reduced compared to PSMA-11 and PSMA-617. Extensive *in vivo* studies have been performed and besides the most promising derivatives DOTAGA.SA.PSMA also TRAM.SA.PSMA and NODAGA.SA.PSMA have been investigated.

Furthermore, there is a great demand in this field for molecules that can be used with versatile nuclides. Even though PSMA-617 including a DOTA chelator is very flexible in terms of nuclide selection, this derivative can usually only be labelled at elevated temperatures, which makes "kit application" considerably more difficult. Promissing alternatives are the hybrid chelates DATA and AAZTA. These were also equipped with an SA.PSMA unit within the context of this work and AAZTA.SA.PSMA was investigated regarding its labeling properties with ^{44}Sc, ^{68}Ga and ^{177}Lu.

Another interesting metal for use in radiopharmaceutical applications is copper. There is a broad variety of isotopes that can be applied for diagnostic (^{64}Cu) as well as for therapeutic purposes (^{64}Cu/^{67}Cu) and would allow for easier dosimetric investigations. In this context both AAZTA^{5}OMe and DATA^{5m}OMe as well as the already mentioned derivative AAZTA.SA.PSMA were investigated with regard to ^{64}Cu. It was found that the labelling can be

completed quickly and with good radiochemical yields, but that the *in vitro* stability in human serum over a period of 24 hours is too low, especially with regard to therapeutic use.

Kurzzusammenfassung

Beim Prostatakarzinom handelt es sich um die dritthäufigste tödliche Krankheit und um die häufigste Krebserkrankung in Industrieländern. Da es sich beim Prostatakarzinom um einen langsam wachsenden Tumor handelt, kann die Lebenserwartung bei einer frühzeitigen Diagnose deutlich erhöht werden. Allerdings endet eine zu späte Diagnose oft tödlich, da typischerweise ein Übergriff auf andere Organe erfolgt. Um eine frühzeitige Diagnose zu ermöglichen, gibt es eine Vielzahl an Methoden. Die wichtigste ist die Bestimmung des PSA-Levels. Nichtsdestotrotz wurde in den letzten Jahren auch vermehrt nuklearmedizinische Konzepte weiterentwickelt. So kann ein Prostatakarzinom verlässlich mittels Positronen-Emissions-Tomographie diagnostiziert werden. Hierfür kommen sogenannte Tracer zum Einsatz, die mit einem radioaktiven Nuklid markiert sind. Wichtigste Vertreter für die Visualisierung von Prostatakarzinomen sind [^{68}Ga]Ga-PSMA-11 und [^{68}Ga]Ga-PSMA-617. Zusätzlich besteht die Möglichkeit, PSMA-617 auch therapeutisch einzusetzen.

Auch wenn die genannten Derivate bereits klinisch etabliert sind und routinemäßig angewendet werden, weisen sie jedoch einige Nachteile wie beispielsweise eine hohe Anreicherung in anderen Organen oder komplexe Synthesen auf. Daher ist der Bedarf an Molekülen, welche flexibler sind und besser Organverteilungen haben, immer noch groß. In diesem Zusammenhang haben sich Quadratsäure gekoppelte KuE-Derivate als vielversprechend herausgestellt. Sie zeigen eine verbesserte Biodistribution, da die Anreicherung der entsprechenden Gallium-Komplexe in Leber und Nieren im Vergleich zu PSMA-11 und PSMA-617 deutlich reduziert ist. Hierzu wurden ausführliche *in vivo*-Studien durchgeführt und neben dem vielversprechendsten Derivat DOTAGA.SA.PSMA wurden ebenso TRAM.SA.PSMA sowie NODAGA.SA.PSMA untersucht.

Des Weiteren besteht ein großer Bedarf an vielseitigen Molekülen, die mit verschiedenen Nukliden eingesetzt werden können. Auch wenn PSMA-617 mit einem DOTA-Chelator sehr flexibel bezüglich der Nuklidauswahl ist, so kann dieses Derivat nur bei erhöhten Temperaturen markiert werden, wodurch eine "Kit-Anwendung" deutlich erschwert wird. Als praktische Alternativen sind hier die hybridischen Chelatoren DATA und AAZTA zu nennen. Diese wurden im Rahmen dieser Arbeit ebenfalls mit einer SA.PSMA-

Einheit versehen und AAZTA.SA.PSMA wurde hinsichtlich seiner Markierungseigenschaften mit ^{44}Sc, ^{68}Ga und ^{177}Lu untersucht.

Eine weiteres interessantes Metall für die Verwendung in radiopharmazeutischen Molekülen ist Kupfer. Die Vielzahl an Isotopen ist hoch und eine Verwendung für die Diagnose (^{64}Cu) als auch ein vielseitiger therapeutischer Einsatz (^{64}Cu/ ^{67}Cu) ist möglich und würde zusätzlich dosimetrische Untersuchungen am Patienten erheblich erleichtern. In diesem Kontext wurden sowohl AAZTA^{5}OMe und DATA^{5m}OMe sowie das bereits erwähnte Derivat AAZTA.SA.PSMA hinsichtlich der Markierung mit ^{64}Cu untersucht. Es konnte festgestellt werden, dass die Markierung schnell und mit guten radiochemischen Ausbeuten abgeschlossen werden kann, die *in vitro*-Stabilitäten in humanem Serum über einen Zeitraum von 24 Stunden allerdings zu gering sind, gerade im Hinblick auf einen therapeutischen Einsatz.

Meinen Eltern

table of contents

Introduction

1.1 PET

There is a variety of imaging methods used in clinical practice for diagnostic purposes (Table 1) with ultrasound (US), X-ray, computed tomography (CT) and magnetic resonance imaging (MRI) probably being the most common. However, they are mainly used to obtain morphological information and cannot map metabolic processes. Only single photon emission computer tomography (SPECT) as well as positron emission tomography (PET) possess this feature. Particularly meaningful data are obtained from the combination of morphological and functional imaging methods such as the established PET/CT or the more recent PET/MRT, which was firstly presented in the end of the 1990s [1]. The individual methods differ not only in the information they give, but also in their sensitivity, temporal and spatial resolution and the used physical effect.

Table 1: Features of available and emerging imaging modalities [2].

modality	**temporal resolution**	**spatial resolution (preclinical)**	**spatial resolution (clinical)**	**sensitivity**	**physical effect**
CT	min	50-200 µm	0.5-1 mm	ND	X-rays
MRI	min-h	25-100 µm	~ 1 mm	10^{-3}-10^{-5} M	magnetic field
PET	s-min	1-2 mm	5-7 mm	10^{-11}-10^{-12} M	β^+- transformation
SPECT	min	1-2 mm	8-10 mm	10^{-10}-10^{-11} M	γ- transformation
US	s-min	1-2 mm	1-2 mm	with microbubbles 10^{-12} M	sound waves

ND, not determined

1.1.1 Physical background

Proton-rich radionuclides decay through the emission of β^+-radiation. A positron and an electron neutrino are emitted by converting a proton into a neutron (equation 1). This means an up-quark is converted into a down-quark. This positron, which is of particular importance for this work, was postulated by Dirac in 1928 and firstly detected by Andersson in 1922 [3, 4]. Equation 2 shows the equation for a β^+-decay.

$$ {}^{1}_{1}p^{+} \rightarrow {}^{1}_{0}n + \beta^{+} + \nu_e \qquad (1) $$

$$ {}^{A}_{Z}X_N \rightarrow {}^{A}_{Z-1}Y_{N+1} + \beta^{+} + \nu_e + Q \qquad (2) $$

The radionuclide must have a Q-value of at least 1.022 MeV. This energy corresponds to twice the electron mass. If the Q-value is higher, this excess of energy is transferred to the resulting particles as kinetic energy. If it is lower, only the competing electron capture (EC) is observed. Herein an s-electron close to the nucleus is captured by the nucleus, a proton is converted into a neutron and an electron neutrino is emitted (equation 3) [5].

$$ {}^{1}_{1}p^{+} + e^{-} \rightarrow {}^{1}_{0}n + \nu_e \qquad (3) $$

The positron can annihilate in two different ways. One is its collision with an electron of the environment. If electron and positron have opposite spins (singlet state), then two γ-quants are emitted in opposite direction (180°± 0.25°), each having an energy of 511 keV, which corresponds exactly to mc^2 (with m = rest mass of electron and c = speed of light). This state has an average lifetime (τ) of 10^{-10} s. In the case of parallel spins of positron and electron (triplet state), three γ-quants are emitted. The energy and angle distribution is much more complex; τ is in the range of 10^{-7} s. Furthermore, annihilation via positronium formation is possible. If the positron has released enough energy on its way through the surrounding matter without annihilating with an electron, the positronium is formed as soon as this

positron meets an electron. For this system two different spin states exist as well, *ortho* (parallel alignment of the spins) and *para* (antiparallel alignment of the spins). The angular distribution and energy is correspondingly 180° and two times 511 keV for the two-body decay, and is much more complex for the *ortho*- positronium, respectivly [6–8].

Precisely these γ-quants, emitted at an angle of 180°, form the basis of PET measurement. They are measured by ring scintillation detectors in a so-called coincidence mode. This means that whenever a simultaneous event occurs on two crystals, annihilation can be reconstructed on the connecting axis of the detectors. (figure 1).

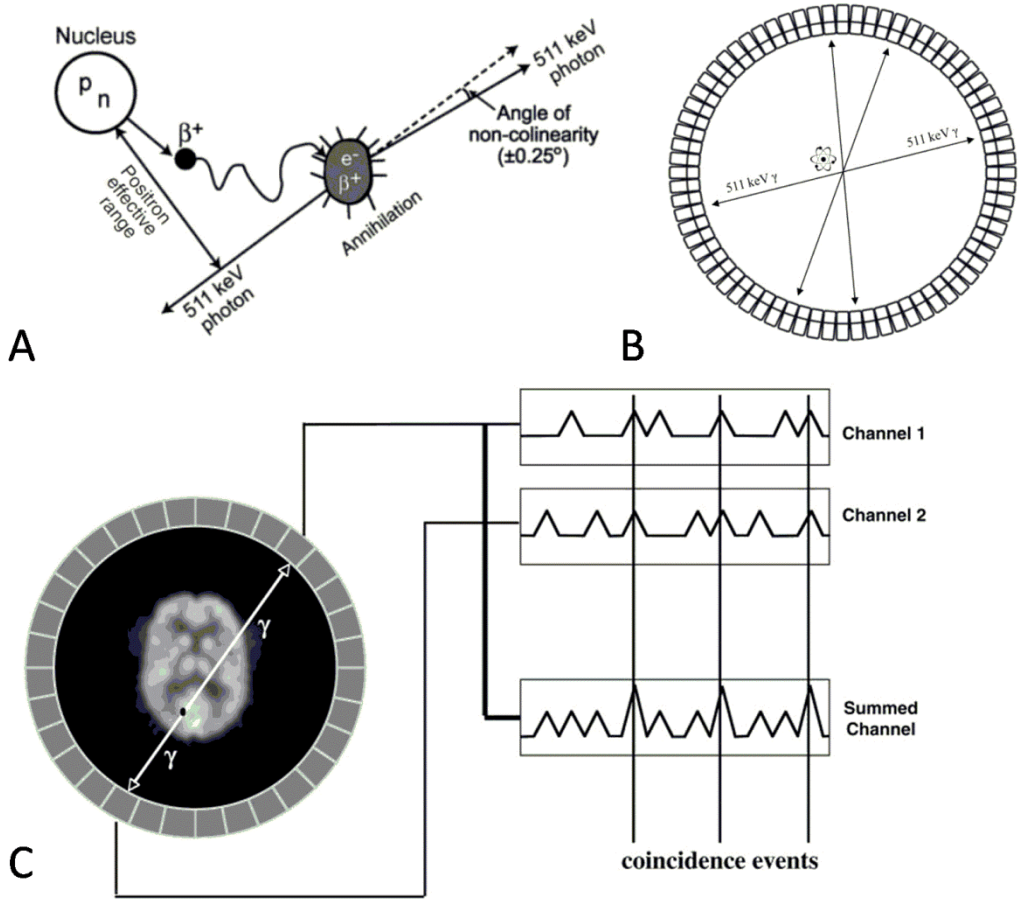

Figure 1: A: Schematic illustration of a β^+-decay with subsequent annihilation **B:** Illustration of the annularly arranged detectors in a coincidence measurement **C:** Simplified schematic representation of the signal generation in coincidence mode. Signals of opposing detectors are combined in a summed channel and coincidence events are determined from this. [9, 10].

The imaginary line between the two quanta is called line of response (LOR), on which the annihilation is located. With a certain blur, which is dependent on the kinetic energy of the positron, this location also corresponds to the localization of the β^+-emitter. In addition to the true desired coincidences as shown in Figure 1, the detectors also register γ-quants that do not originate from such coincidences. Additionally, signals can also be lost. These cases are shown schematically in Figure 2.

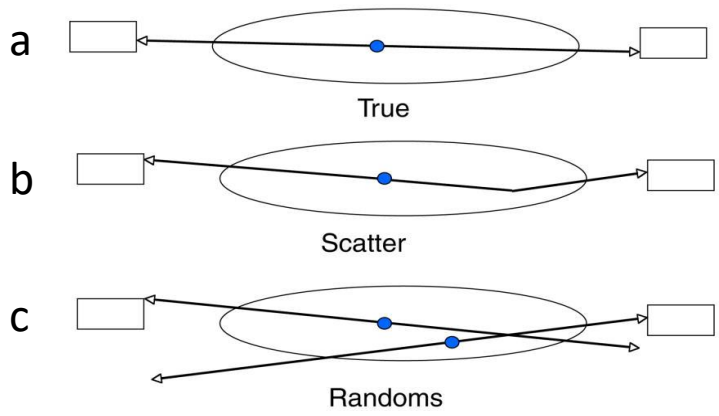

Figure 2: Different scenarios for detections. **A:** A normal true event. This results in a correct signal. **B:** A scatter quantum results in coincidence. This leads to an incorrect signal. **C:** Two random quants result in a coincidence which gives again an incorrect signal [9].

Figure 2a shows the positive case in which a true event is measured coincidentally. However, a γ-quantum can also be scattered resulting in a change of direction of the quantum. This is shown in Figure 2b. The generated LOR therefore is not correct. In a third scenario it is possible that two different quanta of two different decays are detected simultaneously (Figure 2c). Common detector systems consist of 32 individual detector blocks separated by lead shieldings to minimize the number of random coincidences. Frequently used detector materials are inorganic scintillators like bismuth germanate (BGO) or lithium orthosilicate doped with cerium (LOS). The premise for the use of these materials is that they are single ionic crystals with an energy gap conduction and valence band of 4 to 6 eV. The requirements for good materials are luminous efficiency, decay time, death time, the effective mass number of the material, the density as well as the price. Low decay times for

instance are important to minimize the number of random coincidences, and a too long death time of the material leads to lost coincidences. The size of such detector rings is in the range of 1 meter and they are equipped with up to 1152 single detectors per ring. The aim is to ensure the highest possible measuring efficiency [9, 11].

1.1.2 Biological background of PET

The most important basis for PET measurements is the radio tracer principle. Georg de Hevesy (1885-1966) first applied the procedure when he investigated the adsorption and distribution of the natural lead isotope ^{212}Pb in plants. From this he formulated the radio tracer principle and received the Nobel Prize for Chemistry in 1943 for his work [12].

This principle can be transferred to human organism. Thus, by administering a very small amount of a substance (tracer) that does not interfere with biological processes but participates in them, a certain metabolic pathway can be depicted. However, this smallest amount of molecules must be made visible. Radioactivity is particularly suitable for this purpose, since even small amounts are detectable and the expected damaging of the organism is low due to these small doses.

The pioneering work of Hevesy led to the development of nuclear medicine and the use of a large number of radioactive isotopes in various fields. In diagnostics, ^{18}F, ^{11}C and ^{68}Ga are mainly utilized for PET and ^{99m}Tc for SPECT (γ-radiation). Therapeutic nuclides are particle-emitting radiators (α-/β-radiators) like ^{131}I, ^{90}Y, ^{153}Sm, ^{177}Lu or ^{224}Ra. Some of the most often radioisotopes for clinical application are listed in Table 2.

This principle is based on the labeling of a biologically active molecule with a radionuclide. Since different approaches are known for this purpose, various biologically active compounds can be used, e.g. antibodies, proteins, peptides or even small molecules. It is important to note that this labeling should not affect the actual biologic activity of the molecule.

Table 2: Typical isotopes for different radioactive applications

nuclide	$t_{½}$	production	application
^{11}C	20.36 min	cyclotron $^{14}N(p,a)^{11}C$	PET diagnosis
^{13}N	9.97 min	cyclotron $^{16}O(p,a)^{13}N$	
^{15}O	2.04 min	cyclotron $^{15}N(p,n)^{15}O$	
^{18}F	109.6 min	cyclotron $^{18}O(p,n)^{18}F$	
^{68}Ga	67.7 min	$^{68}Ge/^{68}Ga$-generator cyclotron	
^{99m}Tc	6.0 h	$^{99}Mo/^{99m}Tc$-generator cyclotron	SPECT diagnosis
^{111}In	2.80 d	cyclotron $^{112}Cd(p,2n)^{111}In$	
^{123}I	13.22 h	cyclotron $^{124}Xe(p,2n)^{123}Cs \rightarrow {}^{123}Xe \rightarrow {}^{123}I$	
^{90}Y	64.2 h	$^{90}Sr/^{90}Y$-generator cyclotron $^{89}Y(n,\gamma)^{90}Y$	therapy
^{131}I	8.02 d	cyclotron $^{130}Te(n,\gamma)^{131}Te \rightarrow {}^{131}I$	
^{177}Lu	6.7 d	cyclotron $^{176}Yb(n,\gamma)^{177}Lu$	
^{225}Ac	10.0 d	^{228}Th-decay series cyclotron	

1.2 Labeling of molecules

1.2.1 General information

For the labeling of molecules with radionuclides, various aspects have to be considered. A particularly important factor is the half-life ($t_{½}$) because the $t_{½}$of the nuclides have to fit to the different applications. If, for example, a very fast biological process such as blood perfusion has to be imaged, a nuclide with a very short half-life is adequate. For example, $^{15}O[H_2O]$ with a half-life of 2 min is used as a standard. However, if labelled antibodies need to be measured, the half-life of the corresponding nuclide has to be significantly longer because the enrichment as well as the clearance process is significantly slower. As standard, ^{89}Zr ($t_{½}$= 78.5h) is used. Here a measurement after several days is still feasible.

Another point is the availability of the nuclide. Many of the nuclides must be produced at a cyclotron. Herein, the desired radionuclide is generated by bombarding a target with charged particles (projectiles). These projectiles are typically protons, deuterons or α-particles which are accelerated in a magnetic field. A nuclear reaction takes place in the target resulting in the formation of the desired radionuclid. However, this type of production is very expensive to purchase and maintain, which limits its availability. An are radionuclide generators that make nuclides easily accessible. No cyclotron is needed at the facility using the radionuclide for applications. Therefore the principles of transient and secular radioactive equilibria are used, in which a long-lived mother nuclide decays into a short-lived daughter nuclide. By separating the daughter from the mother, fixed on a solid phase, radionuclide generators are able to elegantly obtain the desired radionuclide (daughter).

Another extremely important matter is how the isotope can be introduced into the bioactive molecule and how this changes the pharmacology and pharmacokinetics of the molecule. The simplest examples are probably isotopes of elements found in organic molecules such as ^{11}C, ^{15}O or ^{3}H. Here covalent insertion of the corresponding isotope is fairly easy and the pharmacological property of the molecule is not affected by this. However, if an isotope of a biologically less frequent or a naturally non-existent element is used, it must be considered that this modification can alter the pharmacological properties of the molecule. Common examples of isotopes that are covalently introduced into molecules are halogens, carbons

and hydrogen. A large number of methods have been investigated and published for their insertion [13–15].

Another problem occurs when radioactive metals are used in tracers. These require a chelator moiety, a molecule that is able to capture a metal via coordinative bonds. Normally, these molecules are very large in relation to the bioactive molecule and may therefore influence their pharmacology significantly. The typical arrangement opf tracers that are used in combination with radioactive metals is shown in Figure 3.

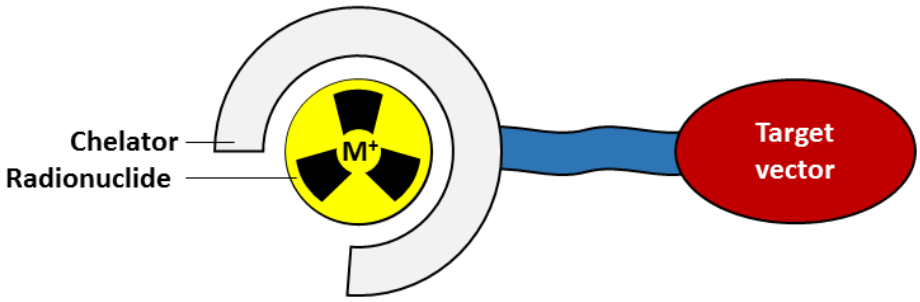

Figure 3: Typical setup of a radiotracer for radiometals.

All tracers of this design have in common that they consist of a biologically active molecule and a chelator that complexes the metal. Additionally, a spacer and a linker can be added, which brings spatial distance between the chelator and the target vector. This can help to minimize negative interaction of the chelate on the targeting vector and cam improve or maintain the pharmacology of the tracer.

1.2.2 Chelates

Chelators, are multidentate ligands. These can have 2 or more donor groups to form a dative bond to a metal with an electron vacancy. The great advantage of these multidentate ligands is that they form much more stable complexes than comparable several monodentate ligands. This advantage is used *in vivo* to protect typical metals towards transmetalation. This stability is called the chelate effect and can typically be explained by two attributes. On the one hand it can be explained thermodynamically. It is assumed that in a complex formation reaction involving a chelate, the number of product molecules increases whereas in a reaction with monodentate ligands it remains the same (see equations 4 and 5). This increase of the number of reaction partners is beneficial to the system in the form of free movement (entropy), which leads to an increased (less positive) free energy of formation, which is reflected in a larger stability constant according to $k_b = \exp(-\Delta G_b/RT)$ [16].

$$[Cd(H_2O)_6]^{2+} + 4NH_2Me \leftrightarrow [Cd(NH_2Me)_4(H_2O)_2]^{2+} + 4H_2O \quad (4)$$

$$[Cd(H_2O)_6]^{2+} + 2\ en \leftrightarrow [Cd(en)_2(H_2O)_2]^{2+} + 4H_2O \quad (5)$$

en = ethylendiamine

On the other hand, there is a kinetic explanation that goes back to G. Schwarzenbach. With the same concentration of a monodentate ligand (L) or a bidentate ligand (L^L), the probability or velocity for the occupation of the first coordination site of a metal ion is approximately the same for both cases. However, the probability of the occupation of the second coordination site is higher for L^L than for L, because the effective concentration of the bidentate ligand at the complex center is usually higher than for L due to its spatial proximity [17].

These factors contribute to the idea that chelators can be used to introduce radiometals into tracers in a stable manner and to ensure the most possible inert behavior *in vivo*. In case of the attachment of a targeting vector to a chelator, as described in Figure 3, the term bifunctional chelator (BFC) is used. In general, a classification can be made between two types of chelators used in nuclear medicine, which are discussed in the following sections.

macrocyclic chelates

The best-known example of a synthetic macrocyclic ligand in radiopharmacy is DOTA (1,4,7,10-tetraazacyclododecan-1,4,7,10-tetraacetic acid) (Figure 1). Its popularity is particularly due to the high variety of metals which can be stabl complexed by DOTA. Possible metals are trivalent d- and f-metals as well as two valent copper [[18–21]. DOTA also represents the typical properties of macrocyclic ligands. On the one hand, DOTA-based complexes provide high kinetic and thermodynamic stability with many metals, so that the biological use is not limited. On the other hand, labeling of DOTA and many other macrocyclic ligands is only possible at elevated temperatures. For the combination of DOTA with gallium, for example, up to 95°C are necessary. However, this is a major disadvantage when bifunctional DOTA derivatives are used for coupling to larger and more sensitive biological molecules such as peptides or antibodies. Here, labeling at high temperatures is inconceivable. Acyclic chelates have been established for the functionalization of such molecules. Other commonly used macrocyclic derivatives are NOTA (1,4,7-Triazacyclononane-1,4,7-triacetic acid) and NOTP (1,4,7-Triazacyclononane-1,4,7-tri(methylene phosphonic acid) (see Figure 4). These two derivatives are compounds that can be labeled even at lower temperatures. However, due to their triazacyclononane scaffold, they do not offer the same flexibility a DOTA and are therefore mostly utilized exclusively for labeling with gallium [22, 23]. This limits the application to diagnostic purposes and excludes a therapeutic approach using the same molecule.

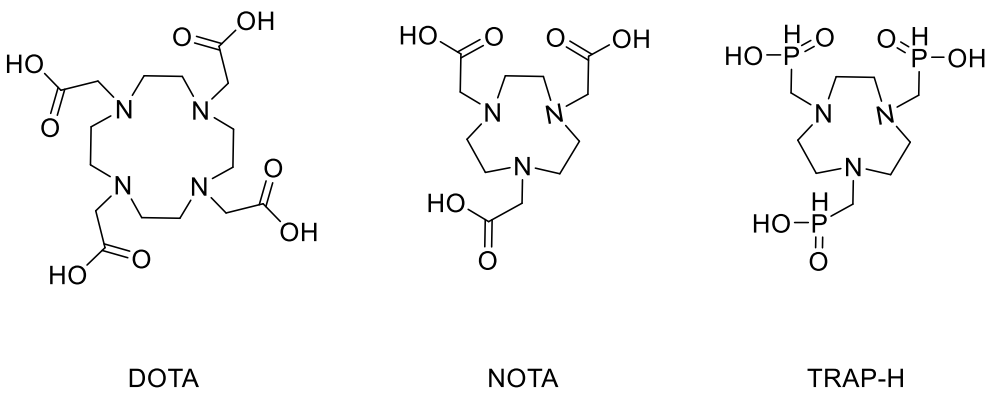

Figure 4: The macrocyclic chelators DOTA, NOTA and TRAP-H. All three show excellent complexation properties with gallium.

However, not every chelator is automatically capable of being a BFC. This often requires modifications. With its N_4O_4 framework, DOTA offers 8 donor moieties for the radiometal. If less than these 8 donors are required, one carboxylic acid group can be used to attach a target vector. This can usually be achieved by formation of a peptide bond between the acid of DOTA and a primary amine of the target vector. Often the acid groups are also activated by NHS esters to ensure a better coupling (see Figure 5). However, it is noteworthy that much more difficult synthesis chemistry has to be applied for preparation of asymmetric DOTA systems. This requires the use of complex protective group chemistry and inevitably results in lower yields and higher prices. If molecules with higher coordination numbers are desired, even special derivatives have to be produced for bifunctionalization, such as DOTAGA or *p*-SCN-Bz-DOTA (see Figure 5). These modifications of the DOTA scaffold can also achieve the coordination number 8 and a TV can be attached to it.

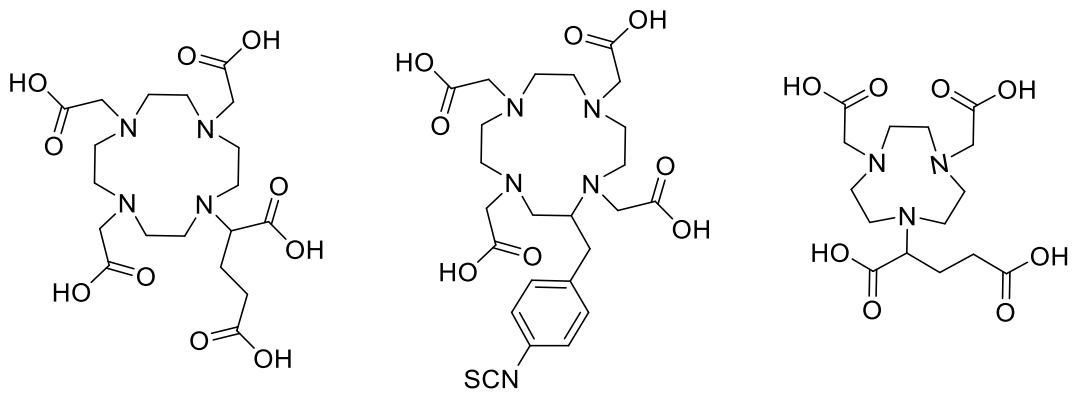

Figure 5: Typical bifunctional derivatives. Normally glutamic acid derivatives are used to enable functionalization (see DOTAGA, NODAGA). Another group besides carboxylic acids used for functionalization is the SCN group. These have a good reactivity towards amines (see *p*-SCN-Bz-DOTA).

Similar modifications are also known for NOTA and are particularly interesting for gallium or other trivalent metals with the coordination number (CN) of 6. The synthesis of derivatives

such as NODAGA or p-SCN-Bn-NOTA (see figure 5) allows the introduction of a target vector while maintaining the N_3O_3 coordination sphere, which in turn allows the complexation of metals with a CN of 6. It is obvious that the synthesis of such derivatives requires even more complex synthesis and protective group strategies than mentioned above.

acyclic chelates

One of the oldest and most commonly used acyclic chelators for radiometals is DTPA (diethylenetriamine pentaacetate; Figure 6). With its N_3O_5 coordination sphere, this ligand is versatile and is able to form complexes with many of the common metals such as gallium, lutetium or even indium [24, 25]. There are also bifunctional variants of this derivative such as the *p*-SCN-Bn-CH_A''-DTPA [26, 27]. In recent years a large number of other acyclic ligands and their bifunctional derivatives have been synthetized for the complexation of gallium. HBED (N,N-bis(2-hydroxybenzyl)ethylenediamine-N,N-diacetic acid, Figure 6) and its corresponding derivatives are of particular importance here [28]. Other chelates that became more important are H_2dedpa (1,2-[[6-carboxy-pyridin-2-yl]-methylamine]ethane) and different trihydropyridone derivatives [29, 30].

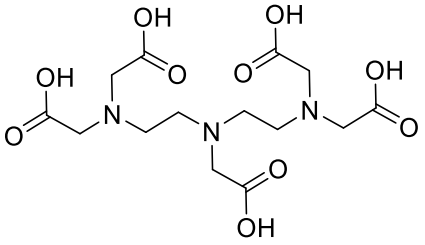

DTPA

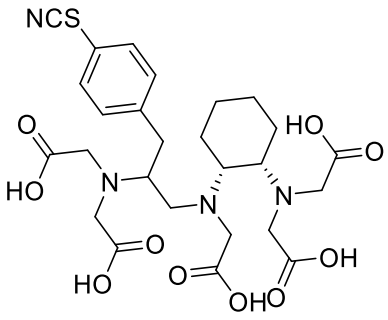

p-SCN-Bn-CHX-A”-DTPA

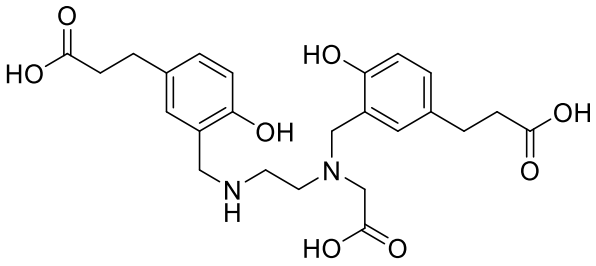

HBED-CC

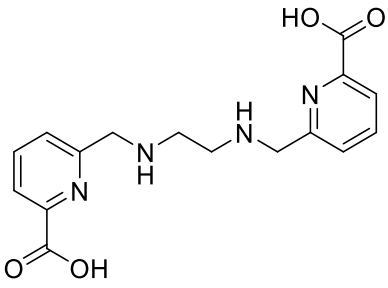

H_2dedpa

Figure 6: Typical acyclic chelators. Top: DTPA and the functionalisable version *p*-SCN-Bn-CHX-A"-DTPA. Bottom: HBED-CC and H_2dedpa. Both can be used bifunctionally.

Advantages of all these derivatives are that they show extremely fast kinetics even at room temperature and are therefore well suited for conjugation with larger and more sensitive peptides. Nevertheless, most of these molecules have the disadvantage of extremely limitation in the choice of suitable metals and in addition most of the corresponding metal ligand complexes indicate a poor *in vivo* stability.

hybrids

Over the last few years, several groups have tried to design molecules that combine the properties of cyclic and acyclic ligands. These are referred to as hybrid chelators. Acyclic chelators are generally considered to be particularly fast in their radiolabeling kinetics and that the process is mostly temperature-independent. A negative property is the decreased kinetic stability, which can be observed with EDTA or DTPA, for example. In contrast to that, macrocyclic chelators form particularly stable complexes (compare DOTA), but require higher labeling temperatures and usually have slower kinetics. The hybrid chelators should combine the positive properties in one structure [31].

The most promising approach in this direction is the use of a diazepine backbone which contributes to complex formation with two endocyclic amines. Introduction of another exocyclic amine provides a third coordination unit. Via alkylation of these amines with three or four carboxylic acids, further donor units can be introduced and either the so-called DATA (6-amino-1,4-diazepine-triacetic acid) or AAZTA (6-amino-1,4-diazepine tetracetic acid) is obtained (Figure 7) [32–34].

Figure 7: Structures of hybrid chelators DATA and AAZTA with coordination numbers of 6 and 7, respectively.

For the transfer of these structures to bifunctional systems a large number of arrangements were investigated. Here the DATA[5m] and the AAZTA[5] turned out to be ideal options. In those systems a C_5-linker with a terminal carboxylic acid is introduced to provide bifunctionality (Figure 8) [35–37].

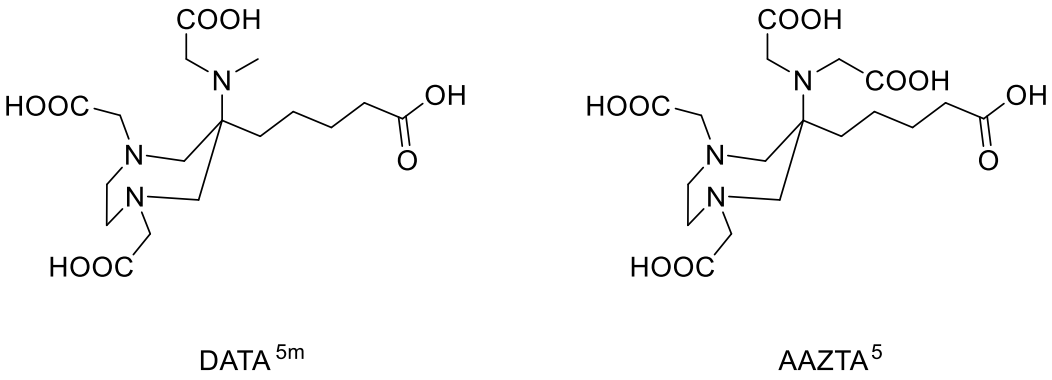

Figure 8: Structures of bifunctional chelators DATA[5m] and AAZTA[5]. In contrast to AAZTA and DATA, these two structures can be coupled by the attached additional carboxylic acids.

So far it is known that DATA has excellent properties for complexing gallium, whereas AAZTA has excels in binding scandium or lutetium. Both chelator classes are able to complex the corresponding metals already at room temperature and the formed complexes show very good stability. Especially for gallium the selection of ligands with comparable possibilities is rather limited. Worth mentioning in this context is TRAP (1,4,7-triazacyclononane phosphinic acid), which can often only be used for multivalent functionalization [22]. In addition, at very mild temperatures gallium is also labeled by the established HBED as well as the H_2dedpa which both, however, form complexes with a positive overall charge [28, 29]. The only completely comparable derivatives in terms of temperature, charge and stability are the THP (Tris(hydroxypyridinone)) variants of Blower *et al.* Here, however, it should be noted that the exact charge distribution of the derivatives has not been clarified [30].

1.2.3 Ligation chemistry

As already mentioned, an extra functional group on a chelator is necessary to attach a target vector. This feature makes it a BFC. In most cases these groups are carboxylic acids, but also amines, alkynes or azides. Common coupling options are described in the following section.

One of the most common binding types is the amide bond. It is formed by the reaction of a carboxylic acid and an amine under water elimination. The so-called amide bond has the advantage that it has an extremely high stability *in vivo*, but unfortunately its synthetic formation is difficult. Direct coupling is usually carried out with the support of active esters formed *in situ*. DCC, HATU or other urea-based reagents are often used. These compounds, however, often show a large number of disturbing side reactions which make processing and spectroscopic examination very difficult. Alternatively, storable active esters can be formed prior to the reaction. NHS (N-hydroxysuccinimide) or pentafluorophenyl esters are frequently used for this purpose. A problem in this case is the sensitivity to hydrolysis, which leads to stabilities of only a few hours for NHS esters [38–40]. For these reaction types, it should be kept in mind that conjugation can only be carried out using complicated protective group chemistry, since a chelator generally contains further reactive groups (carboxylic acids and amines). Therefore, ligations that exhibit complete orthogonality are particularly interesting because they do not require protective groups.

1.3 Isotopes for PET- imaging

The most widely used nuclide is ^{18}F, which is strongly related to the use of ^{18}F-2-Deoxy-2-fluoroglucose ([^{18}F]FDG), an all-purpose tracer that has been clinically applied for more than 40 years [41]. However, due to its physical and chemical properties, ^{18}F does not always provide the perfect conditions and is unsuitable for some applications. For example, for certain utilization the half-life of 110 min can be too short. Also the availability plays a major role since the use of ^{18}F requires a cyclotron in the direct vicinity. For this reason, especially tracers with availability based on radionuclide generators have excelled in recent years.

1.3.1 Gallium-68

In nature, gallium is found in small amounts in zinc salts, among others 0.1 % in zinc blende, 0.1-1 % in germanite or 0.01% in bauxite. The stable isotopes are ^{69}Ga (60.1%) and ^{71}Ga (39.9%). The element was discovered in 1875 by the Frenchman Lecoq de Boisbaudern during spectral analysis of zinc blende. He named the element in honor of his fatherland France (lat. Gaul). In aqueous solutions, gallium normally has the oxidation number +III and, like its nearest relative aluminum, can therefore be classified as a hard Lewis acid. Gallium is thus able to form stable octahedral complexes with a CN of 6 with hard Lewis bases such as amino-, carboxyl- or hydroxyl-groups according to the hard and soft acids and bases (HSAB) principle [16, 42, 43]. The most interesting radioactive isotopes of gallium are ^{67}Ga with a half-life of 3.3 d, which is mainly used in SPECT, and ^{68}Ga with a half-life of 68.3 min, which decays via β^+- transformation and can therefore be used as a PET nuclide [44]. While ^{67}Ga can only be generated at a cyclotron, ^{68}Ga exhibits the advantage that besides cyclotron-based production, it can also be obtained easily, quickly and cost-effectively using a radionuclide generator.

The $^{68}Ga/^{68}Ge$ system provides optimal conditions for use as a generator. ^{68}Ge is long-lived with a half-life of 270.8 days and it decays to the short-lived ^{68}Ga with a half-life of 68.3 minutes, which in turn finally decays to stable ^{68}Zn. ^{68}Ga decays with a high probability (89%)

via β^+- transformation with a maximum of energy of 1.9 MeV. The remaining 11% pathway is electron capture. ^{68}Ge can be produced by a (p, 2n)-reaction of ^{69}Ga at a cyclotron.

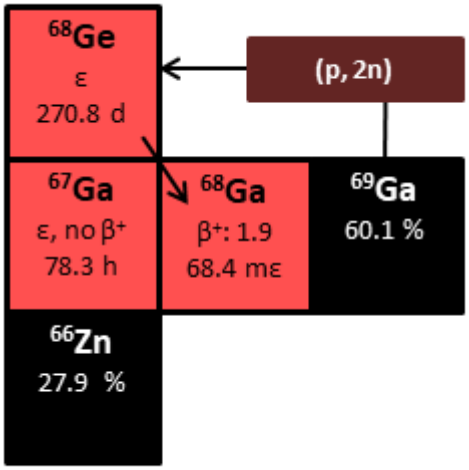

Figure 9: Section from the chart of nuclides. It shows the production of the ^{68}Ge from ^{68}Ga via a (p,2n)-reaction as well as the further decay to ^{68}Ga via ε.

^{68}Ga/^{68}Ge radionuclide generators have become increasingly important in recent years and are now widely used in clinical diagnosis for PET/CT. While the first generators were part of research in the 1960s and the first patient studies were carried out in the USA, interest flattened out in the meantime [19, 45]. This was on one hand due to the type of Ga-eluates of these generators, such as fluorides, oxalates and EDTA complexes. These compounds were difficult to modify or use as a targeted tracer. On the other hand, the contents of impurities like Fe(III), Zn(II), Ti(IV) and Ge(IV) were too high. These two disadvantages could be improved at the beginning of the 21st century. A new type of generator was constructed in which hydrochloric acid was used as eluent. Thus cationic Ga-species (Ga^{3+}) were present ready for versatile complex formation. The first example of this generator type was the Obninsk generator followed by several other types up to today.

In addition, new post-processing methods improved the radionuclide purity of the eluate and consequently, the specific labeling yields and the purity of the labeling solution. In general, elution takes place mostly via ion exchange processes or fractionation. Various

processing methods can now be used, such as acetone-post-processing by Zhernosekov *et al.* or other setups [46–48]. First, impurities are rinsed from the exchanger with various mixtures of solvent and hydrochloric acid before the fixed gallium is rinsed with another solvent/hydrochloric acid mixture.

1.3.2 Scandium-44

Scandium is often considered to be a rare element, but in fact it occurs just as often as lead, cobalt or copper. The reason it is considered so rare is its fine distribution in nature. The only known scandium-containing mineral is thortveitite $(Sc, Y)_2[Si_2O_7]$ with an average of 20-35% Sc_2O_3. In aqueous solutions, scandium is present as an ion with the oxidation state +III and behaves like a hard Lewis acid. Therefore it forms complexes with hard Lewis bases (e.g. amino, carboxyl or hydroxyl groups) with a CN of 6 or higher [16]. The only naturally occurring isotope of scandium is ^{45}Sc. Relevant radioactive isotopes are ^{43}Sc, ^{44}Sc, ^{47}Sc and ^{46}Sc. ^{44}Sc is used as β^+-emitter for PET. Its production is possible via a $^{44}Ca(p,n)^{44}Sc$ nuclear reaction but it can also be obtained via a $^{44}Ti/^{44}Sc$ generator. The mother nuclide ^{44}Ti usually is obtained by bombarding ^{45}Sc with protons or deuterons or by bombarding ^{44}Ca with α-particles at cyclotrons [49, 50]. As pure β-emitter with a half-life of 3.35 d and an E_β of 162 keV, ^{47}Sc is a candidate for radionuclide therapy. This possibility is also offered by ^{46}Sc, which, however, has a significantly longer half-life of 83.79 d. The general diversity of isotopes allows a theranostic use in which the effort for dosimetry examinations can be reduced significantly [51].

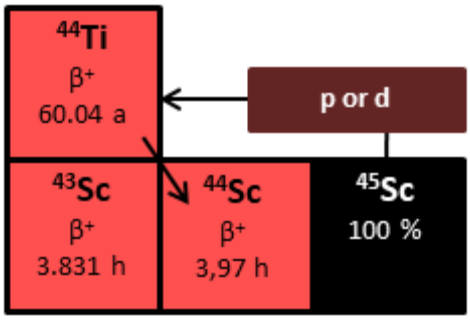

Figure 10: Section from the chart of nuclides. Possible productions for ^{44}Ti are shown as well as the decay to the target nuclide ^{44}Sc.

The initial attempt to build a $^{44}Ti/^{44}Sc$ nuclide generator took place between 1960 and 1970 but were of academic interest only [52–54]. A $^{44}Ti/^{44}Sc$ nuclide generator for easy production of radiopharmaceuticals has been described for the first time from Mainz [55]. Using an

anion exchange matrix, this generator is able to fix the mother nuclide ^{44}Ti ($t_{½}$ = 60 years), which can be obtained by previously described reactions. ^{44}Ti directly decays to the ground state of ^{44}Sc by EC and does not produce any by-products or excited intermediates. The generator is eluted with 20 ml 0.07 M hydrochloric acid / 0.005M oxalic acid (Figure 11). One elution of the Mainz generator yields 175 MBq ^{44}Sc without postprocessing and 130 MBq ^{44}Sc after postprocessing with a ^{44}Ti breakthrough of less than 200 Bq, resulting in an excellent separation factor of 10^6. To reduce the volume of the eluate and to separate the ^{44}Ti breakthrough as well as other metal contaminants, ^{44}Sc is absorbed on a cation exchanger during elution and then eluted with 3 ml 0.25 M ammonium acetate buffer (pH 4) [53]. On average, up to 85% of the ^{44}Sc is recovered from the cation exchanger. The resulting solution contains less than 10 Bq of ^{44}Ti.

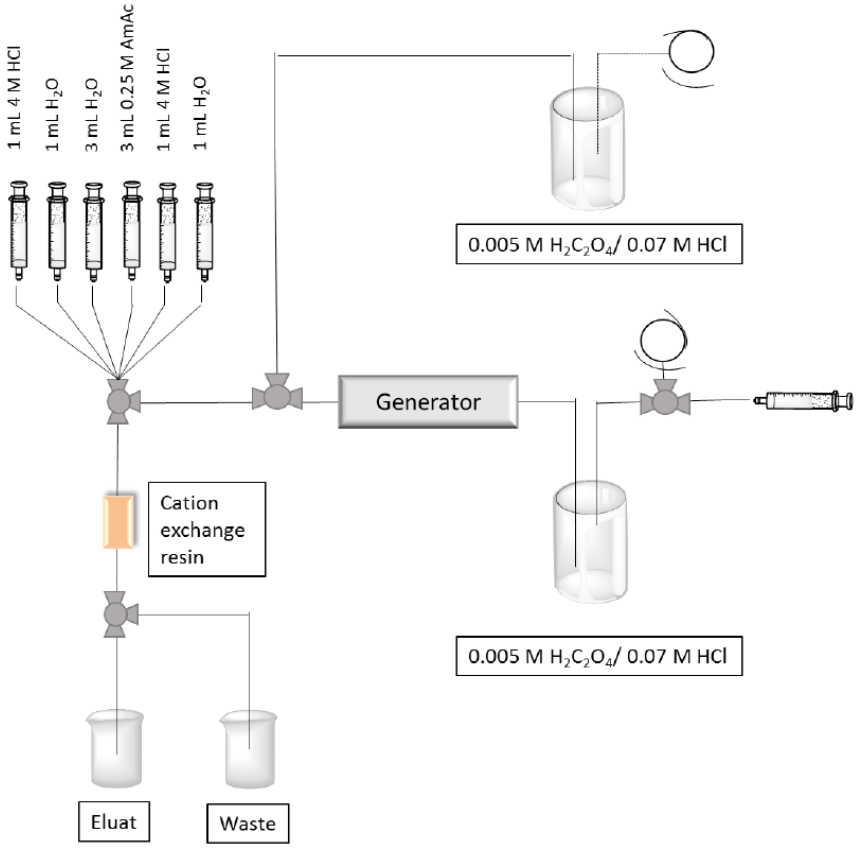

Figure 11: Schematic illustration of the elution of the ^{44}Ti/^{44}Sc generator [56].

1.3.3 Copper-64

Copper is located in the earth's crust with a content of about 0.006 %. As metal, it also occurs mainly in small quantities in North America, Chile and Australia. When bound, it is mainly found as oxide, sulfide or carbonate. Many different copper isotopes are known and in use for a variety of applications [16].

In recent years, ^{64}Cu-derivatives have been increasingly used for PET [57–60]. This is mainly because it provides a relatively long half-life ($t_{½}$ = 12.7 h). In this context, relatively long means, that it is long enough to visualize processes of larger peptides as well as antibodies, but also not too long to visualize processes shown by small molecules with a short biological half-life [61, 62]. A typical radiometal for the examination of molecules with a long biological half-life (3.3 d), in connection with PET, is ^{89}Zr. The disadvantage of ^{89}Zr is the small number of suitable ligands and the average stability of the corresponding complexes *in vitro* and *in vivo* [63]. ^{64}Cu itself has a significantly lower half-life than ^{89}Zr, but with its 12.7 h it offers a sensible compromise between a very long and a short half-life. On top it offers the great advantage that both nuclides, ^{64}Cu and ^{67}Cu, are available for PET, SPECT and therapeutic approaches. For example, ^{67}Cu decays by emitting β^- particle and therefore can be used for therapeutic purpose [64, 65]. The combination with ^{64}Cu offers therefore a perfect pair for theranostic applications [66].

^{64}Cu can decay via a β^+- transformation (18%), electron capture (43 %) as well as a β^--transformation (39%). Therefore, it can theoretically be used as a stand-alone isotope for diagnosis and therapy. In practice, the combination with ^{67}Cu is mostly used as already mentioned.^{64}Cu can be produced both by reactor via a ^{63}Cu(n,y)^{64}Cu reaction and by a cyclotron via a ^{64}Ni(p,n)^{64}Cu reaction. However, due to the poor specific activity obtained as a result of the reactor-based nuclear reaction with a copper target, production at the cyclotron is the preferred method [67].

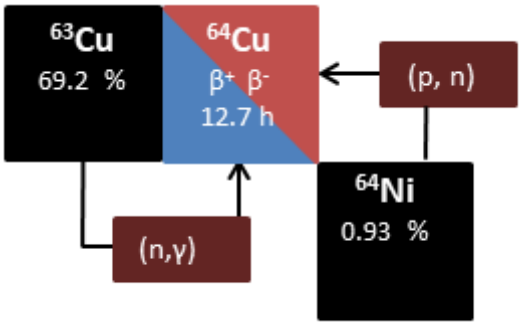

Figure 12: Section from the chart of nuclides. Possible productions for ^{64}Cu are shown.

However, one of the greatest advantages of copper in general is its coordination chemistry, which has been well researched for years [68]. Therefore, a large number of ligands coordinating copper are known. Among others, DOTA (1,4,7,10-tetraazacyclododecane-1,4,7,10-tetraacetic acid) or TETA (1,4,8,11-tetraazacylotetradecane-1,4,8,11-tetracetic acid) are commonly utilized (see Figure 14) [21, 69, 70]. In addition, there are also some different sacrophagine variants, such as DiamSar or SarAr, which are already widely used as Cu-ligands, all with different advantages and disadvantages [71].

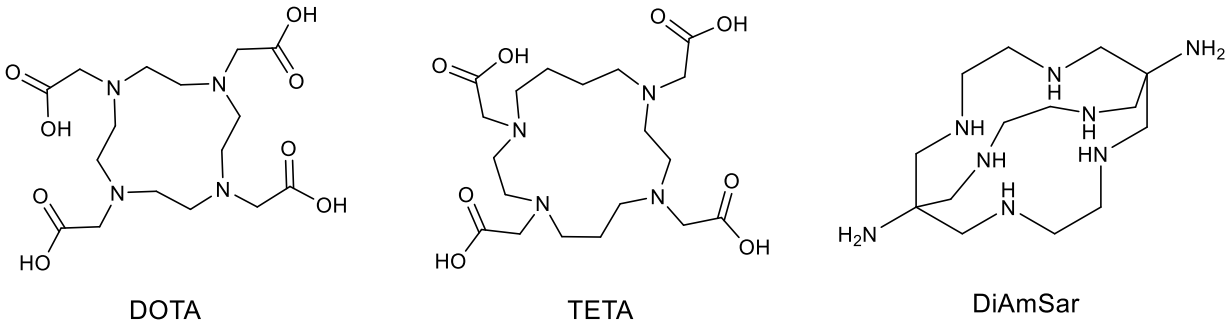

Figure 13: DOTA, TEAT and DiAmSar as typical examples of stable Cu-chelators.

1.4 Isotopes for therapy

Most of the metallic nuclides used in radionuclide therapy or endoradiotherapy are applied as radiopharmaceuticals with a few exceptions. These are the two cations $^{89}Sr^{2+}$ and $^{223}Ra^{2+}$, which are both used for the treatment of bone metastases. In total, nuclides used for therapy emit radiation that is clearly harmful to tissue compared to those used for diagnosis. In most cases, β^-- or α-radiation is used. The distance covered by α-radiation in particular, but also by β^--radiation, is significantly lower than that of γ-radiation, so that damage to the surrounding healthy tissue is minimized.

The linear energy transfer (LET) causes ionization and radical formation, which in tissue mainly creates radicals from water fractions which can lead to DNA damage. It is important that the used radionuclide has a high LET value so that the vitality of the cell is attacked to the greatest possible extent, due to the fact that cells have well-functioning repair mechanisms for this type of damage [72, 73].

1.4.1 Lutetium-177

Lutetium always occurs in the oxidation state +III which leads to a relatively large ionic radius of 1.26 Å which again results in a coordination number of 6 to 12 [16].

Lutetium has a total of 34 isotopes including one stable (^{175}Lu) and another very long-lived (^{176}Lu $t_{½}$ = $3.8 \cdot 10^{10}$ y). Both isotopes also occur naturally with ^{175}Lu accounting for 97.41% [74]. Due to its decay properties ($t_{½}$ = 6.7d), ^{177}Lu is particularly suitable for small tumors.

The most commonly used method to produce ^{177}Lu is using a ^{176}Lu(n,γ)^{177}Lu nuclear reaction. Here, enriched Lu(III)oxide (60.6 % ^{176}Lu) is bombarded with thermal neutrons. Within this reaction, ^{177m}Lu ($t_{½}$= 160 d) occurs as a side product. Even though the contamination content is typically lower than 0.5% it still needs to be taken into account for accurate dosimetry. Furthermore, beside the desired ^{177}Lu, the already mentioned natural nuclides ^{175}Lu and ^{176}Lu occur as additional side products. These cannot be separated chemically and therefore might complicate labelling [75].

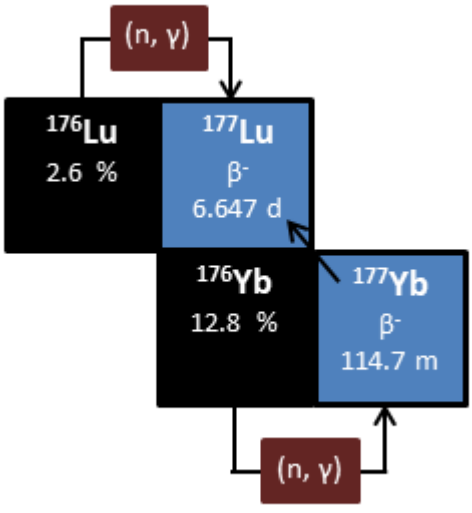

Figure 14: Section from the table of nuclides. Possible productions for ^{177}Lu are shown.

As an alternative there is another method to produce ^{177}Lu which was actually applied for the ^{177}Lu in this work. Here ^{177}Lu can be obtained completely carrier free. Using a ^{176}Yb(n,y,)^{177}Yb→(β^-)→^{177}Lu pathway, the product is obtained after separation from ^{176}Yb without the addition of natural lutetium. ^{176}Yb is bombarded with thermal neutrons and ^{177}Yb is formed. This decays to ^{177}Lu with a half-life of 1.9 h by β^- transformation.

1.4.2 Copper-67

Chemical and physical properties of copper have already been described in section 1.3.3. However, production of ^{67}Cu is different from the ones described for ^{64}Cu.

^{67}Cu is produced by bombardment of ^{67}Zn with neutrons in high flux reactors, or via cyclotron by irradiation of ^{nat}Zn or enriched ^{68}Zn with protons. These are the most commonly used methods besides other less practicable methods such as irradiation with α-particles [64].

1.5 Prostate cancer

Prostate cancer is the most common cancer in industrial countries and the third most deadly disease [77]. Tumor growth in prostate is a slow process, so an early stage diagnosis can increase the 5-year survival rate to nearly 100%. In contrast, if the disease is discovered after the tumor has spread, the survival rate decreases dramatically. Once detected, prostate cancer requires an immediate, but balanced, therapeutic intervention, because a too aggressive treatment can be detrimental to the patient´s quality of life [78, 79]. Therefore, timely diagnosis and reliable assessment of both, disease progress and response to therapy are indispensable for management of long-term survival and the patients' life quality.

The standard procedure for diagnosis of prostate cancer is to palpate. Particularly in preventive medicine, this is the method of choice. Furthermore, tumor markers in the patient's blood can be determined. The marker prostate-specific antigen (PSA), which is produced in the prostate gland and liquefies sperm, is usually analyzed. In general, the concentration of PSA in the blood is rather low, so that an elevated concentration can be interpreted as a disease of the prostate. However, the probability of a false positive is very high using this method [80, 81].

Another very important structure for diagnosing prostate cancer is the prostate-specific-membrane-antigen (PSMA), a membrane-bound glycoprotein belonging to the enzyme class of the carboxy peptidases (E.C. 3.4.16). The preferred substrate of PSMA is a peptide with a C-terminal glutamate, e.g. N-acetyl-aspartyl-glutamate (NAAG) or folic acid-(poly)-γ-glutamate [81]. PSMA is barely present in healthy tissue, but is expressed in high levels in prostate cancer cells [82, 83]. Additionally, the concentration of expressed PSMA correlates well with the stage of the disease [82, 84]. Furthermore, bone metastases, as well as lymph nodes, show a significantly increased expression of PSMA [85].

In radiopharmaceutical chemistry and nuclear medicine, different approaches to visualize PSMA have been used over the years. The most common strategy is the usage of antibodies that bind to the protein structure of PSMA [86–88]. Alternatively, binding pockets at the active site of the enzyme can be targeted using small molecules as shown in Figure 16.

Besides the main pocket, where two Zn^{2+} ions are located, there is a secondary pocket showing high affinity towards planar, aromatic structures [89, 90].

For any ligand to bind to the active site of PSMA, a glutamate motif resembling the natural substrate must be present. In order to enhance binding and to avoid dissociation of the bound ligand, this structure should contain a reactive group to form a covalent bond to an amino-acid residue of the active center that cannot be cleaved by the enzyme. One of the most potent PSMA inhibitors is 2-phosphonomethyl pentanedioic acid (2-PMPA), which combines the glutamate binding structure with a non-cleavable phosphonate. In addition, thiols are not processed by the enzyme as well. A large group of urea-based PSMA inhibitors found to be clinically relevant are the radiopharmaceuticals PSMA-11 and PSMA-617 [81, 91].

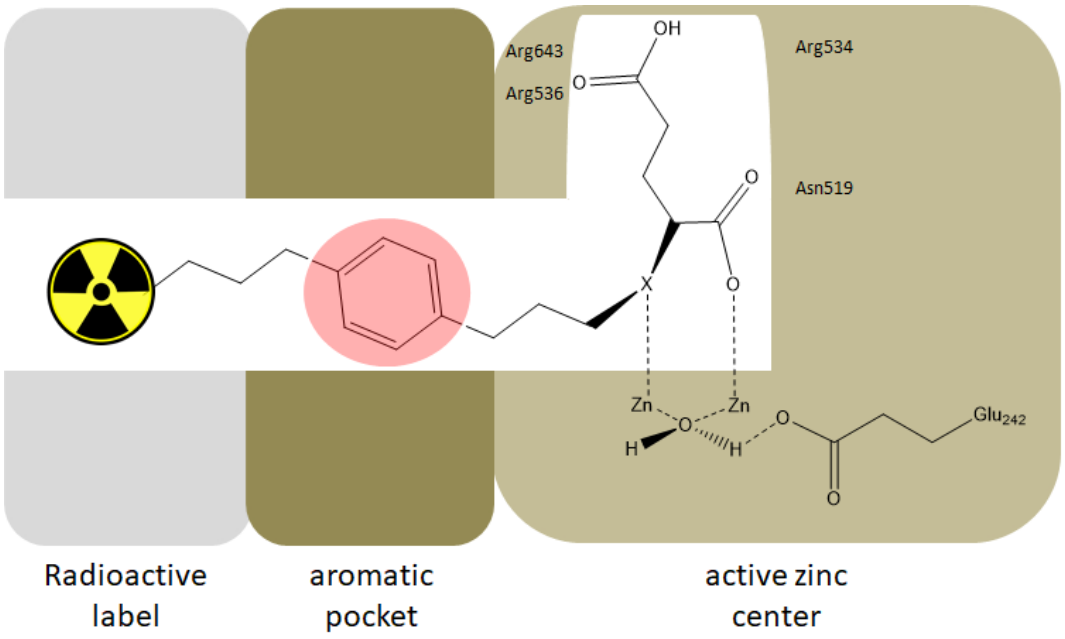

Figure 15: Schematic illustration of the binding of a radio-labelled small molecule PSMA-inhibitor to the binding pocket of PSMA. The glutamate binding motif binds to the active zinc center of the enzyme. It is linked by a non-cleavable bond to an aromatic linker that interacts with the aromatic binding pocket of the targeting molecule. This is illustrated here schematically by a benzyl residue. On the left side of the molecule, the radioactive label is attached covalently (for e.g. radioahalogenides) or non-covalently (for radiometals, which requires a covalently bound bifunctional chelator).

Concerning the structure of the aromatic binding pocket in PSMA, the insertion of a aromatic moiety into the inhibitor has proven to be advantageous. For example, the enzyme inhibition potential increases with addition of a tetrazole to 2,2'-(carbonylbis(azanediyl))bis(5-amino-5-oxopentanoic acid) (Figure 16, molecule 4). A similar pattern was observed in the development of chelator-PSMA-inhibitor derivatives. Coupling of ((4-amino-1-carboxybutyl)carbamoyl)glutamine (KuE) to the aromatic HBED chelator via an octanedioic acid linker and subsequent 68Ga-labelling results in the potent radiopharmaceutical ^{68}Ga-HBED-PSMA-11 (6). Using DOTA instead of HBED, losses in affinity occur(6) [92].

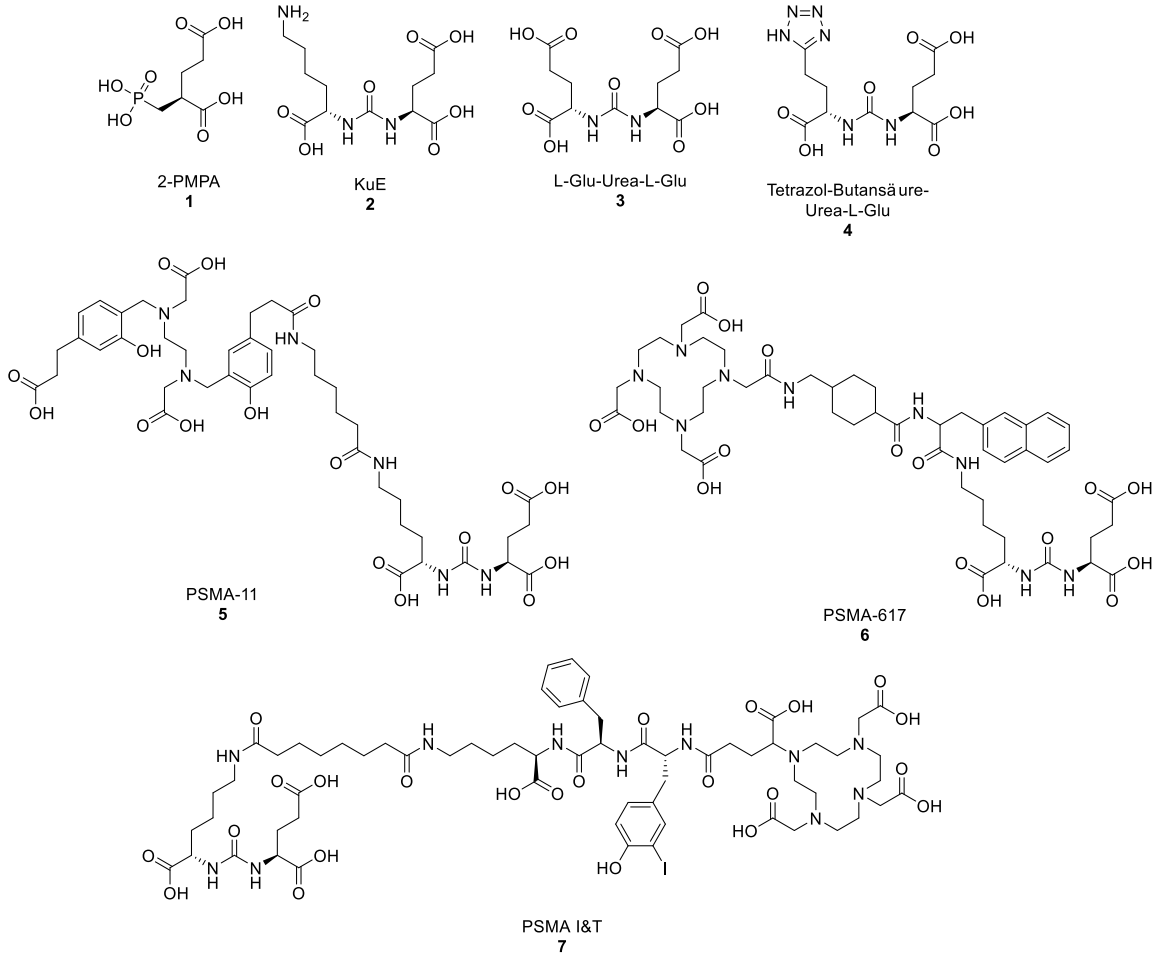

Figure 16: Different PSMA-inhibitors. The inhibitor Lys-Urea-Glu (KuE) (**2**) shows good affinities bound to the aromatic chelator HBED (PSMA-11, K_i = 12.0 nM) (**5**). The affinity of the Glu-Urea-Glu (EuE)-derivative (**3**) (K_i = 1.5 nM) can be increased by introducing an aromatic tetrazole group (K_i = 0.9 nM). By inserting an aromatic linker, a good affinity can be maintained despite the DOTA ligand (PSMA-617, K_i = 2.3 nM) (**6**) which is not the case for coupling the plain structure of KuE to DOTAA (K_i = 37.8 nM). Another potent molecule with aromatic part and DOTAGA-chelator is the PSMA I&T (**7**).

Squaric acid

3,4-dihydroxycyclobu-3-ene-1,2-dione, also known as quadratic acid or squaric acid (SA) is a multi-purpose tool for different chemical applications [93, 94] with a long history at the Johannes Gutenberg-University, Mainz [95]. SA has various interesting physical and chemical properties. One example is the name, which is derived from an almost square geometry (c.f. Figure 17), proven by X-ray crystallography [96, 97]. In addition, the dianion follows Hückel´s rule for aromatic systems , which explains the high acidity of the protonated compound (pK1 = 0.5-1.2; pK2 = 2.2-3.5) [98].

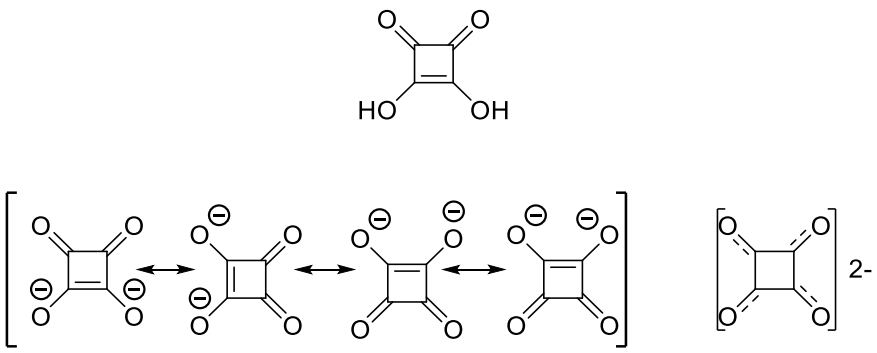

Figure 17: Schematic representation of mesomeric stabilization of the squaric acid dianion explaining the aromaticity.

When applying SA for coupling, the diester is used. It can be formed under harsh conditions via direct reaction of the acid or by converting the SA with thionyl chloride to the corresponding dichloride followed by ester-formation via nucleophilic attack of an alcohol (Figure 18) [99].

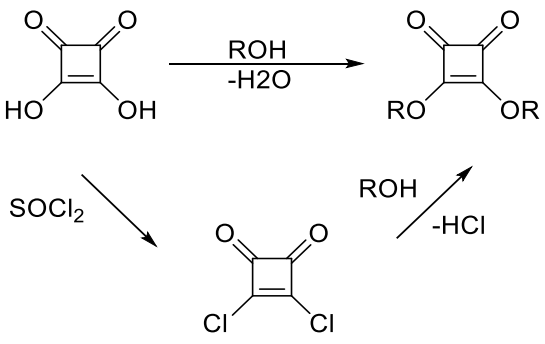

Figure 18: Synthesis pathway for the production of SADM.

Coupling by SA diesters avoids a lot of synthetic problems like challenging protection group chemistry when coupling with other coupling reagents. SA diesters offer the possibility of selectively combining two amines (c.f. Figure 19). This is done by a stepwise, pH-dependent, asymmetric amidation of the diester under mild conditions, both in aqueous buffers and in organic solvents [100]. The stepwise pH-dependent course of the reaction can be explained by a change in the aromaticity of the intermediate stages.

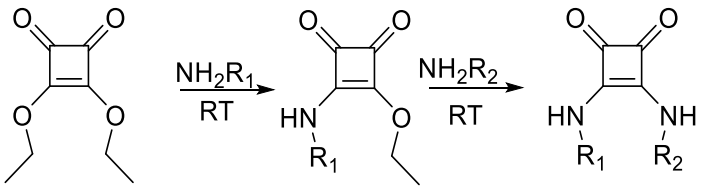

Figure 19: Scheme of the selective reaction of squaric acid diester.

This selectivity results in an enormous advantage of coupling by means of SA esters. In contrast to alkynes and azides for azide-alkyne cycloaddition reactions, amines are present in many biomolecules and do not have to be introduced with synthetic efforts. Amines are also used for coupling with active esters, but the use of SA esters for coupling renders the protection of other nucleophilic groups unnecessary. Another positive property is that the monoamide intermediate is stable and can be isolated. This results in a squaric acid monoester (SAME), which in turn can be connected to amines. However, SAMEs have a much higher stability than e.g. *N*-hydroxy succinimide (NHS) esters. In solution at pH 9, SAME are stable for several days, while NHS esters are affected by hydrolysis already after minutes. Additionally, SADE are used in several fields of organic chemistry for example to couple carbohydrates to proteins [101, 102]. These properties make SA derivatives an interesting alternative for coupling chelators to target vectors. Ideally, a bifunctional chelator with a primary amine is brought to react with a SA diester and transformed into a bench-stable building block. This particularly elegant approach makes protective groups redundant. Subsequently, coupling to an unprotected target vector containing an amine function takes place. After purification, the resulting chelator-target vector conjugate can be

used directly. A further deprotection step, which could possibly be critical for a sensitive target vector, is not necessary.

Interestingly, despite the well-known properties of SA, the application of this strategy in radiopharmaceutical chemistry is rather limited. Only very few examples for usage of SA to connect bioactive molecules to chelators for nuclear imaging are known. However, the ones reported used SA exclusively to link proteins or antibodies to the chelator desferrioxamine (DFO), which has a peptide like structure [103, 104].

When SA is applied for coupling, however, the characteristic structure of SA becomes a feature of the product. This is comparable to triazole formation for the "click" coupling of azides and alkynes. Consequently, the influence of the squaric acid on the pharmacophore and the biological activity of the final compound must be considered. Comparisons were made between the SA structure with phosphate [105], urea [106] and guanidine structures [107] with regard to their impact on biological behavior. The aromatic character of the SA diamide renders the group comparable to imidazole or triazole structures. For the coupling of chelators though, it should be kept in mind that SA has complexing properties itself [108] and may therefore influence the complexation properties of the bound chelator – a feature never considered in the design of radiometal-chelator-based radiopharmaceuticals.

Objectives

The development of novel PSMA inhibitors has been very successful in recent years. In addition to the established PSMA-11 and PSMA-617 derivatives for ^{68}Ga and ^{177}Lu, further derivatives are found in clinical studies that also allow for ^{18}F or ^{99m}Tc labeling. Nevertheless, their synthesis is often very complex and complicated. In addition, the intermediate products can seldomly be stored for longer periodes resulting in high costs for syntheses. Therefore a more simple system would be desirable, which should allow a modular construction with building blocks leading to versatile inhibitors.

This thesis focuses on the synthesis and evaluation of novel PSMA targeting molecules in order to make them accessible for nuclear medicine. It is based in the preliminary work described in the dissertation paper of Nils Engelbogen, Joahnnes Gutenberg-Universität Mainz, 2017. In his work, he was able to show for the first time that typical molecules for PSMA-targeting experience an increase in affinity if they contain a squaric acid moiety. The molecules he examined are shown in Figure 20.

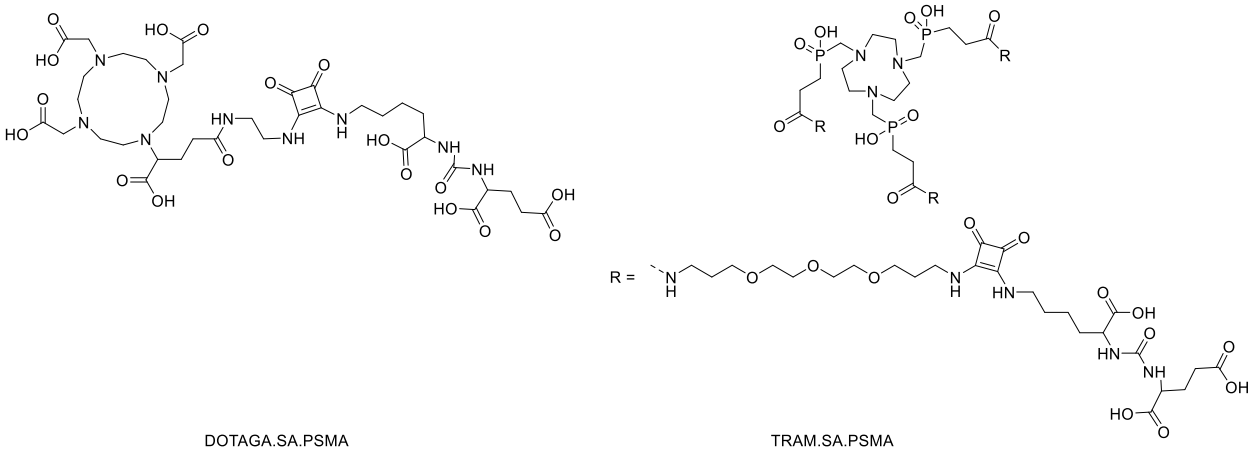

Figure 20: First generation molecules. Both molecules were introduced in the dissertation of Nils Engelbogen.

For the first time, he was able to investigate those two novel molecules *in vivo* and to establish the hypothesis, that they are superior compared to known structures being described in the literature. The results of his work and a comparison with other tracers are summarized in Table 3.

Table 3: Reported comparison between literature known PSMA inhibitors with ^{68}Ga and the two SA.PSMA derivatives from Fig. 20 [109] in term of SUV, %ID/g and animal model. Some values are missing because they are not presented in literature.

compound	SUV	%ID/g	animal-model	compound	SUV	%ID/g	animal-model
[^{68}Ga]Ga.DOTAGA.SA.PSMA	1.2	5.6	NMRI$^{nu/nu}$	[^{68}Ga]Ga-PSMA-11		3.5[110]	BALB/c$^{nu/nu}$
[^{68}Ga]Ga.TRAM.SA.PSMA	1.0		NMRI$^{nu/nu}$	[^{68}Ga]Ga-PSMA-617	0.6	4.1[111]	BALB/c$^{nu/nu}$
				[^{68}Ga]Ga-PSMA-I&T		4,9[112]	CD-1$^{nu/nu}$

Even if these data may indicate a superiority of the new tracers, they are hardly meaningful since different animal models. Furthermore, information on actual values of the established tracers are hard to obtain because they are not presented in literature. Therefore, the first two aims of this work were: (1) Synthesis, purification and labeling of the already known products, mainly focussing on DOTAGA.SA.PSMA. (2) Generation of *in vivo* data of the new tracers and comparison to literature known tracers (PSMA-11 and PSMA-617) within the same experiment series and in the same animal models to ensure superiority.

A third (3) aim was to synthesize a derivative with a different overall charge than the already known ones (NODAGA.SA.PSMA) in order to investigate its possible influence. It is known that PSMA binding pockets at the direct binding location prefer negative charges. However, it is not known yet how the charge in the ligand area affects the binding. Therefore NODAGA.SA.PSMA was chosen because its structure is very similar to that of DOTAGA.SA.PSMA. With its ^{68}Ga label it is considered to have an overall neutral charge whereas the DOTAGA derivative is charged negatively.

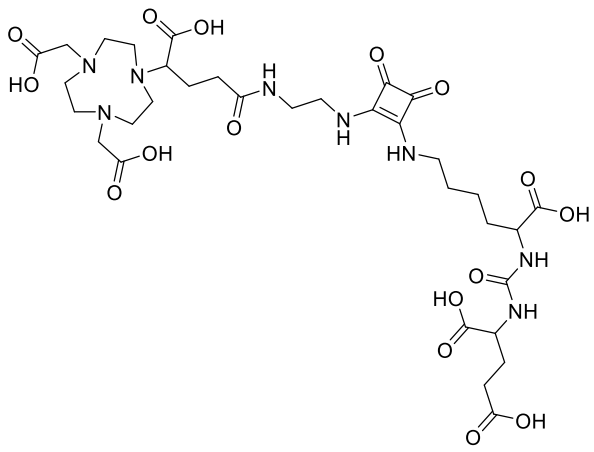

Figure 21: The synthesized compound NODAGA.SA.PSMA as a tool for investigation of the influence of charge on enrichment on the target on binding affinity.

After detailed studies on DOTAGA.SA.PSMA, NODAGA.SA.PSMA and TRAM.SA.PSMA, as a fourth task (4), several new systems were synthesized which will make the unit SA.PSMA available for other ligands or nuclides. Here, the hybrid chelators DATA and AAZTA should be used first, as these have promising properties and the system itself is already well established. For a suitable connection to the SA.PSMA unit, the functional group of the chelator´s side chain must be first exchanged from a typical carboxyl moiety to a primary amine.

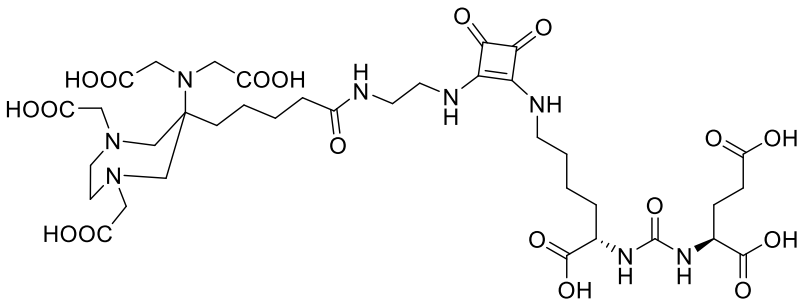

Figure 22: Structure of AAZTA.SA.PSMA

The last part (5) of this work is the first labeling of hybrid type chelators AAZTA and DATA with ^{64}Cu. Labeling of AAZTA with stabel copper is already known [113], but there have been no studies on radioactive labeling so far. In this work, this was performed utilizing DATA^{5m}OMe and AAZTA^{5}OMe. Furthermore, the corresponding SA.PSMA derivatives of DATA^{5m} and AAZTA^{5} were investigated not only for labeling with ^{64}Cu but also with ^{44}Sc, ^{64}Ga and ^{177}Lu especially focusing on the versatile character of AAZTA.SA.PSMA.

References

1. Shao Y, Cherry SR, Farahani K, Meadors K, Siegel S, Silverman RW, Marsden PK. Simultaneous PET and MR imaging. Phys Med Biol. 1997;42:1965–70.
2. James ML, Gambhir SS. A molecular imaging primer: modalities, imaging agents, and applications. Physiol Rev. 2012;92:897–965.
3. Dirac PAM. The Quantum Theory of the Electron. Proceedings of the Royal Society A: Mathematical, Physical and Engineering Sciences. 1928;117:610–24.
4. Anderson CD. The Positive Electron. Phys. Rev. 1933;43:491–4.
5. Lieser KH. Einführung in die Kernchemie. 3rd ed. Weinheim: VCH; 1991.
6. Rösch F. Nuclear- and Radiochemistry: Volume 1: Introduction. Berlin, Boston: De Gruyter; 2014.
7. Vallery RS, Zitzewitz PW, Gidley DW. Resolution of the orthopositronium-lifetime puzzle. Phys Rev Lett. 2003;90:203402.
8. Ache HJ. Chemie des Positrons und Positroniums. Angew. Chem. 1972;84:234–55.
9. Lewellen TK. Recent developments in PET detector technology. Phys Med Biol. 2008;53:R287-317.
10. Saha PGB, Saha GB. Basics of PET Imaging: Physics, Chemistry, and Regulations. 3rd ed. Cham: Springer International Publishing; 2015.
11. Humm JL, Rosenfeld A, Del Guerra A. From PET detectors to PET scanners. Eur J Nucl Med Mol Imaging. 2003;30:1574–97.
12. Hevesy G. The Absorption and Translocation of Lead by Plants: A Contribution to the Application of the Method of Radioactive Indicators in the Investigation of the Change of Substance in Plants. Biochem J. 1923;17:439–45.
13. Alauddin MM. Positron emission tomography (PET) imaging with 18F-based radiotracers. Am J Nucl Med Mol Imaging. 2011;2:55–76.
14. Tredwell M, Gouverneur V. ^{18}F-Markierung von Arenen. Angew. Chem. 2012;124:11590–602.
15. Deng X, Rong J, Wang L, Vasdev N, Zhang L, Josephson L, Liang S. Chemistry for Positron Emission Tomography: Recent Advances in ^{11}C-, ^{18}F-, ^{13}N- and ^{15}O-labeling Reactions. Angew Chem Int Ed Engl 2018.
16. Holleman AF, Wiberg E, Wiberg N. Lehrbuch der anorganischen Chemie. 102nd ed. Berlin: De Gruyter; 2007.
17. Schwarzenbach G. Der Chelateffekt. Helv. Chim. Acta. 1952;35:2344–59.
18. Aime S, Botta M, Fasano M, Marques MPM, Geraldes CFGC, Pubanz D, Merbach AE. Conformational and Coordination Equilibria on DOTA Complexes of Lanthanide Metal Ions in Aqueous Solution Studied by 1 H-NMR Spectroscopy. Inorg. Chem. 1997;36:2059–68.
19. Spang P, Herrmann C, Roesch F. Bifunctional Gallium-68 Chelators: Past, Present, and Future. Semin Nucl Med. 2016;46:373–94.

20. Estorch M. Tratamiento con 177Lu-DOTATATE: pasado, presente y futuro. Rev Esp Med Nucl Imagen Mol. 2017;36:69–71.
21. Wadas TJ, Wong EH, Weisman GR, Anderson CJ. Coordinating Radiometals of Copper, Gallium, Indium, Yttrium and Zirconium for PET and SPECT Imaging of Disease. Chem Rev. 2010;110:2858–902.
22. Notni J, Pohle K, Wester H-J. Comparative gallium-68 labeling of TRAP-, NOTA-, and DOTA-peptides: practical consequences for the future of gallium-68-PET. EJNMMI Res. 2012;2:28.
23. Notni J, Šimeček J, Hermann P, Wester H-J. TRAP, a powerful and versatile framework for gallium-68 radiopharmaceuticals. Chemistry. 2011;17:14718–22.
24. Maecke HR, Riesen A, Ritter W. The molecular structure of indium-DTPA. J Nucl Med. 1989;30:1235–9.
25. Price EW, Orvig C. Matching chelators to radiometals for radiopharmaceuticals. Chem Soc Rev. 2014;43:260–90.
26. Kobayashi H, Wu C, Yoo TM, Sun BF, Drumm D, Pastan I, et al. Evaluation of the in vivo biodistribution of yttrium-labeled isomers of CHX-DTPA-conjugated monoclonal antibodies. J Nucl Med. 1998;39:829–36.
27. Ackova DG, Smilkov K, Janevik-Ivanovska E. Physicochemical evaluation of Lyophilized Formulation of p-SCN-Bn-DOTA- and p-SCN-Bn-DTPA-rituximab for NHL Radio Immunotherapy. Iran J Pharm Res. 2016;15:295–302.
28. Schuhmacher J, Klivényi G, Hull WE, Matys R, Hauser H, Kalthoff H, et al. A bifunctional HBED-derivative for labeling of antibodies with ^{67}Ga, ^{111}In and ^{59}Fe. Comparative biodistribution with ^{111}In-DPTA and ^{131}I-labeled antibodies in mice bearing antibody internalizing and non-internalizing tumors. International Journal of Radiation Applications and Instrumentation. Part B. Nuclear Medicine and Biology. 1992;19:809–24.
29. Boros E, Ferreira CL, Cawthray JF, Price EW, Patrick BO, Wester DW, et al. Acyclic chelate with ideal properties for (68)Ga PET imaging agent elaboration. J Am Chem Soc. 2010;132:15726–33.
30. Berry DJ, Ma Y, Ballinger JR, Tavaré R, Koers A, Sunassee K, et al. Efficient bifunctional gallium-68 chelators for positron emission tomography: tris(hydroxypyridinone) ligands. Chem Commun (Camb). 2011;47:7068–70.
31. Tsionou MI, Knapp CE, Foley CA, Munteanu CR, Cakebread A, Imberti C, et al. Comparison of macrocyclic and acyclic chelators for gallium-68 radiolabelling. RSC Adv. 2017;7:49586–99.
32. Seemann J, Waldron BP, Roesch F, Parker D. Approaching 'Kit-Type' Labelling with ^{68}Ga: The DATA Chelators. ChemMedChem. 2015;10:1019–26.
33. Waldron BP, Parker D, Burchardt C, Yufit DS, Zimny M, Roesch F. Structure and stability of hexadentate complexes of ligands based on AAZTA for efficient PET labelling with gallium-68. Chem Commun (Camb). 2013;49:579–81.

34. Aime S, Calabi L, Cavallotti C, Gianolio E, Giovenzana GB, Losi P, et al. Gd-AAZTA-: a new structural entry for an improved generation of MRI contrast agents. Inorg. Chem. 2004;43:7588–90.
35. Seemann J, Waldron B, Parker D, Roesch F. DATATOC: a novel conjugate for kit-type ^{68}Ga labelling of TOC at ambient temperature. EJNMMI Radiopharm Chem 2016.
36. Farkas E, Nagel J, Waldron BP, Parker D, Tóth I, Brücher E, et al. Equilibrium, Kinetic and Structural Properties of Gallium(III) and Some Divalent Metal Complexes Formed with the New DATAm and DATA5m Ligands. Chemistry. 2017;23:10358–71.
37. Nagy G, Szikra D, Trencsényi G, Fekete A, Garai I, Giani AM, et al. AAZTA: An Ideal Chelating Agent for the Development of ^{44} Sc PET Imaging Agents. Angew Chem Int Ed Engl. 2017;56:2118–22.
38. Knorr R, Trzeciak A, Bannwarth W, Gillessen D. New coupling reagents in peptide chemistry. Tetrahedron Letters. 1989;30:1927–30.
39. Montalbetti CAGN, Falque V. Amide bond formation and peptide coupling. Tetrahedron. 2005;61:10827–52.
40. Kalkhof S, Sinz A. Chances and pitfalls of chemical cross-linking with amine-reactive N-hydroxysuccinimide esters. Anal Bioanal Chem. 2008;392:305–12.
41. World Scientific (Firm). Handbook of nuclear medicine and molecular imaging: Principles and clinical applications. Singapore, Hackensack, N.J: World Scientific Pub. Co; 2012.
42. Wade K, Banister AJ, Bailar JC, Emeléus HJ, Nyholm R. The Chemistry of Aluminium, Gallium, Indium and Thallium: Comprehensive Inorganic Chemistry. 1st ed. s.l.: Elsevier Reference Monographs; 1973.
43. Downs AJ, editor. Chemistry of aluminium, gallium, indium and thallium. 1st ed. London: Blackie Acad. & Professional; 1993.
44. Al-Suqri B, Al-Bulushi N. Gallium-67 Scintigraphy in the Era of Positron Emission Tomography and Computed Tomography: Tertiary centre experience. Sultan Qaboos Univ Med J. 2015;15:e338-43.
45. Greene MW, Tucker WD. An improved gallium-68 cow. ApplRadiatIsot. 1961;12:62–3.
46. Zhernosekov KP, Filosofov DV, Baum RP, Aschoff P, Bihl H, Razbash AA, et al. Processing of generator-produced ^{68}Ga for medical application. J Nucl Med. 2007;48:1741–8.
47. Eppard E, Wuttke M, Nicodemus PL, Rösch F. Ethanol-Based Post-processing of Generator-Derived ^{68}Ga Toward Kit-Type Preparation of ^{68}Ga-Radiopharmaceuticals. J Nucl Med. 2014;55:1023–8.
48. Roesch F. Maturation of a key resource - the germanium-68/gallium-68 generator: development and new insights. Curr Radiopharm. 2012;5:202–11.
49. Duchemin C, Guertin A, Haddad F, Michel N, Métivier V. Production of scandium-44m and scandium-44g with deuterons on calcium-44: cross section measurements and production yield calculations. Phys Med Biol. 2015;60:6847–64.
50. Szkliniarz K, Sitarz M, Walczak R, Jastrzębski J, Bilewicz A, Choiński J, et al. Production of medical Sc radioisotopes with an alpha particle beam. Appl Radiat Isot. 2016;118:182–9.
51. Walczak R, Krajewski S, Szkliniarz K, Sitarz M, Abbas K, Choiński J, et al. Cyclotron production of ^{43}Sc for PET imaging. EJNMMI Phys. 2015;2:33.

52. Greene MW, Hillman M. A scandium generator. J.Appl.Rad.Isotopes. 1967;18:540–1.
53. Pruszyński M, Loktionova NS, Filosofov DV, Rösch F. Post-elution processing of ^{44}Ti/^{44}Sc generator-derived ^{44}Sc for clinical application. J.Appl.Rad.Isotopes.2010;68:1636–41.
54. Roesch F. Scandium-44: benefits of a long-lived PET radionuclide available from the ^{44}Ti/^{44}Sc generator system. Curr Radiopharm. 2012;5:187–201.
55. Filosofov DV, Loktionova NS, Rösch F. A ^{44}Ti/^{44}Sc radionuclide generator for potential application of ^{44}Sc-based PET-radiopharmaceuticals. Radiochimica Acta. 2010;98:152.
56. de la Fuente Joaniquet. Radiolabelling, in vitro and in vivo evaluation of metal-labelled biomolecules for PET imaging: [Dissertation]. Mainz: Johannes-Gutenberg-Universität; 2016.
57. Anderson CJ, Ferdani R. Copper-64 Radiopharmaceuticals for PET Imaging of Cancer: Advances in Preclinical and Clinical Research. Cancer Biother Radiopharm. 2009;24:379–93.
58. Niccoli Asabella A, Cascini GL, Altini C, Paparella D, Notaristefano A, Rubini G. The copper radioisotopes: a systematic review with special interest to ^{64}Cu. Biomed Res Int. 2014;2014:786463.
59. Shokeen M, Anderson CJ. Molecular imaging of cancer with copper-64 radiopharmaceuticals and positron emission tomography (PET). Acc Chem Res. 2009;42:832–41.
60. Wu N, Kang CS, Sin I, Ren S, Liu D, Ruthengael VC, et al. Promising Bifunctional Chelators for Copper 64-PET imaging: Practical ^{64}Cu Radiolabeling and High In Vitro and In Vivo Complex Stability. J Biol Inorg Chem. 2015;21:177–84.
61. Kumar A, Hao G, Liu L, Ramezani S, Hsieh J-T, Öz OK, Sun X. Click-chemistry strategy for labeling antibodies with copper-64 via a cross-bridged tetraazamacrocyclic chelator scaffold. Bioconjug Chem. 2015;26:782–9.
62. Banerjee SR, Pullambhatla M, Foss CA, Nimmagadda S, Ferdani R, Anderson CJ, et al. ^{64}Cu-Labeled Inhibitors of Prostate-Specific Membrane Antigen for PET Imaging of Prostate Cancer. J Med Chem. 2014;57:2657–69.
63. Zeglis BM, Lewis JS. The Bioconjugation and Radiosynthesis of ^{89}Zr-DFO-labeled Antibodies. J Vis Exp 2015.
64. Novak-Hofer I, Schubiger PA. Copper-67 as a therapeutic nuclide for radioimmunotherapy. Eur J Nucl Med Mol Imaging. 2002;29:821–30.
65. Smith NA, Bowers DL, Ehst DA. The production, separation, and use of ^{67}Cu for radioimmunotherapy: a review. Appl Radiat Isot. 2012;70:2377–83.
66. Ahmedova A, Todorov B, Burdzhiev N, Goze C. Copper radiopharmaceuticals for theranostic applications. Eur J Med Chem. 2018;157:1406–25.
67. Vértes A, editor. Handbook of nuclear chemistry. 2nd ed. Dordrecht: Springer; 2011.
68. Conry RR. Copper: Inorganic & Coordination ChemistryBased in part on the article Copper: Inorganic & Coordination Chemistry by Rebecca R. Conry & Kenneth D. Karlin which appeared in the Encyclopedia of Inorganic Chemistry, First Edition. In: King RB, Crabtree RH, Lukehart CM, Atwood DA, Scott RA, editors. Encyclopedia of Inorganic Chemistry. Chichester, UK: John Wiley & Sons, Ltd; 2006. p. 2309.

69. Wadas TJ, Wong EH, Weisman GR, Anderson CJ. Copper chelation chemistry and its role in copper radiopharmaceuticals. Curr Pharm Des. 2007;13:3–16.
70. Nurchi VM, Crisponi G, Crespo-Alonso M, Lachowicz JI, Szewczuk Z, Cooper GJS. Complex formation equilibria of Cu(II) and Zn(II) with triethylenetetramine and its mono- and di-acetyl metabolites. Dalton Trans. 2013;42:6161–70.
71. Cai Z, Anderson CJ. Chelators for copper radionuclides in positron emission tomography radiopharmaceuticals. J Labelled Comp Radiopharm. 2013;57:224–30.
72. Kassis AI, Adelstein SJ. Radiobiologic principles in radionuclide therapy. J Nucl Med. 2005;46 Suppl 1:4S-12S.
73. Zoller F, Eisenhut M, Haberkorn U, Mier W. Endoradiotherapy in cancer treatment--basic concepts and future trends. Eur J Pharmacol. 2009;625:55–62.
74. Audi G, Bersillon O, Blachot J, Wapstra AH. The Nubase evaluation of nuclear and decay properties. Nuclear Physics A. 2003;729:3–128.
75. Pillai MRA, Chakraborty S, Das T, Venkatesh M, Ramamoorthy N. Production logistics of ^{177}Lu for radionuclide therapy. Appl Radiat Isot. 2003;59:109–18.
76. Lebedev NA, Novgorodov AF, Misiak R, Brockmann J, Rösch F. Radiochemical separation of no-carrier-added ^{177}Lu as produced via the ^{176}Yb(n,gamma)^{177}Yb--^{177}Lu process. Appl Radiat Isot. 2000;53:421–5.
77. Torre LA, Bray F, Siegel RL, Ferlay J, Lortet-Tieulent J, Jemal A. Global cancer statistics, 2012. CA Cancer J Clin. 2015;65:87–108.
78. Afshar-Oromieh A, Malcher A, Eder M, Eisenhut M, Linhart HG, Hadaschik BA, et al. PET imaging with a [^{68}Ga]gallium-labelled PSMA ligand for the diagnosis of prostate cancer: biodistribution in humans and first evaluation of tumour lesions. Eur J Nucl Med Mol Imaging. 2013;40:486–95.
79. Davidson PJ, van den Ouden D, Schroeder FH. Radical prostatectomy: prospective assessment of mortality and morbidity. Eur Urol. 1996;29:168–73.
80. DeMarzo AM, Nelson WG, Isaacs WB, Epstein JI. Pathological and molecular aspects of prostate cancer. Lancet. 2003;361:955–64.
81. Pillai MRA, Nanabala R, Joy A, Sasikumar A, Russ Knapp FF. Radiolabeled enzyme inhibitors and binding agents targeting PSMA: Effective theranostic tools for imaging and therapy of prostate cancer. Nucl Med Biol. 2016;43:692–720.
82. Silver DA, Pellicer I, Fair WR, Heston WD, Cordon-Cardo C. Prostate-specific membrane antigen expression in normal and malignant human tissues. Clin Cancer Res. 1997;3:81–5.
83. Perner S, Hofer MD, Kim R, Shah RB, Li H, Möller P, et al. Prostate-specific membrane antigen expression as a predictor of prostate cancer progression. Hum Pathol. 2007;38:696–701.
84. Mosquera J-M, Perner S, Demichelis F, Kim R, Hofer MD, Mertz KD, et al. Morphological features of TMPRSS2-ERG gene fusion prostate cancer. J Pathol. 2007;212:91–101.
85. Elgamal A-AA, Holmes EH, Su SL, Tino WT, Simmons SJ, Peterson M, et al. Prostate-specific membrane antigen (PSMA): Current benefits and future value. Semin. Surg. Oncol. 2000;18:10–6.

86. Bařinka C, Rojas C, Slusher B, Pomper M. Glutamate carboxypeptidase II in diagnosis and treatment of neurologic disorders and prostate cancer. Curr Med Chem. 2012;19:856–70.
87. Wüstemann T, Bauder-Wüst U, Schäfer M, Eder M, Benesova M, Leotta K. Design of Internalizing PSMA-specific Glu-ureido-based Radiotherapeuticals. Theranostics. 2016;6:1085–95.
88. Zhang AX, Murelli RP, Barinka C, Michel J, Cocleaza A, Jorgensen WL. A remote arene-binding site on prostate specific membrane antigen revealed by antibody-recruiting small molecules. J Am Chem Soc. 2010;132:12711–6.
89. Lütje S, Heskamp S, Cornelissen AS, Poeppel TD, van den Broek SAMW, Rosenbaum-Krumme S, et al. PSMA Ligands for Radionuclide Imaging and Therapy of Prostate Cancer: Clinical Status. Theranostics. 2015;5:1388–401.
90. Witkowska-Patena E, Mazurek A, Dziuk M. ^{68}Ga-PSMA PET/CT imaging in recurrent prostate cancer: Where are we now? Cent European J Urol. 2017;70:37–43.
91. Kozikowski AP, Zhang J, Nan F, Petukhov PA, Grajkowska E, Wroblewski JT, et al. Synthesis of urea-based inhibitors as active site probes of glutamate carboxypeptidase II: efficacy as analgesic agents. J Med Chem. 2004;47:1729–38.
92. Eder M, Schäfer M, Bauder-Wüst U, Hull W-E, Wängler C, Mier W, et al. 68 Ga-Complex Lipophilicity and the Targeting Property of a Urea-Based PSMA Inhibitor for PET Imaging. Bioconjugate Chem. 2012;23:688–97.
93. Ian Storer R, Aciro C, Jones LH. Squaramides: physical properties, synthesis and applications. Chem. Soc. Rev. 2011;40:2330.
94. Neuse E, Green B. Amidierung von Quadratsäure-estern. Justus Liebigs Ann. Chem. 1973;1973:619–32.
95. Wurm FR, Klok H-A. Be squared: expanding the horizon of squaric acid-mediated conjugations. Chem. Soc. Rev. 2013;42:8220.
96. Samuelsen EJ, Semmingsen D. Squaric acid, a two-dimensional hydrogen-bonded material with a phase transition. Solid State Communications. 1975;17:217–9.
97. Wang Y, Stucky GD, Williams JM. Is squaric acid square? A combined X-ray and neutron diffraction study of 3,4-dihydroxycyclobut-3-ene-1,2-dione. J. Chem. Soc., Perkin Trans. 2. 1974:35.
98. Wurm FR, Klok H-A. Be squared: expanding the horizon of squaric acid-mediated conjugations. Chem Soc Rev. 2013;42:8220–36.
99. Schmidt AH. Reaktionen von Quadratsäure und Quadratsäure-Derivaten. Synthesis. 1980;1980:961–94.
100. Tietze LF, Arlt M, Beller M, Gl üsenkamp K-H, Jähde E, Rajewsky MF. Anticancer Agents, 15. Squaric Acid Diethyl Ester: A New Coupling Reagent for the Formation of Drug Biopolymer Conjugates. Synthesis of Squaric Acid Ester Amides and Diamides. Chem. Ber. 1991;124:1215–21.
101. G. Davis B. Recent developments in glycoconjugates. J. Chem. Soc., Perkin Trans. 1. 1999:3215.

102. Gamblin DP, Scanlan EM, Davis BG. Glycoprotein synthesis: an update. Chem Rev. 2009;109:131–63.
103. Rudd SE, Roselt P, Cullinane C, Hicks RJ, Donnelly PS. A desferrioxamine B squaramide ester for the incorporation of zirconium-89 into antibodies. Chem. Commun. 2016;52:11889–92.
104. Yoganathan S, Sit CS, Vederas JC. Chemical synthesis and biological evaluation of gallidermin-siderophore conjugates. Org. Biomol. Chem. 2011;9:2133.
105. Sato K, Seio K, Sekine M. Squaryl group as a new mimic of phosphate group in modified oligodeoxynucleotides: synthesis and properties of new oligodeoxynucleotide analogues containing an internucleotidic squaryldiamide linkage. J Am Chem Soc. 2002;124:12715–24.
106. Rostami A, Colin A, Li XY, Chudzinski MG, Lough AJ, Taylor MS. N, N' -Diarylsquaramides: General, High-Yielding Synthesis and Applications in Colorimetric Anion Sensing. J. Org. Chem. 2010;75:3983–92.
107. Lee C-W, Cao H, Ichiyama K, Rana TM. Design and synthesis of a novel peptidomimetic inhibitor of HIV-1 Tat–TAR interactions: Squaryldiamide as a new potential bioisostere of unsubstituted guanidine. Bioorganic & Medicinal Chemistry Letters. 2005;15:4243–6.
108. Gauger J, Manecke G. Kondensationsprodukte der Quadratsäure mit primären und sekundären Aminen, II. Chem. Ber. 1970;103:3553–62.
109. Engelbogen N. Quadratsäurediester als Brücke zwischen Chelatoren und Biomolekülen in der Radiopharmazie: Synthese und Evaluierung von Radiopharmaka zur Diagnose von Leberfibrose sowie zur Diagnose und Therapie von Tumorerkrankungen [Dissertation]. Mainz: Johannes-Gutenberg-Universität; 2017.
110. Eder M, Schäfer M, Bauder-Wüst U, Hull W-E, Wängler C, Mier W. ^{68}Ga-complex lipophilicity and the targeting property of a urea-based PSMA inhibitor for PET imaging. Bioconjug Chem. 2012;23:688–97.
111. Benešová M, Schäfer M, Bauder-Wüst U, Mier W, Haberkorn U, Kopka K, Eder M. Preclinical Evaluation of a Tailor-Made DOTA-Conjugated PSMA Inhibitor with Optimized Linker Moiety for Imaging and Endoradiotherapy of Prostate Cancer. J Nucl Med. 2015;56:914–20.
112. Weineisen M, Schottelius M, Simecek J, Baum RP, Yildiz A, Beykan S, et al. ^{68}Ga- and ^{177}Lu-Labeled PSMA I&T: Optimization of a PSMA-Targeted Theranostic Concept and First Proof-of-Concept Human Studies. J Nucl Med. 2015;56:1169–76.
113. Baranyai Z, Uggeri F, Maiocchi A, Giovenzana GB, Cavallotti C, Takács A, et al. Equilibrium, Kinetic and Structural Studies of AAZTA Complexes with Ga3+, In3+ and Cu2+. Eur. J. Inorg. Chem. 2013;2013:147–62.
114. Sengar RS, Nigam A, Geib SJ, Wiener EC. Syntheses and crystal structures of gadolinium and europium complexes of AAZTA analogues. Polyhedron. 2009;28:1525–31.
115. Tei L, Gugliotta G, Fekete M, Kálmán FK, Botta M. Mn(II) complexes of novel hexadentate AAZTA-like chelators: a solution thermodynamics and relaxometric study. Dalton Trans. 2011;40:2025–32.

116. Vágner A, D'Alessandria C, Gambino G, Schwaiger M, Aime S, Maiocchi A, et al. A rigidified AAZTA-like ligand as efficient chelator for ^{68}Ga radiopharmaceuticals. ChemistrySelect. 2016;1:163–71.
117. Nagy G, Szikra D, Trencsényi G, Fekete A, Garai I, Giani AM, et al. AAZTA: An Ideal Chelating Agent for the Development of ^{44}Sc PET Imaging Agents. Angew. Chem. 2017;129:2150–4.
118. Nock BA, Kaloudi A, Nagel J, Sinnes J-P, Roesch F, Maina T. Novel bifunctional DATA chelator for quick access to site-directed PET ^{68}Ga-radiotracers: preclinical proof-of-principle with Tyr3octreotide. Dalton Trans. 2017;46:14584–90.
119. Bass LA, Wang M, Welch MJ, Anderson CJ. In Vivo Transchelation of Copper-64 from TETA-Octreotide to Superoxide Dismutase in Rat Liver. Bioconjugate Chem. 2000;11:527–32.
120. Moi MK, Meares CF, McCall MJ, Cole WC, DeNardo SJ. Copper chelates as probes of biological systems: Stable copper complexes with a macrocyclic bifunctional chelating agent. Analytical Biochemistry. 1985;148:249–53.
121. McQuade P, Miao Y, Yoo J, Quinn TP, Welch MJ, Lewis JS. Imaging of melanoma using ^{64}Cu- and ^{86}Y-DOTA-ReCCMSH(Arg11), a cyclized peptide analogue of alpha-MSH. J Med Chem. 2005;48:2985–92.
122. Chen X, Hou Y, Tohme M, Park R, Khankaldyyan V, Gonzales-Gomez I, et al. Pegylated Arg-Gly-Asp peptide: ^{64}Cu labeling and PET imaging of brain tumor alphavbeta3-integrin expression. J Nucl Med. 2004;45:1776–83.
123. Anderson CJ, Jones LA, Bass LA, Sherman EL, McCarthy DW, Cutler PD, et al. Radiotherapy, toxicity and dosimetry of copper-64-TETA-octreotide in tumor-bearing rats. J Nucl Med. 1998;39:1944–51.
124. Chen X, Park R, Tohme M, Shahinian AH, Bading JR, Conti PS. MicroPET and autoradiographic imaging of breast cancer alpha v-integrin expression using ^{18}F- and 64Cu-labeled RGD peptide. Bioconjugate Chem. 2004;15:41–9.
125. Chen X, Sievers E, Hou Y, Park R, Tohme M, Bart R, et al. Integrin αvβ3-Targeted Imaging of Lung Cancer1. Neoplasia. 2005;7:271–9.
126. Anderson CJ, Dehdashti F, Cutler PD, Schwarz SW, Laforest R, Bass LA, et al. ^{64}Cu-TETA-octreotide as a PET imaging agent for patients with neuroendocrine tumors. J Nucl Med. 2001;42:213–21.

Manuscripts

Mild and efficient ^{64}Cu labeling of 1,4-diazepine derivatives for potential use with large peptides, proteins and antibodies

Lukas Greifenstein

Institute of Nuclear Chemistry, Johannes Gutenberg University, Mainz, German, Fritz-Straßmann-Weg 2, 55128 Mainz

Submitted to Radiochimica Acta, May 8, 2019

Abstract

DATA (6-Amino-1,4-diazapine-triacetate) and AAZTA (6-Amino-1,4-diazapine-tetracetate) chelators represent a novel approach representing hybrid-chelates: possessing significant cyclic and acyclic character. It is believed that flexibility of the acyclic part facilitates rapid complexation, whilst the preorganized cyclic part minimizes the energy barrier to complexation and inhibits decomplexation processes. So far, these chelators have been used exclusively with ^{44}Sc and ^{68}Ga only. Recent results with ^{nat}Cu predict high stabilities for Cu-AAZTA, yet no radioactive labeling of AAZTA or DATA with ^{64}Cu or any additional radioactive isotope has been reported. We present the one pot synthesis of the bifunctional derivatives AAZTA^{5}OMe and DATA^{5m}OMe and their labeling with ^{64}Cu. In addition, *in vitro* stability of the respective comlexes are presented.

Introduction

In recent years, ^{64}Cu derivatives have been increasingly used for positron emission tomography (PET) [1-4]. This is mainly motivated by its positron emisson branch and its relatively long half-life ($t_{½}$ = 12.7 h). Relatively long in this context means, that it is long enough to visualize processes of distribiution and accumulation of molecules targeting vectos such as peptides as well as antibodies, but also not too long to visualize processes shown by small molecules with a short biological halflive as well [5,6]. The isotope ^{67}Cu decays by emitting a β^--particle and therefore can be used for therapeutic purpose [7,8] combination with ^{64}Cu it appear to be a perfect pair for theranostic use [9]. Despite nuclear parameters, one of the greatest advantages of copper is the coordination chemistry [10]. A large number of chelates coordinating copper is known. Among others, DOTA (1,4,7,10-tetraazacyclododecane-1,4,7,10-tetraacetic acid) or TETA (1,4,8,11-tetraazacylotetradecane-1,4,8,11-tetracetic acid) are the most often used ones (see Figure 1a) [11-13]. In addition, there is also a variety of Sacrophag variants, such as DiamSar or SarAr, which are already used as ligand for ^{64}Cu, all with different advantages and disadvantages [14]. It is noteworthy, that these structures are macrocyclic and therefore may need high temperatures to guarantee fast labeling kinetics.

Over the last years, a new class of chelates has attracted attention having a diazepane as their lead structure. First results were published for a Gd-AAZTA-derivative [15]. Further investigations on this system showed that the flexibility of the lead structure allows a multitude of metals to be complexed under mild conditions [16-19]. For the complexation of gallium, for example, the derivative DATA^m appeared to be ideal [20]. while the AAZTA derivatives appear to be better suited for the complexation of metals such as Lu or Sc [21]. There are no substantial differences for all mentioned derivatives with regard to the labeling conditions. In contrast to DOTA and TETA all labeling can be carried out under very mild conditions, both with regard to temperature and the necessary pH values [22]. However, stabilities of the various radiometal-1,4-diazepane complexes are much different. With regard to copper, there are studies and experiments indicating that diazepane derivatives complex copper quiet well, but so far no results are known with radioactive copper. Baranyai and coworkers showed in 2013 that Cu complexes of AAZTA are stable and they were able to

crystalize a Cu-AAZTA complex [17]. In 2017 Frakas et al. were able to determine stabilities of Cu-DATA complexes and to show that these complexes are more stable than the corresponding Ga complex [20]. Nevertheless both studies do not provide complexation under radiochemical conditions.

Because the above mentioned derivatives do not offer the possibility to enable a bifunctional derivative, special derivatives (e.g. DATA^{5m}, AAZTA^{5}, see Figure 1) were established and have been used in different studies [23]. The derivatives used in this paper still carry a methyl ester on the side chain to enable that carboxylic acid from interfering with coordination chemistry. In the following sections, we describe the formation of ^{64}Cu complexes with DTA^{5m}OMe and AAZTA^{5}OMe under typical conditions.

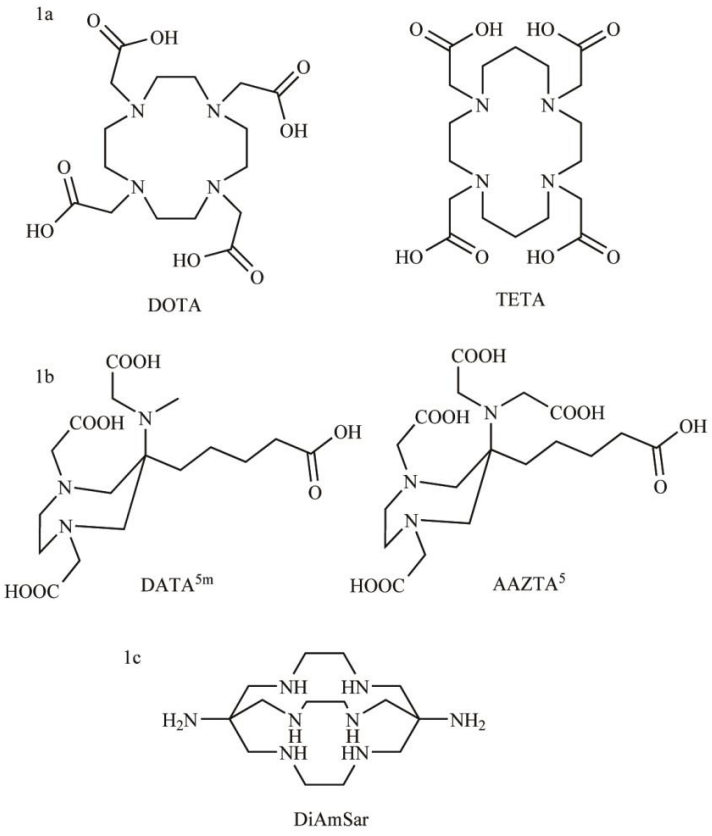

Figure. 1: Typical chelates for copper complexation: DOTA and TETA. It is noteworthy that these structures are macrocyclic and therefore often need high temperatures to guarantee fast labeling kinetics. 1b: Completely deprotected structures of DATA^{5m} and AAZTA^{5}. The hybrid structure of AAZTA and DATA are shown in contrast to DOTA and TETA and therefore more mild conditions can be used for labeling with different metals. The derivatives used in this paper still carry a methyl ester on the side chain to enable that carboxylic acid for functionalization from interfering with coordination chemistry. 1c: One of the typically used Sacophag ligands DiAmSar.

Materials and methods

Synthetic part

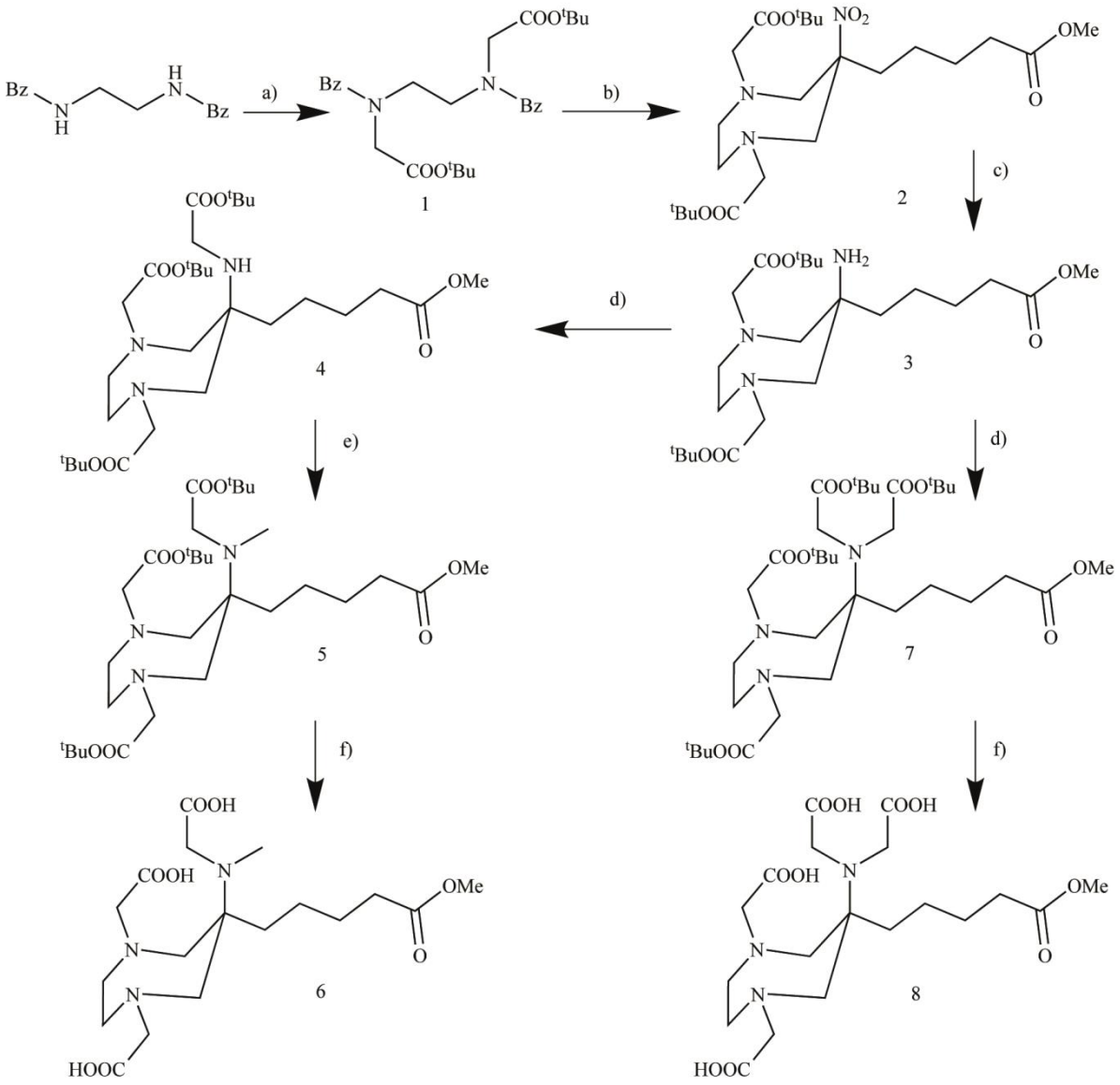

Figure 2: Synthesis of the derivatives DATA^{5m}OMe (**6**) and AAZTA^{5}OMe (**8**): a) *tert*-Butylbromoacetate, Na_2CO_3, MeCN, 81 %; b) i) Pd/C, H_2, formic acid, EtOH; ii) 2-Nitrocycloheanone, Amberlyst® A21, paraformaldehyde, MeOH, 74 %; c) Ni/H_2, EtOH; d) *tert*-Butylbromoacetate, DIPEA, MeCN, 23 % product **4**, 21 % product **7**; e) Formalin, AcOH, $NaBH_4$, MeCN, 87 %; f) TFA/DCM (50:50/ v:v), 32 % product **6**, 45 % product **8**.

In this paper, the DATA^{5m} **6** and AAZTA^5 **8** chelators are synthesized in a slightly different way than already published [20]. Herein a route of synthesizing both molecules in one reaction pathway is established. Molecules **6** and **8** represent the desired products. It is noteworthy, that the carboxylic acid of the sidechain remains unprotected during all experiments. In the first step, N,N´-dibenzylethylenediamine is alkylated with *tert*-butylbromoacetate.

Afterwards the key step, the Nitro-Mannich reaction, was carried out to yield the diazepane derivative **2**. After the reduction with Raney-nickel and hydrogen, derivative **3** was further alkylated with *tert*-butylbromoacetate to yield **4** and **7**. Those derivatives are isolated by column chromatography. Derivative **4** was alkylated with formaline and $NaBH_4$ to yield **5**. Both **7**and **5** are deprotected with TFA in DCM to yield **6** or **8**. After precipitation, the crude product was purified by means of HPLC.

Radiolabeling

[^{64}Cu]$CuCl_2$ was purchased from Universitätsklinikum Tübingen and was supplied in 20-50 µL of 0.1 M HCl solution with 200-350 MBq activity. This solution was diluted with 0.1 M HCl to a total concentration of 2 MBq/µL. The solution of $^{64}CuCl_2$ was added to different concentrations of **6** and **8** in 300 µL of NH_4OAc buffer (0.2 M, pH = 5.5). Shaking for 30 min at 25 °C afford the ^{64}Cu complexes. Radiochemical yield and purity were determined by radio-thin layer chromatography (TLC) using Merck Silica F254 TLC plates as the stationary phase and either citric acid buffer (0.1 M, pH 4.0) or NH_4Ac/MeOH 9:1 (v/v) the mobile phase. Radio-TLC analysis was carried out using a CR-35 Bio Test-Imager from Raytest and the software AIDA (Raytest).

[^{64}Cu]Cu-**6** and [^{64}Cu]Cu-**8** were evaluated regarding their *in vitro* stability in human serum (HS) as well as phosphate buffered saline (PBS, pH 7.4).

Results

Radiolabeling of DATA^{5m}OMe

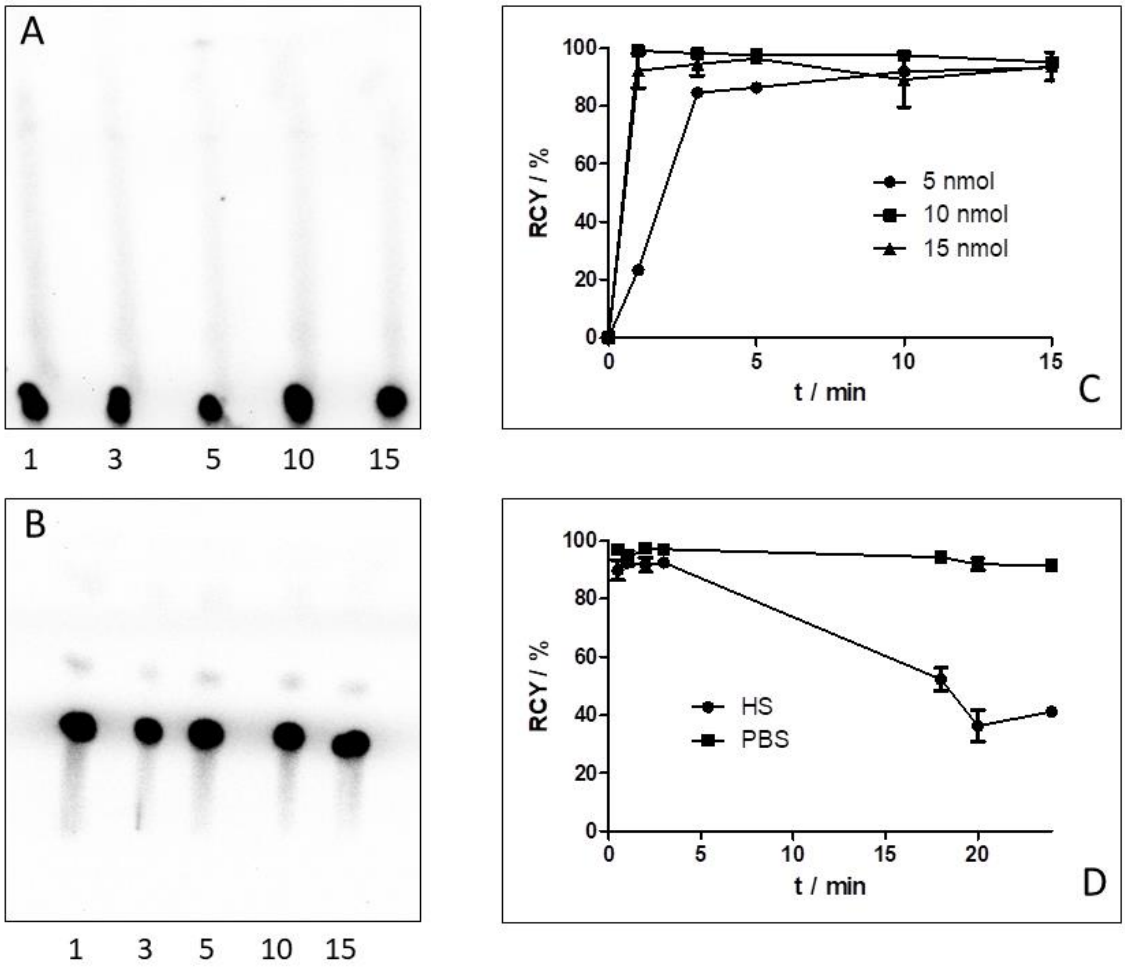

Figure. 3: Radiolabeling and stability of [^{64}Cu]Cu-DATA^{5m}OMe in NaOAc (0.2 M, pH 5.5) at ambient temperature with 35 MBq ^{64}Cu: **A**: Radio-TLC using citricacid buffer (0.1 M, pH 4.0) as mobile phase. More than 95% of the activity at all time points has an R_f = 0.0. Free, uncomplexed ^{64}Cu has an R_f = 0.9 under same conditions. **B**: The complimentary TLC with NH_4Ac/MeOH 9:1 (v/v) as mobile phase. More than 95% of the activity has an R_f of 0.5. Free activity has an R_f of 0.0 under the same conditions. Both TLC systems provide comparable radiochemical yields. **C**: Radiolabeling kinetics of [^{64}Cu]Cu-DATA^{5m}OMe with ^{64}Cu in NaOAc (0.2 M, pH 5.5) using 5, 10 and 15 nmol precursor at 25 °C (n=1, n=1, n=3), respectively. The image represent the yields calcualted from TLC **A** (10 nmol) but correspond well with the results from TLC **B D**: [^{64}Cu]Cu-DATA^{5m}OMe in PBS (pH = 7.4) and human serum at 37 °C over 24 h (n = 3).

Radiolabeling of DATA^{5m}OMe with [^{64}Cu]$CuCl_2$ provided radiochemical yields (RCY) of >98 % within 5 min with precursor amounts of ≥10 nmol (see Figure 3 C). Even precursor amounts of 5 nmol yield in more than 70 % labeling yield after 5 min. This could be determined by TLC in a 0.1 M citrate buffer (pH = 4.0) (Figure 3A) as well as in a solvent mixture of ammonium acetate and methanol 9:1 (Figure 3B). For the citrate buffer, the ^{64}Cu-complex has an R_f value

of 0.0, whereas free copper has an R_f value of 1.0. Inverse is the case for the mobile phase of ammonium acetate/methanol, where the ^{64}Cu-complex has an R_f value of 0.5 and the free copper has an R_f value of 0.0. RCY derived from both TLC methods and results are identical for both systems.

[^{64}Cu]Cu-DATA^{5m}OMe was evaluated regarding its *in vitro* stability in human serum as well as in phosphate buffered saline (PBS, pH 7.4) as injection solvent. The complex showed a stability of >85 % in PBS over 24 h, which corresponds to about 2 half-lives of ^{64}Cu. For the same periode stabilities detected in HS were 40%. This could be due to the presence of superoxide dismutase (SOD) in human serum, which could be explained by a potential transchelation by superoxide dismutase. This effect was already proven in *in vivo* experiments by Baas et al. for a [^{64}Cu]-TETA-octreotide species in Sprague-Dawley rats. It was shown that 70 % of the activity of [^{64}Cu]-TETA-OC were transchelated by the SOD [24]. Nevertheless, it is noteworthy that over 3 hours the stability in HS remained at 85 %.

Radiolabeling of AAZTA^{5}OMe

Labeling studies for AAZTA^{5}OMe were performed under the same conditions previously described. With regard to this derivative, hardly any differences in labeling behavior or stability could be detected. Radiolabeling of AAZTA^{5}OMe with [^{64}Cu]$CuCl_2$ provided radiochemical yields of >95 % within 5 min with precursor amounts of ≥10 nmol (see Figure 3 C). However, labeling with lower amounts of precursor resulted in lower yields compared to the DATA^{5m}OMe derivative. TLC data can be interpreted in analogy to the DATA^{5m}OMe - derivative identifying more than 99% of the activity as product (Fig. 4 A and B). [^{64}Cu]Cu-AAZTA^{5}OMe was evaluated towards its *in vitro* stability in human serum and phosphate buffered saline (PBS, pH 7.4) yielding comparable stabilities in both media. The only visible difference is the slightly lower stability in HS with values between 50 and 60 % after 24 h. This low stability may be caused by the SOD activity again.

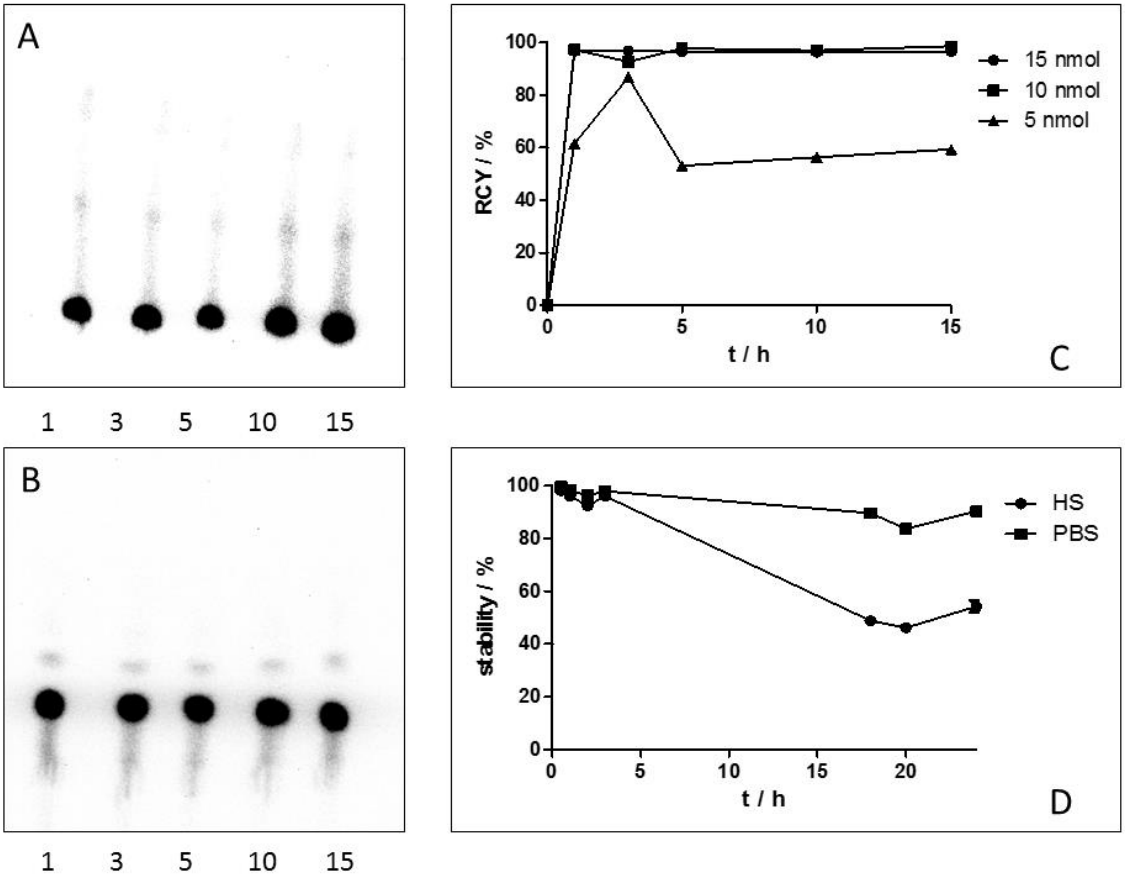

Figure 4: Radiolabeling and stability of [^{64}Cu]Cu-AAZTA^{5}OMe in NaOAc (0.2 M, pH 5.5) at ambient temperature with 35 MBq ^{64}Cu: **A**: Radio-TLC using citric acid-buffer (0.1 M, pH 4.0) as mobile phase. More than 95% of the activity at all time points has an R_f = 0.0. Free, uncomplexed Cu has an R_f = 0.9 under same conditions. **B**: The complimentary TLC with NH_4Ac/MeOH 9:1 (v/v) as mobile phase. More than 95% of the activity has an R_f of 0.5. Free activity has an R_f of 0.0 under the same conditions. Both TLC systems provide comparable radiochemical yields. **C**: Radiolabeling kinetics of [^{64}Cu]Cu-AAZTA^{5}OMe in NaOAc (0.2 M, pH 5.5) using 5, 10 and 15 nmol precursor at 25 °C (n=1, n=1, n=3), respectively. The image represent the yields of the TLC **A** (10 nmol) but correspond well with the results from TLC B **D**: [^{64}Cu]Cu-AAZTA^{5}OMe in PBS (pH = 7.4) and human serum at 37 °C over 24 h (n = 3). Yields were calculated from TLC **A**.

Discussion

The two new hybrid chelators AAZTA^{5}OMe and DATA^{5m}OMe were successfully evaluated regarding their labeling properties with ^{64}Cu and the stability of [^{64}Cu]Cu-**6** and [^{64}Cu]Cu-**8** in HS and PBS buffer. Concerning labelling yields, [^{64}Cu]Cu-DATA^{5m}OMe is slightly superior to [^{64}Cu]Cu-AAZTZA^{5}OMe as it provides a higher yield at 5 nmol. In total, however, both derivatives are similar as they quantitatively label both at low amounts of 10 and 15 nmol at 25°C within less than 3 minutes.

A comparison of the stability of both derivatives shows that both derivatives have acceptable stability over 24 hours in PBS buffer. The DATA derivative is slightly more stable compared to the AAZTA. If the stability in HS is considered, both derivatives show very good stability over the period up to 4 hours. At this point the DATA derivative has a stability of 93% and the AAZTA derivative a stability of 96%, which makes [^{64}Cu]Cu-**8** a slightly more stable complex for ^{64}Cu. This trend continues over a period of 24 hours. Here, the DATA derivative shows a stability of 41% and the AAZTA derivative a stability of 54% ,both indicat the appearance of a new copper species (Figure 5).

A comparison of ^{64}Cu chelate complexes with the complexes used in the literature appears difficult, since the results on the various ligands used are quite contradictory. In general, it can be said that DTPA, EDTA and their derivatives are comparable in terms of stability in HS. Stabilities of 4 to 35 % after 3 days were measured for various DTPA and EDTA derivatives [25]. Overall, ^{64}Cu-DOTA labelled compounds are more unstable than ^{64}Cu-TETA complexes and must be labelled at higher temperatures. TETA, on the other hand, can usually be labelled at room temperature and shows very good *in vitro* stability, with levels of 95% after 2 d in HS [26, 27]. In some cases it is also reported that the labeling of DOTA and TETA is not complete and subsequent purification of the labeled substance using a cartridge is necessary [27-31]. This was neither observed for DATA nor for AAZTA. The complex formation was always quantitative, so no separation was necessary. Furthermore, for ^{64}Cu-DOTA complexes it is reported that temperatures higher than 25°C up to 60°C may be essential and reaction times of more than 10 minutes are not sufficient [27,29,30]. Neither DATA nor AAZTA derivative showed this behaviour. Both derivatives showed a fast kinetics even at 25 °C. Overall, DATA^{5m}OMe and AAZTA^{5}OMe allow for a fast, quantitative and robust labeling with ^{64}Cu and facilitate radiolabeling compared to establish Cu-complexes. Additionally, both

diazepin ligands can be labeled with other nuclides in an easy fashion, for example DATA^{5m} with ^{68}Ga [22]. Stabilities for both complexes were good in PBS buffer over two half-lives of ^{64}Cu. However stabilities in HS were moderate with 40% respectively 50% after 24h. Due to an active transport of copper *in vivo* carried out by SOD. As this behavior also applies to the majority of all other common ligands, none of the two ligands seems less suitable than most of the established ones [11].

Overall, it has been shown that both DATA^{5m} and AAZTA^{5} are suitable chelators for labeling with ^{64}Cu and offer excellent labeling kinetics and yields in combination with mild conditions.

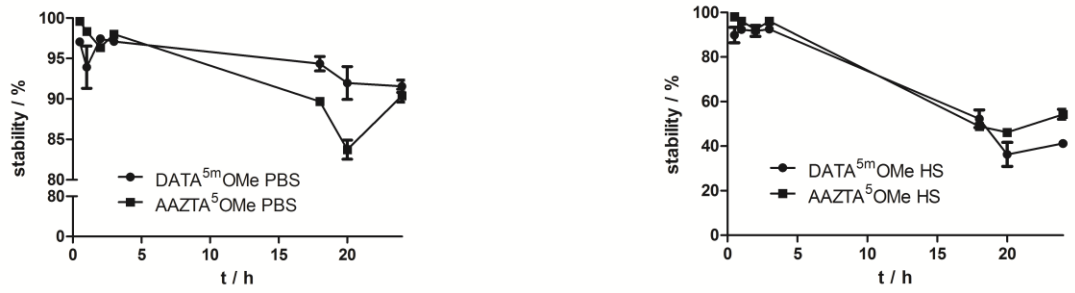

Figure 5: Comparison of the stability of [^{64}Cu]Cu-DATA^{5m}OMe and [^{64}Cu]Cu-AAZTA^{5}OMe. A: in PBS, pH =7, 37°C, B: in HS, 37°C.

Conclusion

DATA^{5m}OMe and AAZTA^{5}OMe can complex copper very well. This complexation can also be carried out at room temperature and the quantities of chelate can be kept very low. Mild pH conditions can be used, allowing the use of peptides and antibodies. Nevertheless, both complexes are only moderate stable in the presence of HS.

Experimental

Chemicals and instrumentation

All chemicals were commercially available at Acros Organics (Nidderau, Germany), Merck (Darmstadt, Germany), Sigma Aldrich (Steinheim, Germany) or VWR (Darmstadt, Germany) and were used without further purification. Deuterated solvents for NMR spectroscopy were purchased from Deutero (Kastellaun, Germany). Silica gel (particle size: 0.040 – 0.063 mm) for column chromatography was purchased from VWR (Darmstadt, Germany). The measurements of ^{1}H- and ^{13}C-NMR spectra were performed on a Bruker Avance II 400 (400 MHz). Mass spectra were recorded on an Agilent Technologies 6130B Single Quadrupole LC/MS system. Semipreparative HPLC was performed on a Merck Hitachi LaChrom L-7100. Following column was used: Phenomenex Luna C18 (250 x 10 mm) 10 µm.

Synthesis of AATZA^{5}OMe and DATA^{5m}Ome

Synthesis of N,N'-dibenzyl-N,N'-di-(*tert*-butylacetate)-ethylenediamine (1):

A mixture of N,N'-dibenzylethylenediamine (3.00 g, 12.48 mmol, 1 eq) and Na_2CO_3 in dry acetonitrile (50 mL) was stirred at room temperature for 30 min. A solution of *tert*-butylbromoacetate (4.64 g, 3.52 mL, 23.78 mmol, 1.9 eq) in dry acetonitrile (10 mL) was added dropwise over 30 min. Then the mixture was heated under reflux for 16 h. The suspension was filtrated and the filtrate was concentrated under reduced pressure. The crude product was purified by recrystallization (H/EA; 6:1) and product **1** was obtained as colorless solid (4.75 g, 10.14 mmol, 81 %).

^{1}H-NMR (400 MHz, $CDCl_3$): δ (ppm) = 7.36 – 7.22 (m, 10H), 3.80 (s, 4H), 3.28 (s, 4H), 2.83 (s, 4H), 1.46 (s, 18H).^{13}C-NMR (100 MHz, $CDCl_3$): δ (ppm) = 171.0, 139.2, 129.1, 128.3, 127.1, 80.9, 58.4, 55.3, 28.3. MS (ESI^+): m/z (%): calculated for $C_{28}H_{40}N_2O_4$: 468.30 $[M]^+$, found: 469.3 $[M+H]^+$.

Synthesis of 1,4-di(tert-butylacetate)-6-methylpentanoate-6-nitroperhydro-1,4-diazepane (2):

1 (3.28 g, 7.00 mmol, 1 eq) was dissolved in ethanol (20 mL) and formic acid (528 µL, 14.00 mmol, 2 eq). Palladium on activated charcoal (10 %, 0.53 g, 16 wt%) was added and the solution was stirred under H_2 at room temperature for 16 h. The mixture was filtered through celite and the solvent was evaporated under vacuum. The crude product (1.99 g, 6.93 mmol, 99 %) was used without further purification. MS (ESI^+): m/z (%): calculated for $C_{14}H_{28}N_2O_4$: 288.20 $[M]^+$, found: 289.2 $[M+H]^+$.

A mixture of 2-nitrocyclohexanone (1.00 g, 6.99 mmol, 1 eq) and Amberlyst A21 (2.00 g, 2 mass-eq) in dry methanol (30 mL) was heated under reflux for 1 h. Then **2a** (1.99 g, 6.93 mmol, 1 eq) and paraformaldehyde (0.76 g, 25.31 mmol, 3.6 eq) were added and the suspension was heated 24 h under reflux. The suspension was filtrated and the filtrate was concentrated under reduced pressure. Purification by column chromatography (H/EA; 2:1; R_f = 0.50) afforded product **2** as yellow oil (2.50 g, 5.13 mmol, 74 %).

^{1}H-NMR (400 MHz, $CDCl_3$): δ (ppm) = 3.66 (s, 3H), 3.62 (d, *J* = 14.6 Hz, 2H), 3.47 (d, *J* = 17.3 Hz, 2H), 3.32 (d, *J* = 17.3 Hz, 2H), 3.14 (d, *J* = 14.6 Hz, 2H), 2.86 (m, 4H), 2.29 (t, 2H), 1.85 (m, 2H), 1.59 (m, 2H), 1.48 (s, 18H), 1.20 (m, 2H). ^{13}C-NMR (100 MHz, $CDCl_3$): δ (ppm) = 173.7, 170.9, 95.1, 81.3, 61.6, 61.2, 56.9, 51.7, 37.3, 33.7, 28.4, 24.8, 23.0. MS (ESI^+): m/z (%): calculated for $C_{23}H_{41}N_3O_8$: 487.29 $[M]^+$, found: 488.3 $[M+H]^+$.

Synthesis of 1,4-Di(tert-Butylacetat)-6-methylpentanoat-6-aminoperhydro-1,4-diazepan (3):

2 (1.60 g, 3.28 mmol, 1 eq) was dissolved in ethanol. Raney nickel (washed 5 times with ethanol) was added to the solution and the mixture was stirred under H_2 at 40 °C for 24 h. After completion the mixture was filtered through Celite and the filtrate was concentrated under vacuum. The crude product **3** was obtained as greenish-blue oil (1.50 g, 3.28 mmol, 100 %) and was used without further purification.

MS (ESI^+): m/z (%): calculated for $C_{23}H_{43}N_3O_6$: 457.32 $[M]^+$, found: 458.3 $[M+H]^+$.

Synthesis of 1,4-di(tert-butylacetate)-6-methylpentanoate-6-amino-tert-butylacetate-perhydro-1,4-diazepane (4):

A solution of **3** (1540 mg, 3.36 mmol, 1 eq) and DIPEA (430 mg, 580 µL, 3.36 mmol, 1 eq.) in dry acetonitrile (15 mL) was stirred under argon at room temperature for 30 min. *Tert*-butylbromoacetate (980 mg, 740 µL, 5.04 mmol, 1.5 eq) was added dropwise to the solution. The solution was stirred under argon at room temperature for 72 h. The solvent was evaporated under reduced pressure and the residue, which contained **4** and **7**, was purified via column chromatography. The monoalkylated product **4** was separated from the dialkylated product **7** by first eluting **7** (H/EA; 5:1; R_f = 0.20) and then eluting **4** (H/EA; 1:1; TLC: H/EA; 3:1; R_f = 0.14). **4** was obtained as yellowish oil (392 mg, 0.7 mmol, 23 %).

^{1}H-NMR (CDCl3, 400 MHz, δ [ppm]): 3.64 (s, 3 H); 3.28 (s, 4 H); 3.21 (s, 2 H); 2.77 (m, 4 H); 2.67 (m, 4 H); 2.30 (t, 3 H); 1.59(m, 2 H); 1.45 (s, 9 H); 1.44 (s, 18 H); 1.28 (m, 4 H); 13C-NMR

(CDCl3, 100 MHz, δ [ppm]): 174.25 (s), 171.97 (s), 171.09 (s), 81.05 (s), 80.96 (s), 63.58 (s), 62.12 (s), 58.10 (s), 57.46 (s), 51.58 (s), 44.78 (s), 35.34 (s), 34.18 (s), 28.36 (s), 28.27 (s), 25.86 (s), 22.73 (s) MS (ESI^+): m/z (%): calculated for $C_{29}H_{53}N_3O_8$: 571.38 $[M]^+$, found: 572.4 $[M+H]^+$.

Synthesis of 1,4-di(tert-butylacetate)-6-methylpentanoate-6-(amino(methyl)-tert-butylacetate)-perhydro-1,4-diazepane (5):

(34.1 mg, 0.06 mmol, 1 eq) was dissolved in dry acetonitrile. Formalin solution (17.9 mg, 16.4 µL, 0.60 mmol, 10 eq) and acetic acid (10.7 mg, 10.2 µL, 0.18 mmol, 3 eq) were added and the solution was stirred at room temperature for 15 min. $NaBH_4$ (6.8 mg, 0.18 mmol, 3 eq) was added in portions and the mixture was stirred at room temperature for 2 h. After completion the solution was quenched with water and extracted with chloroform (3 x 5 mL). The combined organic layers were dried over sodium sulfate and filtrated. The filtrate was concentrated under reduced pressure to give product **5** as yellowish oil (30.4 mg, 0.05 mmol, 87 %).

^{1}H-NMR (CDCl3, 400 MHz, δ [ppm]):3.64 (s, 3 H); 3.46 (s, 2 H); 3.25 (m, 4 H); 2.94 (d, 2 H); 2.84-2.65 (m, 6 H); 2.31 (t, 2 H); 1.57 (m, 4 H); 1.45 (s, 18 H); 1.44 (s, 9 H); 1.35 (s, 2 H); 13C-NMR (CDCl3, 100 MHz, δ [ppm]): 174.23 (s), 172.17 (s), 170.72 (s), 80.90 (s), 80.35 (s), 77.34 (s), 62.52 (s), 62.34 (s), 58.80 (s), 53.99 (s), 51.42 (s), 37.34 (s), 36.61 (s), 34.09 (s), 28.22 (s), 28.12 (s), 25.73 (s), 21.91 (s) MS (ESI^+): m/z (%): calculated for $C_{30}H_{55}N_3O_8$: 585.40 $[M]^+$, found: 586.4 $[M+H]^+$.

Synthesis of 1,4-diacetate-6-methylpentanoate-6-(amino(methyl)-acetate)-perhydro-1,4-diazepane (6):

5 (19.8 mg, 0.03 mmol) was dissolved in dichloromethane (500 µL) and trifluoroacetic acid (500 µL) was added. The mixture was stirred at room temperature for 3 h. After completion dichloromethane and trifluoroacetic acid were evaporated under reduced pressure and the crude product was purified via semipreparative HPLC (column: Phenomenex Luna C18 (250 x 10 mm) 10 µm; flow: 5 mL/min; solvent: H_2O/MeCN + 0.1 % TFA; isocratic: 18 % MeCN; R_t = 11.0 min). After lyophilization product **6** was obtained as colorless solid (4.5 mg, 0.01 mmol, 32 %).

MS (ESI$^+$): m/z (%): calculated for $C_{18}H_{31}N_3O_8$: 417.21 $[M]^+$, found: 418.2 $[M+H]^+$.

Synthesis of 1,4-di(*tert*-butylacetate)-6-methylpentanoate-6-amino-di(*tert*-butylacetate)-perhydro-1,4-diazepane (7):

cf. **4**. Product **7** was obtained as yellow oil (480 mg, 0.70 mmol, 21 %).

^{1}H-NMR (400 MHz, $CDCl_3$): δ (ppm) = 3.66 (s, 4H), 3.61 (s, 4H), 3.22 (s, 3H), 2.99 (d, *J* = 14.1 Hz, 2H), 2.85 – 2.65 (m, 4H), 2.63 (d, *J* = 14.1 Hz, 2H), 2.31 (t, *J* = 7.4 Hz, 2H), 1.63 – 1.53 (m, 4H), 1.44 (s, 18H), 1.43 (s, 18H), 1.25 (m, 2H). ^{13}C-NMR (100 MHz, $CDCl_3$): δ (ppm) = 174.4, 172.9, 170.9, 80.9, 80.4, 65.3, 63.2, 62.6, 59.4, 52.1, 51.6, 37.3, 34.3, 28.3, 28.2, 25.9, 21.9. MS (ESI$^+$): m/z (%): calculated for $C_{35}H_{63}N_3O_{10}$: 685.45 $[M]^+$, found: 686.5 $[M+H]^+$.

Synthesis of 1,4-diacetate-6-methylpentanoate-6-amino-diacetate-perhydro-1,4-diazepane (8):

7 (64.1 mg, 0.09 mmol) was dissolved in dichloromethane (500 µL) and trifluoroacetic acid (500 µL) was added. The mixture was stirred at room temperature for 20 h. After completion the solution was concentrated under reduced pressure and the crude product was purified via semipreparative HPLC (column: Phenomenex Luna C18 (250 x 10 mm) 10 µm; flow: 5 mL/min; solvent: H_2O/MeCN + 0.1 % TFA; gradient: 15-30 % MeCN in 20 min; R_t = 11.4 min). After lyophilization product **6** was obtained as colorless solid (18.7 mg, 0.04 mmol, 45 %).

MS (ESI$^+$): m/z (%): calculated for $C_{19}H_{31}N_3O_{10}$: 461.20 $[M]^+$, found: 462.2 $[M+H]^+$.

References

1. Anderson, C. J., Ferdani, R.: Copper-64 Radiopharmaceuticals for PET Imaging of Cancer: Advances in Preclinical and Clinical Research. Cancer Biotherapy & Radiopharmaceuticals. **24**, 379–393 (2009).
2. Niccoli Asabella, A., Cascini, G. L., Altini, C., Paparella, D., Notaristefano, A., Rubini, G.: The copper radioisotopes: a systematic review with special interest to 64Cu. BioMed research international. **2014**, 786463 (2014).
3. Shokeen, M., Anderson, C. J.: Molecular imaging of cancer with copper-64 radiopharmaceuticals and positron emission tomography (PET). Accounts of chemical research. **42**, 832–841 (2009).
4. Wu, N., Kang, C. S., Sin, I., Ren, S., Liu, D., Ruthengael, V. C., Lewis, M. R., Chong, H.-S.: Promising Bifunctional Chelators for Copper 64-PET imaging: Practical 64Cu Radiolabeling and High In Vitro and In Vivo Complex Stability. J. Biol. Chem, **21**, 177–184 (2015).
5. Kumar, A., Hao, G., Liu, L., Ramezani, S., Hsieh, J.-T., Öz, O. K., Sun, X.: Click-chemistry strategy for labeling antibodies with copper-64 via a cross-bridged tetraazamacrocyclic chelator scaffold. Bioconjug Chem. **26**, 782–789 (2015).
6. Banerjee, S. R., Pullambhatla, M., Foss, C. A., Nimmagadda, S., Ferdani, R., Anderson, C. J., Mease, R. C., Pomper, M. G.: 64Cu-Labeled Inhibitors of Prostate-Specific Membrane Antigen for PET Imaging of Prostate Cancer. J Med CHem. **57**, 2657–2669 (2014).
7. Novak-Hofer, I., Schubiger, P. A.: Copper-67 as a therapeutic nuclide for radioimmunotherapy. EJNMMI, **29**, 821–830 (2002).
8. Smith, N. A., Bowers, D. L., Ehst, D. A.: The production, separation, and use of 67Cu for radioimmunotherapy: a review.Appl Radiat Isot. **70**, 2377–2383 (2012).
9. Ahmedova, A., Todorov, B., Burdzhiev, N., Goze, C.: Copper radiopharmaceuticals for theranostic applications. Eur. J. Med. Chem. **157**, 1406–1425 (2018).
10. Conry, R. R.: Copper: Inorganic & Coordination ChemistryBased in part on the article Copper: Inorganic & Coordination Chemistry by Rebecca R. Conry & Kenneth D. Karlin which appeared in the Encyclopedia of Inorganic Chemistry, First Edition. In: *Encyclopedia of Inorganic Chemistry* (R. B. King, R. H. Crabtree, C. M. Lukehart, D. A. Atwood, R. A. Scott, eds.). John Wiley & Sons, Ltd, Chichester, UK 2006, p. 2309.
11. Wadas, T. J., Wong, E. H., Weisman, G. R., Anderson, C. J.: Copper chelation chemistry and its role in copper radiopharmaceuticals. Curr Pharm Des. **13**, 3–16 (2007).
12. Nurchi, V. M., Crisponi, G., Crespo-Alonso, M., Lachowicz, J. I., Szewczuk, Z., Cooper, G. J. S.: Complex formation equilibria of Cu(II) and Zn(II) with triethylenetetramine and its mono- and di-acetyl metabolites. Dalton Trans. **42**, 6161–6170 (2013).
13. Wadas, T. J., Wong, E. H., Weisman, G. R., Anderson, C. J.: Coordinating radiometals of copper, gallium, indium, yttrium, and zirconium for PET and SPECT imaging of disease. Chem. Rev. **110**, 2858–2902 (2010).

14. Cai, Z., Anderson, C. J.: Chelators for copper radionuclides in positron emission tomography radiopharmaceuticals. J Labelled Comp Radiopharm. **57**, 224–230 (2013).
15. Aime, S., Calabi, L., Cavallotti, C., Gianolio, E., Giovenzana, G. B., Losi, P., Maiocchi, A., Palmisano, G., Sisti, M.: Gd-AAZTA-: a new structural entry for an improved generation of MRI contrast agents. Inorg. Chem. **43**, 7588–7590 (2004).
16. Sengar, R. S., Nigam, A., Geib, S. J., Wiener, E. C.: Syntheses and crystal structures of gadolinium and europium complexes of AAZTA analogues. Polyhedron. **28**, 1525–1531 (2009).
17. Baranyai, Z., Uggeri, F., Maiocchi, A., Giovenzana, G. B., Cavallotti, C., Takács, A., Tóth, I., Bányai, I., Bényei, A., Brucher, E., Aime, S.: Equilibrium, Kinetic and Structural Studies of AAZTA Complexes with Ga3+ In3+ and Cu2+. Eur. J. Inorg. Chem. **2013**, 147–162 (2013).
18. Tei, L., Gugliotta, G., Fekete, M., Kálmán, F. K., Botta, M.: Mn(II) complexes of novel hexadentate AAZTA-like chelators: a solution thermodynamics and relaxometric study. Dalton trans. **40**, 2025–2032 (2011).
19. Vágner, A., D'Alessandria, C., Gambino, G., Schwaiger, M., Aime, S., Maiocchi, A., Tóth, I., Baranyai, Z., Tei, L.: A rigidified AAZTA-like ligand as efficient chelator for ^{68}Ga radiopharmaceuticals. Chemistry Select. **1**, 163–171 (2016).
20. Farkas, E., Nagel, J., Waldron, B. P., Parker, D., Tóth, I., Brücher, E., Rösch, F., Baranyai, Z.: Equilibrium, Kinetic and Structural Properties of Gallium(III) and Some Divalent Metal Complexes Formed with the New DATAm and DATA5m Ligands. Chemistry. **23**, 10358–10371 (2017).
21. Nagy, G., Szikra, D., Trencsényi, G., Fekete, A., Garai, I., Giani, A. M., Negri, R., Masciocchi, N., Maiocchi, A., Uggeri, F., Tóth, I., Aime, S., Giovenzana, G. B., Baranyai, Z.: AAZTA: An Ideal Chelating Agent for the Development of 44 Sc PET Imaging Agents. Angew. Chem. **129**, 2150–2154 (2017).
22. Seemann, J., Waldron, B., Parker, D., Roesch, F.: DATATOC: a novel conjugate for kit-type 68Ga labelling of TOC at ambient temperature. EJNMMI. **1** (2016).
23. Nock, B. A., Kaloudi, A., Nagel, J., Sinnes, J.-P., Roesch, F., Maina, T.: Novel bifunctional DATA chelator for quick access to site-directed PET 68Ga-radiotracers: preclinical proof-of-principle with Tyr3octreotide. Dalton trans. **46**, 14584–14590 (2017).
24. Bass, L. A., Wang, M., Welch, M. J., Anderson, C. J.: In Vivo Transchelation of Copper-64 from TETA-Octreotide to Superoxide Dismutase in Rat Liver. Bioconjugate Chem. **11**, 527–532 (2000).
25. Moi, M. K., Meares, C. F., McCall, M. J., Cole, W. C., DeNardo, S. J.: Copper chelates as probes of biological systems: Stable copper complexes with a macrocyclic bifunctional chelating agent. Analytical Biochem. **148**, 249–253 (1985).
26. McQuade, P., Miao, Y., Yoo, J., Quinn, T. P., Welch, M. J., Lewis, J. S.: Imaging of melanoma using 64Cu- and 86Y-DOTA-ReCCMSH(Arg11), a cyclized peptide analogue of alpha-MSH.J. Med. Chem. **48**, 2985–2992 (2005).
27. Chen, X., Hou, Y., Tohme, M., Park, R., Khankaldyyan, V., Gonzales-Gomez, I., Bading, J. R., Laug, W. E., Conti, P. S.: Pegylated Arg-Gly-Asp peptide: 64Cu labeling and PET imaging of brain tumor alphavbeta3-integrin expression. J. Nuc. Med.. **45**, 1776–1783 (2004).

28. Anderson, C. J., Jones, L. A., Bass, L. A., Sherman, E. L., McCarthy, D. W., Cutler, P. D., Lanahan, M. V., Cristel, M. E., Lewis, J. S., Schwarz, S. W.: Radiotherapy, toxicity and dosimetry of copper-64-TETA-octreotide in tumor-bearing rats. J. Nuc. Med. **39**, 1944–1951 (1998).
29. Chen, X., Park, R., Tohme, M., Shahinian, A. H., Bading, J. R., Conti, P. S.: MicroPET and autoradiographic imaging of breast cancer alpha v-integrin expression using 18F- and 64Cu-labeled RGD peptide. Bioconjugate Chem. **15**, 41–49 (2004).
30. Chen, X., Sievers, E., Hou, Y., Park, R., Tohme, M., Bart, R., Bremner, R., Bading, J. R., Conti, P. S.: Integrin αvβ3-Targeted Imaging of Lung Cancer. Neoplasia. **7**, 271–279 (2005).
31. Anderson, C. J., Dehdashti, F., Cutler, P. D., Schwarz, S. W., Laforest, R., Bass, L. A., Lewis, J. S., McCarthy, D. W.: 64Cu-TETA-octreotide as a PET imaging agent for patients with neuroendocrine tumors. J. Med. Chem. 42, 213–221 (2001).

Synthesis, labeling and preclinical evaluation of a squaric acid containing PSMA-inhibitor labeled with ^{68}Ga – a comparison with PSMA-11 and PSMA-617

Lukas Greifenstein

Submitted to ChemMedChem, May 14, 2019

Abstract

The L-lysine urea-L-glutamate (KuE) represents a key motif in recent diagnostic and therapeutic radiopharmaceuticals targeting the prostate specific membrane antigen PSMA. The most potent derivatives all present in addition to the KuE motif an aromatic unit which fulfills requirements for binding in the PSMA enzyme binding pocket. In our previous work we already showed obtained good results *in vivo* with a TRAP-TEG-Amin (TRAM) derivative using a squaric acid molecule to connect chelate and KuE unit leading to a TRAM.QS.KuE. When SA is used for coupling, however, the peculiar structural of SA becomes a feature of the product. This is comparable to triazole formation for the "click" coupling of azides and alkynes. Consequently, the influence of squaric acid pharmacophore on the biological activity of the final compound must be considered. TRAM.QS.KuE, DOTAGA.QS.KuE and NODAGA.QS.KuE were all synthesized in straight forward organic reactions and purified by HPLC afterwards. DIfferents amounts of tracer were labelled at different temperatures with different nuclides including ^{68}Ga, ^{44}Sc, ^{64}Cu, ^{177}Lu and ^{225}Ac. PET examinations were performed on $NMRI_{nu/nu}$ nude mice with an LNCaP tumor on the right hind leg inclouding *ex vivo* investiagtions of the organs. For comparison, ^{68}Ga-derivatives of PSMA-11 and PSMA-617 were as well investigated in the same animal model.

Introduction

Prostate cancer is the most common cancer in industrial countries and the third most deadly disease (*1*). Tumor growth in prostate is a slow process so that an early stage diagnosis can increase the 5-year survival rate to nearly 100 %. In contrast, if the disease is discovered after the tumor has spread, the survival rate decreases dramatically. Once detected, prostate cancer requires an immediate, however balanced, therapeutic intervention, because a too aggressive treatment can be detrimental to the patients' quality of life (*2,3*). Therefore, a timely diagnosis and reliable assessment of both, the progress and response to therapy of the disease are indispensable for management of long-term survival and the patient's life quality.

A very important structure for targeting prostate cancer is the prostate-specific-membrane-antigen (PSMA), a membrane-bound glycoprotein belonging to the enzyme class of the carboxy peptidases. The preferred substrate of PSMA is a peptide with a C-terminal glutamate, e.g. N-acetyl-aspartyl-glutamate (NAAG) and folic acid-(poly)-γ-glutamate (*4*). Besides the main pocket, where two Zn^{2+} ions are located, there is a secondary pocket showing high affinity towards planar, aromatic structures (*11,12*). PSMA is barely present in normal tissue but is expressed in prostate cancer cells in high levels (*5,6*). Additionally, the concentration of expressed PSMA correlates well with the stage of the disease (*7,5*).

In radiopharmaceutical chemistry and nuclear medicine, different approaches for visualization of the PSMA-target have been used over the last years. A common strategy is the usage of antibodies which bind to the protein structure of PSMA (*8–10*). Alternatively, the binding pocket at the active site of the enzyme can be targeted using small molecules as shown in Fig. 1.

For any ligand to bind to the active site of PSMA, a glutamate motif resembling the natural substrate is madatory. In order to enhance binding and avoid dissociation of the bound ligand, this structure should contain a reactive group to form a covalent bond to an amino-acid residue in the active center, that cannot be cleaved by the enzyme.

A large group of urea-based PSMA inhibitors found to be relevant in nuclear medicine diagnoses using PET/CT are the radiopharmaceuticals [^{68}Ga]Ga-PSMA-11 and [^{68}Ga]Ga-PSMA-617 (see Figure 1) (*4,13*). Both structures include an aromatic part which as well has

been proven to be benefical regarding affinitiy. This is due to an additional pocket in the entrance funnel of the PSMA which favours aromatic units (6)(*14*). Even if PSMA-11 and PSMA-617 already showed promising results in preclinical as well as in clinical routine application they both suffer from different drawbacks. PSMA-11 for instance uses N,N'-bis(2-hydroxybenzyl)ethylendiamine-N,N'-diacetic acid (HBED) as a chelator, which has perfect properties for the labeling of ^{68}Ga, but is not able to form complexes with other radiometals. This can be disadvantageous for any theranostic purpose where trivalent radiometals such as ^{177}Lu and ^{225}Ac are important. PSMA-617, on the other hand, uses a 1,4,7,10-tetraazacyclododecane-1,4,7,10-tetraacetic acid ligand (DOTA) instead of HBED which avoids this problem. Yet, PSMA-617 shows significant accumulation in organs other than the tumor, which is a disadvantage for therapeutic application.

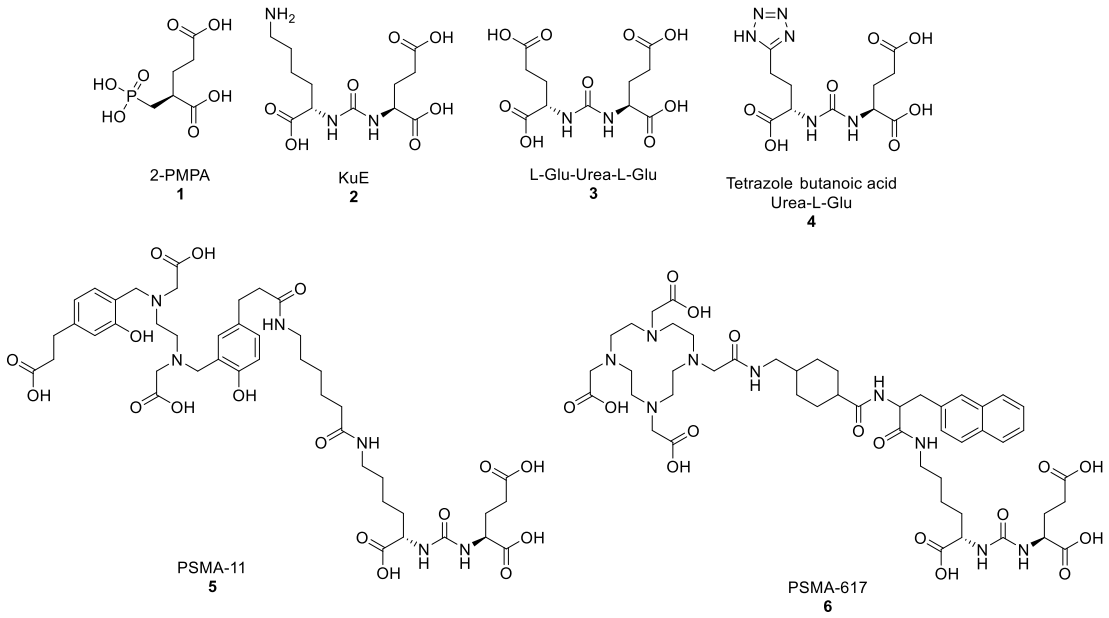

Figure 1: Structures of PSMA-inhibitors used for diagnosis and therapy of PCa in nuclear medicine. For some the *in vitro* affinities are given. The affinity of the Glu-Urea-Glu (EuE)-derivative (3) (K_i = 1.5 nM) can be increased by introducing an aromatic tetrazole group (K_i = 0.9 nM). The inhibitor Lys-Urea-Glu (KuE) (2) bound to the aromatic chelator HBED shows good affinities (PSMA-11, K_i = 12.0 nM) (5). By inserting an aromatic linker, a good affinity can be maintained despite the substitution with DOTA ligand (PSMA-617, K_i = 2.3 nM) (6).

Squaric acid

3,4-dihydroxycyclobu-3-ene-1,2-dione, also known as squaric acid (SA), is a multi-purpose tool in different chemical applications (*15,16*). SA is a very interesting molecule for different reasons. For example, the dianion follows the Hückel rule for aromatic systems, which explains the high acidity of the SA (pK1 = 0.5-1.2; pK2 = 2.2-3.5) (*17*). Furthermore, its diester 3,4 dibutoxy-3-cyclobutene-1,2-dione (SADE) can be used for coupling reactions in a very elegant way. Coupling by SADE avoids a lot of synthetic problems, i.e. challenging protection group chemistry necessary when coupling with other coupling reagents. In addition, SADE offers the possibility of selectively combining two amines. This is done by a stepwise, pH-dependent, asymmetric amidation of the diester under mild conditions, both in aqueous buffers and in organic solvents (Fig. 2) (*18*). The stepwise pH-dependent course of the reaction can be explained by a change in the aromaticity of the intermediate stages (*19*).

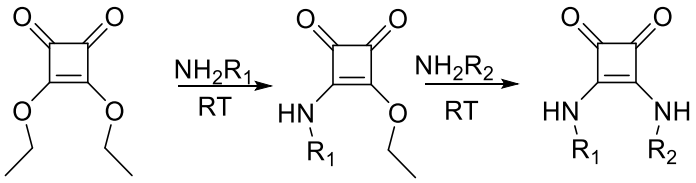

Figure 2: Scheme of the selective reaction of the SADE. Both reactions are driven by the change in aromaticity. For the connection of each amine therefore different pH values are necessary. The first amidation occurs at a pH of 7 whereas the second amidation takes place at pH 9.

This selectivity results in an enormous advantage of coupling by means of SADE. In contrast to alkynes and azides for azide-alkyne cycloaddition reactions, amines are present in many biomolecules and do not have to be introduced into the molecule with synthetic effort. Amines are also used for coupling with active esters, but the use of SADE for coupling makes the protection of other nucleophilic groups unnecessary. Another positive feature is, that the monoamine intermediate is stable and can be isolated. This product is called squaric acid monoester (SAME) and has a much higher stability than e.g. N-hydroxy succinimide (NHS)

esters. In solution at pH 9, SAME is stable for several days, while NHS esters show hydrolysis already after minutes under these conditions. All properties are traditionally used in several fields of organic chemistry for example to couple carbohydrates to proteins (*20,21*) Interestingly, SA derivatives appear to be an coupling alternative for connecting chelators to targeting vectors. Ideally, a bifunctional chelator with a primary amine is reacted with SA diester and transformed into a bench stable building block. This particularly elegant approach makes protective groups redundant. Subsequently, the coupling to an unprotected targeting vector with an amine function for coupling takes place. After purification, the chelator-target vector conjugate can be used directly. A further deprotection, which could possibly be a problem for a sensitive targeting vector, is not necessary. Interestingly, despite the well-known properties of SADE, the use of this strategy in radiopharmaceutical chemistry is rather limited. The only two reportes used SA exclusively to link proteins or antibodies to the chelator desferrioxamine (DFO), which has a peptide like structure (*22,23*).

When SA is used for coupling as a "chemical" tool, however, the peculiar structural of SA becomes a pharmacological feature of the product molecule. Consequently, the influence of squaric acid on parameters such as biological activity, the lipophilicity, the metabolism etc. of the final compound must be considered. Some comparisons were made between the SA structure with phosphate (*24*), urea (*25*) and guanidine structures (*26*) with regard to their impact on their biological behavior in general. The aromatic character of the SA diamide renders the group comparable to imidazole or triazole structures.

For example, SA could as well be a feature of the product when used in PSMA-inhibitors to introduce aromaticity into the inhibitors. Furthermore, for the coupling of chelators to targeting vectors it must be kept in mind in particular, that SA itself has complexing properties itself (*27*) and may therefore influence the chelator-radiometal complexation properties of the bound chelator – a feature never considered in the design of radiometal-chelator-based radiopharmaceuticals. In the present study three structures connecting the typical PSMA-inhibitor motif KuE with the chelators 2,2',2"-(10-(4-((2-aminoethyl)amino)-1-carboxy-4-oxobutyl)-1,4,7,10-tetraazacyclododecane-1,4,7-triyl)triacetic acid (DOTAGA-NH_2), ((1,4,7-triazonane-1,4,7-triyl)tris(methylene))tris((1-amino-15-oxo-4,7,10-trioxa-14-azaheptadecan-17-yl)phosphinic acid) (TRAM) and 2,2'-(7-(4-((2-aminoethyl)amino)-1-carboxy-4-oxobutyl)-1,4,7-triazonane-1,4-diyl)diacetic acid (NODAGA-NH_2) via a SA are

presented (Figure 5). Synthesis, labeling with ^{68}Ga and *in vivo* as well as *ex vivo* experiments are conducted. It is demonstrated that the synthetic and analytical chemistry is easy to perform, that ^{68}Ga-radiolabeling is efficient and that the new SA-based radiopharmaceuticals show *in vivo* binding affinities and biodistributions in LNCaP cell lines and LNCaP-tumor bearing mice comparabal to the established PSMA inhibitors PSMA-11 and PSMA-617.

Materials and Methodes

Synthesis of the PSMA unit (KuE)

One of the exciting advantages of using SADE is the simple synthesis strategy. This can easily be applied to any conceivable system in two steps without complications. SADEs are characterized by their selective reactivity with amines. Thus, no sophisticated protective group chemistry is required for coupling. Furthermore, coupling of the chelating component and the PSMA component is pH-controlled. A one-step synthesis of the KuE precursors is carried out.

The PSMA inhibitor lysin-urea-glutamic acid (KuE) is synthesized via solid phase peptide synthesis methods according to literature (*28,29*). Since the linker function of the final compound is located on the chelator and no further reactions at the side chain of the lysine at the solid phase have to be carried out, the amino acids are not protected as usual with an orthogonal protective group, but with an acid-labile *tert*-butyl ester. This is a huge advantage compaired to the standard protocol.

First, the protected glutamic acid (1) is reacted with triphosgene in the presence of *N,N*-Diisopropylethylamine (DIPEA) in dry dichloromethane (DCM) yielding the isocyanate. This is afterwards coupled to the solid phase bound lysine (2) yielding the urea containing motif. The product is cleaved from the solid phase and simultaneously completely deprotected in one step with trifluoroacetic acid (TFA). After removal of the TFA the product is separated from remaining free lysine using semi-preparative HPLC yielding KuE. During the execution of this synthesis, several parameters have to be considered in order to achieve high yields. On the one hand, the reaction must be kept at 0°C during reaction period under all

circumstances. Even a few degrees above can reduce the yield significantly. On the other hand, the dripping speed of the triphosgene is sensitive. If triphosgene is added too quickly, the yield of the final product can be reduced by up to 80%.

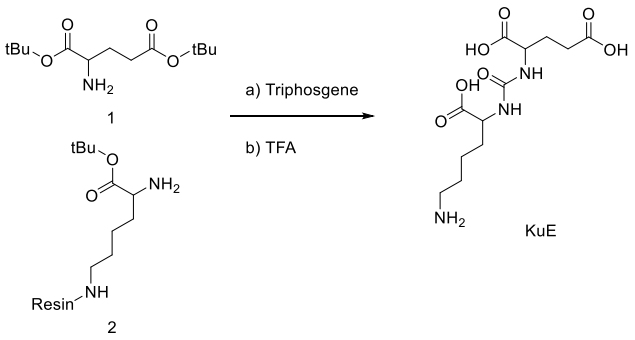

Figure 3: Synthesis of the KuE unit. a) i) DIPEA, triphosgene, DCM, 0°C, 4h ii) **2** DCM, RT, 16h b) TFA, 0.5h, 71%.

The KuE precursor can next be coupled to any component carrying a squaric acid ethylester. This can be done in an aqueous medium at room temperature.

Preparation of the Chelator.SA moiety

All three chelators with a terminal amine are commercially available except the TRAM ligand, which is prepared from commercially available TRAP coupled to the corresponding triethylene glycole amine in a standard peptide coupling reaction.

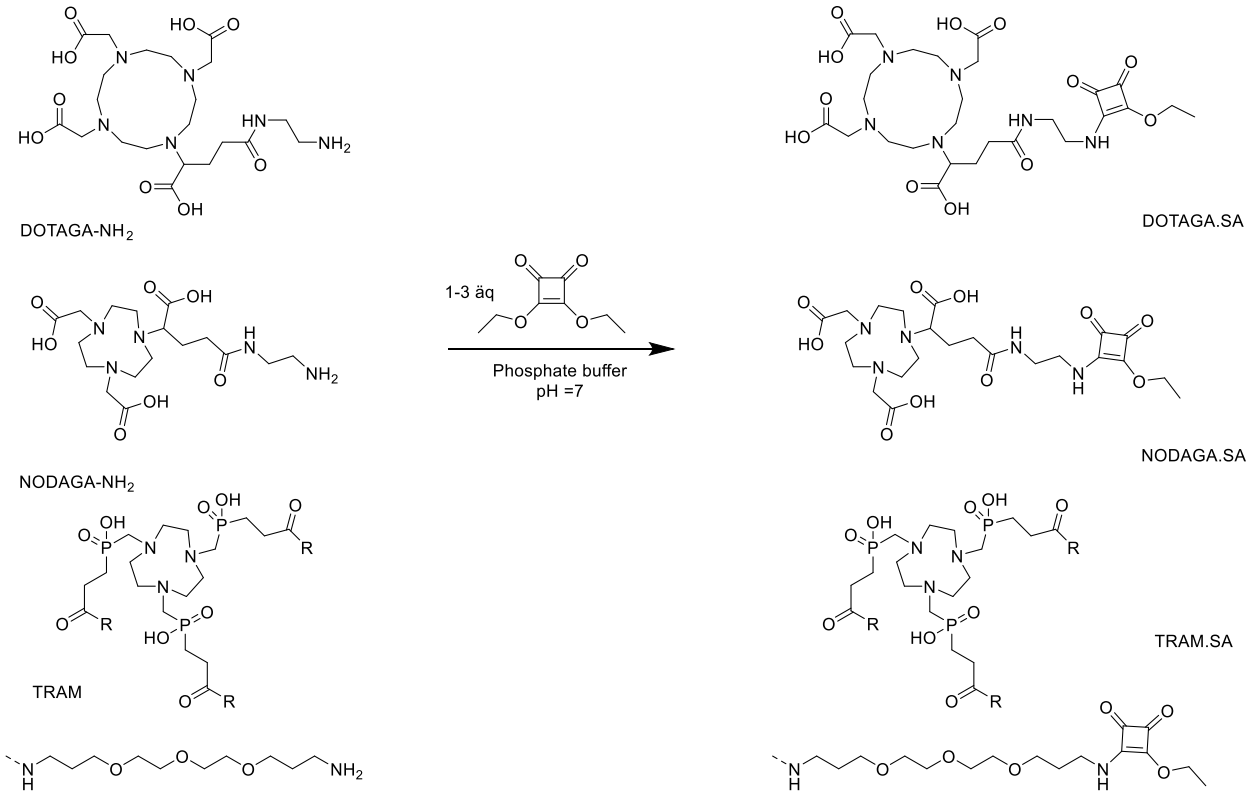

Figure 4: Coupling of the chelators with SADE at pH7 in phosphate buffer at room temperature. In case of the TRAM derivative 3 equivalents are necessary for complete reaction. In the other cases 1 equivalent is sufficient. The substituents of the TRAM ligands are summarized as R and are given under the respective structure.

For the coupling described in Fig. 4 all components were dissolved in corresponding ratios in phosphate buffer (0.2 M, pH = 7.0) and shaken overnight at ambient temperature to yield the products. The pH value of the reaction mixture was checked every one to three hours and if necessary, the pH was recalibrated to pH = 7 by using a few drops of 0.1 M NaOH. If the reaction is very fast, it could be necessary to adjust the pH with 1 M NaOH due to minimization of the volume. The formation of all products was proven by LC-MS and

purification was performed using semi-preparative HPLC. It is noteworthy that chelator.SA derivatives can be stored at 0-5°C for several months in contrast to typical chelates ready for functionalization like SCN-derivatives. This was again confirmed by a continuous examination of the compounds by LC-MS, where no decomposition was observed.

Synthesis of DOTAGA.SA.PSMA, NODAGA.SA.PSMA and TRAM.SA.PSMA

The storable chelator.SA moieties were coupled to the KuE motif using phosphate buffer (0.2 M, pH = 9.0). Mixing both components in equimolar ratios resulted in the formation of the desired PSMA inhibitors given in figure 5 after shaking them for 1 day at ambient temperature. Recalibration of the pH was again performed with 0.1 M and 1 M NaOH as well but needed more calibration steps because the buffer area of phosphate buffer is not suitable for this pH value.

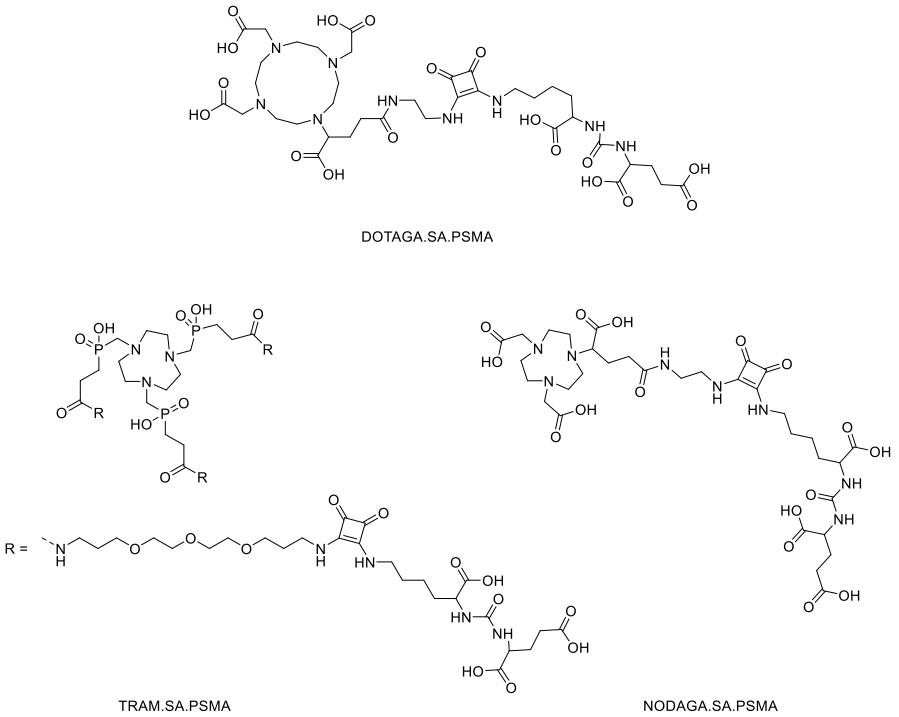

Figure 5: The final SA-based KuE derivatives with different chelators.

Radiolabeling

For radiochemical evaluation with ^{68}Ga, a $^{68}Ge/^{68}Ga$ generator (TiO_2-based matrix, Cyclotron Co. Obninsk, Russia) was used with online acetone post-processing separating iron and zinc impurities as well as ^{68}Ge breakthrough [17, 18].

Labeling was performed in 1 ml of 0.2 M ammonium acetate buffer pH 4.5 or in 0.5 M HEPES buffer pH 4.5. Reactions were carried out at room temperature (25 °C) or at 95 °C. Labeling kinetics for DOTAGA.SA.PSMA, TRAM.SA.PSMA and NODAGA.SA.PSMA were recorded with precursor amounts of 5, 10 and 15 nmol. The pH was controlled at start of labeling and after labeling was finished.

For reaction control, TLC with citrate buffer, pH 7, as eluent and radio HPLC (Merck Chromolith® RP-18e-column, Water : MeCN with 0.1% TFA, 5 to 95% MeCN in 10 min) was used. TLC´s were measured in RITA TLC imager (Elysia Raytest). The citrate TLC showed free radiometal with an Rf of 0.9 and all labelled compounds with an Rf of 0.1 to 0.3. Radio-HPLC was used in addition to exclude the presence of colloidal radio metals not visible on TLC.

***In vitro*-stability studies**

Stability studies were performed in HS and PBS solution (pH adjusted to 7 by PBS buffer) in triplicate. HS (human male AB plasma, USA origin) were bought from Sigma Aldrich, phosphate buffered saline (PBS) pH= 7.4 was purchased from Sigma Aldrich as well. The final procedure used 50-70 µl of the labeling solution (5-10 MBq) added to 1 ml of either HS or PBS. The pH was controlled to ensure no influence of the labeling buffer on the solution.

***In vivo*-experiments**

The mice were housed in the animal laboratory of the Helmholtz-Zentrum Dresden-Rossendorf and experiments were performed according to the guidelines of the European and German Regulations for Animal Welfare approved by the local Ethics Committee for Animal Experiments (Landesdirektion Dresden; file numbers 24-9165.40-4/2013, 24-9168.21-4/2004-1).

Male Rj:NMRI-*Foxn1*$^{nu/nu}$ mice, T-cell-deficient, hairless, in the age between 5 and 8 weeks, (Janvier Labs, France) were kept in a pathogen-free facility with *ad libitum* access to water and food. The mice were subcutaneously injected with 100 µL PBS containing 2x10^6 LNCaP cells into the right hind leg. The tumor volume was calculated from caliper measurements by $V = \pi / 6 \times ((\text{tumor length}-0.8) \times (\text{tumor width}-0.8)^2)$. The tumor lengths were corrected for the skin thickness with approximately 0.8 mm according to MRI measurements.

The PET experiments and biodistribution evaluation of the radiotracers were carried out when the tumors reached a volume between 400 and 1300 mm^3.

Biodistribution studies were performed with [^{68}Ga]Ga-DOTAGA.SA.PSMA (control n=3, co-injection of 10 mg/kg body weight 2-PMPA, blocked, n=2), [^{68}Ga]Ga-NODAGA.SA.PSMA (control, n=5), [^{68}Ga]Ga-TRAM.SA.PSMA (control, n=8), [^{68}Ga]Ga-PSMA-11 (control, n=3), [^{68}Ga]Ga-PSMA-617 (control, n=4). Animals were sacrificed at 60 min post-injection (p.i.). Blood, tumor and the major organs were collected, weighed, and counted in a cross-calibrated γ-counter (Isomed 1000, Isomed GmbH) and Wallac WIZARD Automatic Gamma Counter (PerkinElmer). The activity of the tissue samples was decay-corrected and calibrated by comparing the counts in tissue with the counts in aliquots of the injected radiotracer that had been measured in the γ-counter at the same time. The activity in the selected organs was expressed as percent-injected activity per organ (%ID) and the activity concentration in tissues and organs as standardized uptake value (SUV in [MBq activity/g tissue] / [MBq injected activity/g body weight]). Values are quoted as mean±standard deviation for each group of animals.

PET scans were performed using dedicated rodent PET/CT scanner (NanoPET/CT, Mediso, Hungary) or microPET P4 (Siemens, US). The PET experiments were carried out with mice

under general anesthesia that was induced and maintained by inhalation of 12 % and 9 % (v/v) desflurane in 30/10 % (v/v) oxygen/air, respectively.

Anesthetized mice were positioned on a warmed bed along the scanner axis. The ^{68}Ga-labeled radiotracers with an average activity of 20 MBq in 300 µL isotonic NaCl was infused over one minute into a tail vein. PET images were acquired beginning with the injection over 1 h and were reconstructed in dynamic mode with 32 frames and 0.5 mm^3 voxel size. Region-of-interest (ROI) quantification was performed with ROVER (ABX GmbH, Germany). The ROI values were not corrected for recovery and partial volume effects. The values were expressed as SUV_{mean}.

Results

Radiolabeling and stability studies

DOTAGA.SA.PSMA

For DOTAGA.SA.PSMA three different amounts of precursor were labeled at 95 °C with 100 MBq of ^{68}Ga. Kinetics from TLC of all reactions are given in Fig 6. For 10 and 15 nmol, the reactions reached more than 95 % RCY after 1 minute. For 5 nmol, the reaction is slightly slower and reaches 95 % after 10 minutes only. However, all reactions guaranteed for more than 95 % RCY after 15 minutes, making further purification not necessary.

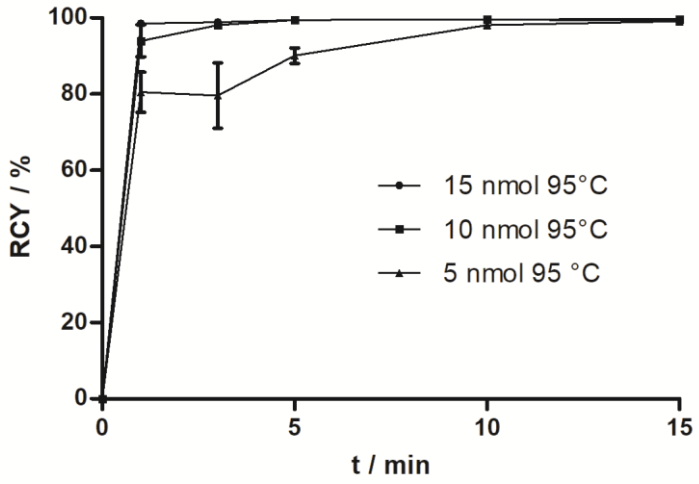

Figure 6: Labeling kinetics of DOTAGA.SA.PSMA with 100 MBq of ^{68}Ga measured from radio-TLC developed in citric acid buffer at pH 4.5. The ligand reaches more than 95 % RCY after 15 minutes for all conditions.

All results were confirmed by radio-HPLC given in Figure 7. Less than 1% uncomplexed ^{68}Ga with a retention time of 1 minute was present 30 minutes after start of the reaction whereas the labeled complex appeared at 2.4 minutes. The image shows the results from a reaction of 10 nmol precursor at 95 °C labeled with 100 MBq ^{68}Ga.

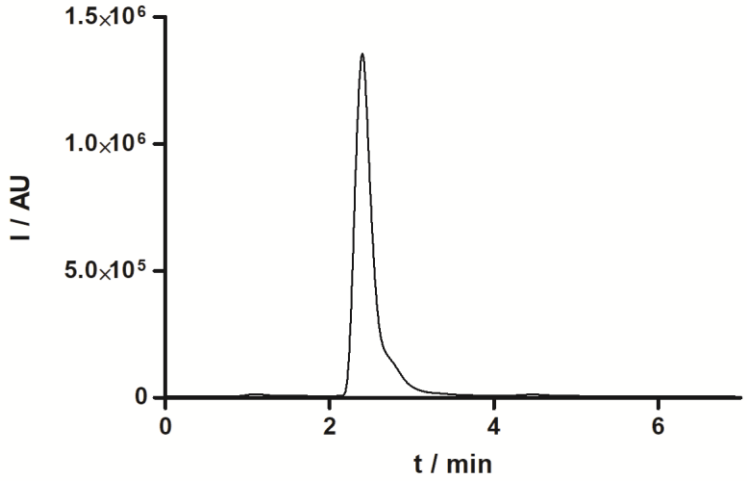

Figure 7: Radio-HPLC of the 10 nmol reaction of DOTAGA.SA.PSMA 30 minutes after reaction started. Less the 1% of uncomplexed ^{68}Ga appeared at a retention time of 1 min.

Stabilities for all tracers were investigated in human serum and in PBS-buffer (pH 7.4) at 37 °C within two half-lives of ^{68}Ga. Results were measured via radio-TLC as well as radio-HPLC and are given in Figure 8.

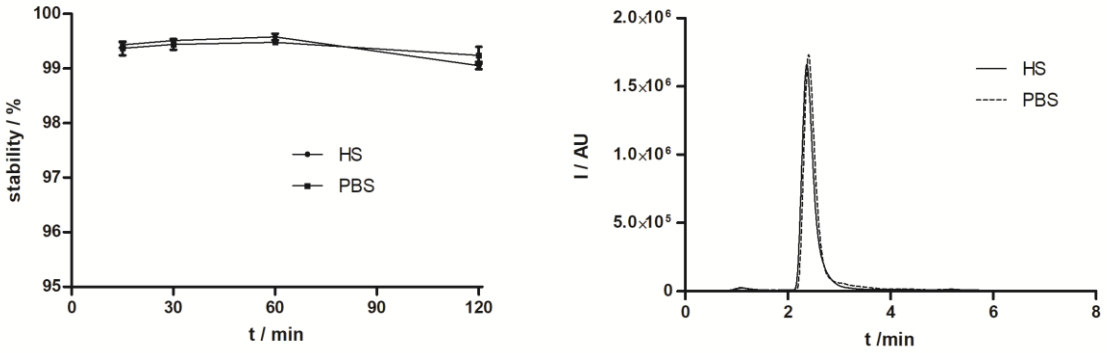

Figure 8: Stability of [^{68}Ga]Ga-DOTAGA.SA.PSMA in human serum and PBS at 37°C. Left: Radio-TLC developed with citric acid buffer pH 4.5. The ligand shows more than 99 % stability after 2 hours in both media. Right: Radio-HPLC after 120 min. Uncomplexed gallium at 1 min., product at 2.4 min. Less than 1% free gallium is observed.

Both methods show in agreement that the compound is stable over a period of 2 hours in both human serum and PBS buffer with values greater than 99 %.

NODAGA.SA.PSMA

The NODAGA.SA.PSMA derivative was subjected to the same investigations as the DOTAGA derivative. In contrast to DOTAGA the reactions were carried out at room temperature. Both radio-TLC and radio-HPLC results showed consistently more than 95 % RCY. In addition, the radio-TLC shows that even at room temperature and small amounts of tracer a complete labelling is already obtained after 1 minute.

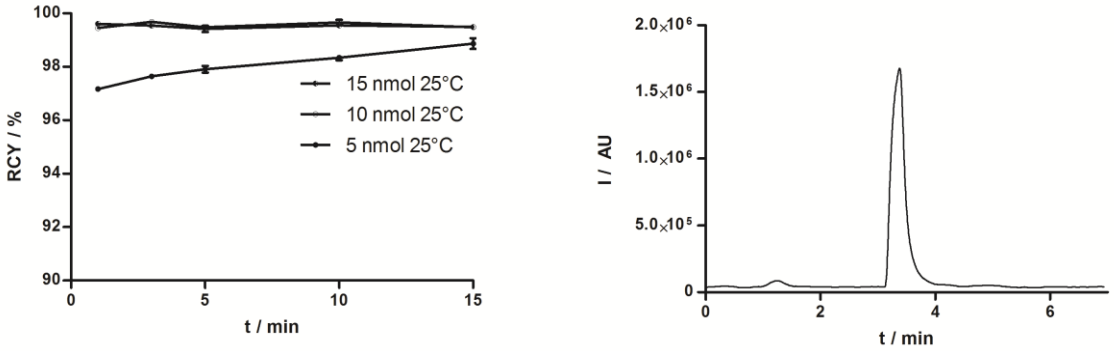

Figure 9: Labeling kinetics of NODAGA.SA.PSMA with 100 MBq of ^{68}Ga measured from radio-TLC developed in citric acid buffer at pH 4.5. [^{68}Ga]Ga-NODAGA.SA.PSMA reaches more than 95 % RCY after 15 minutes for all conditions. left: radio-TLC developed in citric acid buffer pH 4.5. right: radio-HPLC after 30 min. Uncomplexed gallium at 1 min, product at 3.4 min.

Stabilities were again determined with radio-HPLC and radio-TLC. The stabilities measured with radio-HPLC after 120 min in HS and PBS at 37 °C are given in Fig. 10. [^{68}Ga]Ga-NODAGA.SA.PSMA remains stable after 120 min in both media with values greater than 95 %.

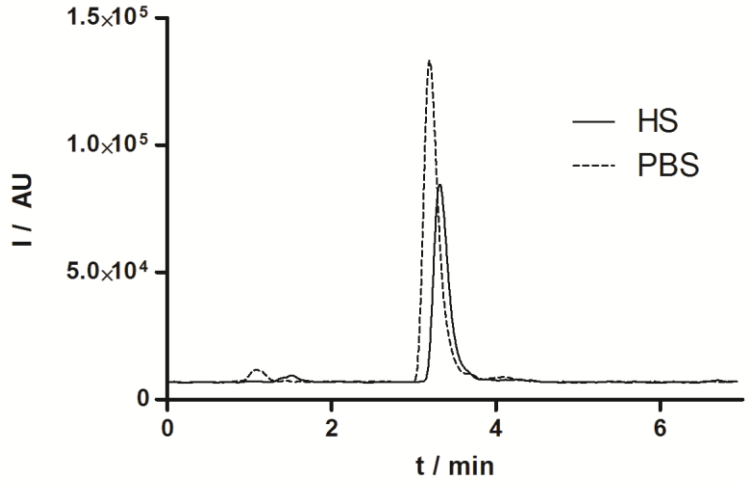

Figure 10: radio HPLC showing the stability of [^{68}Ga]Ga-NODAGA.SA.PSMA in human serum and PBS at 37 °C. Uncomplexed gallium at 1 min, product at 3.4 min.

TRAM.SA.PSMA

The TRAP chelator is known to have perfect properties for the labeling of ^{68}Ga. In this case, however, the SA unit has a huge impact on the labeling because sufficient RCY was not achieved at 25 °C. This may be due to steric hindrance and precomplexation caused by the three bulky SA-substituents of the TRAM ethylene glycol linker. They are able to obstruct the coordination sphere of the TACN part of TRAM and therefore prevent gallium from entering. Furthermore, SA has self-complexing properties as previously described. This may as well prevent gallium from reaching the coordination sphere of the actual chelate but form intermediate complexes with SA. Elevated temperatures and higher precursor amounts lead to RCYs greater than 95 % for the [^{68}Ga]Ga-TRAM.SA.PSMA as well (Fig. 11 left). The high RCY was confirmed by radio-HPLC showing 99 % yield after 30 minutes. (Fig. 11 right)

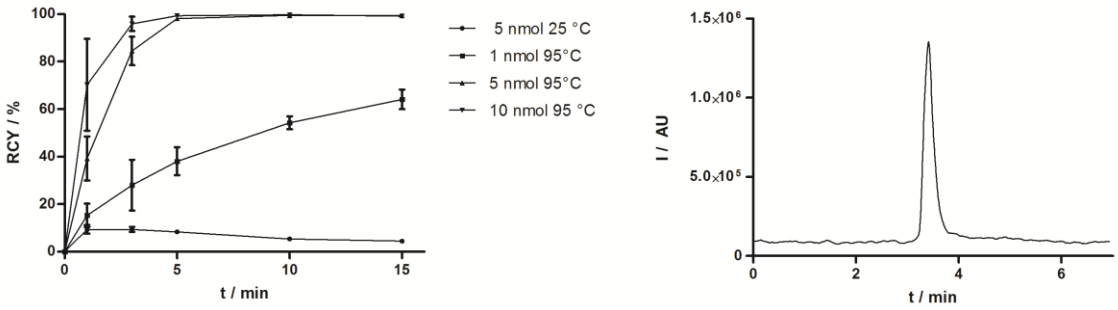

Figure 11: Labeling kinetics of [^{68}Ga]Ga-TRAM.SA.PSMA with 100 MBq of ^{68}Ga measured from radio-TLC developed in citric acid buffer at pH 4.5. The ligands reaches more than 95 % RCY after 15 minutes at 95°C for higher quantities of chelate. For 25°C no efficient labeling is observed. left: radio-TLC developed in citric acid buffer pH 4.5. right: radio-HPLC after 30 min. Uncomplexed gallium at 1 min, product at 3.4 min.

The stability of [^{68}Ga]Ga-TRAM.SA.PSMA after 120 min is shown in Fig. 12. The radio-HPLC data show that the stability of [^{68}Ga]Ga-TRAM.SA.PSMA is slight reduced compared to the other derivatives with values of 89 % in HS and 92 % in PBS, respectively. Nevertheless, these are acceptable stabilities for the use of this compound for further investigations.

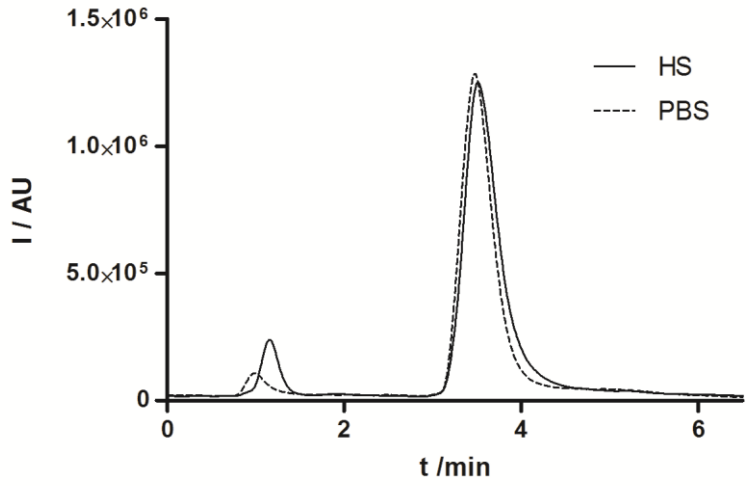

Figure 12: Stability of the[^{68}Ga]-TRAM.SA.PSMA in human serum and PBS at 37°C. Uncomplexed gallium at 1 min, product at 3.4 min.

ex vivo-comparison of [^{68}Ga]Ga-DOTAGA.SA.PSMA, [^{68}Ga]Ga-NODAGA.SA.PSMA and [^{68}Ga]Ga-TRAM.SA.PSMA

Fig. 13 shows the *ex vivo*-comparison of the three designated tracers labeled with ^{68}Ga. The diagram indicates that all SA.PSMA show significant accumulation in the tumor. However, [^{68}Ga]Ga-NODAGA.SA.PSMA shows a significantly lower uptake in the tumor with 3.44 %ID/g compared to the other the tracers which can be due to the different total charge of [^{68}Ga]Ga-NODAGA. [^{68}Ga]Ga-DOTAGA.SA.PSMA and [^{68}Ga]Ga-TRAM.SA.PSMA demonstrate nearly same values with 5.64 %ID/g and 5.59 %ID/g, respectively.

The only clear off target enrichment for all tracers can be observed in the kidneys which is a typical result for radiolabeled PSMA inhibitors containing the KuE-unit (*30*). Here, the [^{68}Ga]Ga-TRAM.SA.PSMA-derivative shows a significant higher uptake with 8.45 %ID/g compared to the [^{68}Ga]Ga-DOTAGA.SA.PSMA and [^{68}Ga]Ga-NODAGA.SA.PSMA derivatives with values of 1.08 and 1.14 %ID/g, respectively.

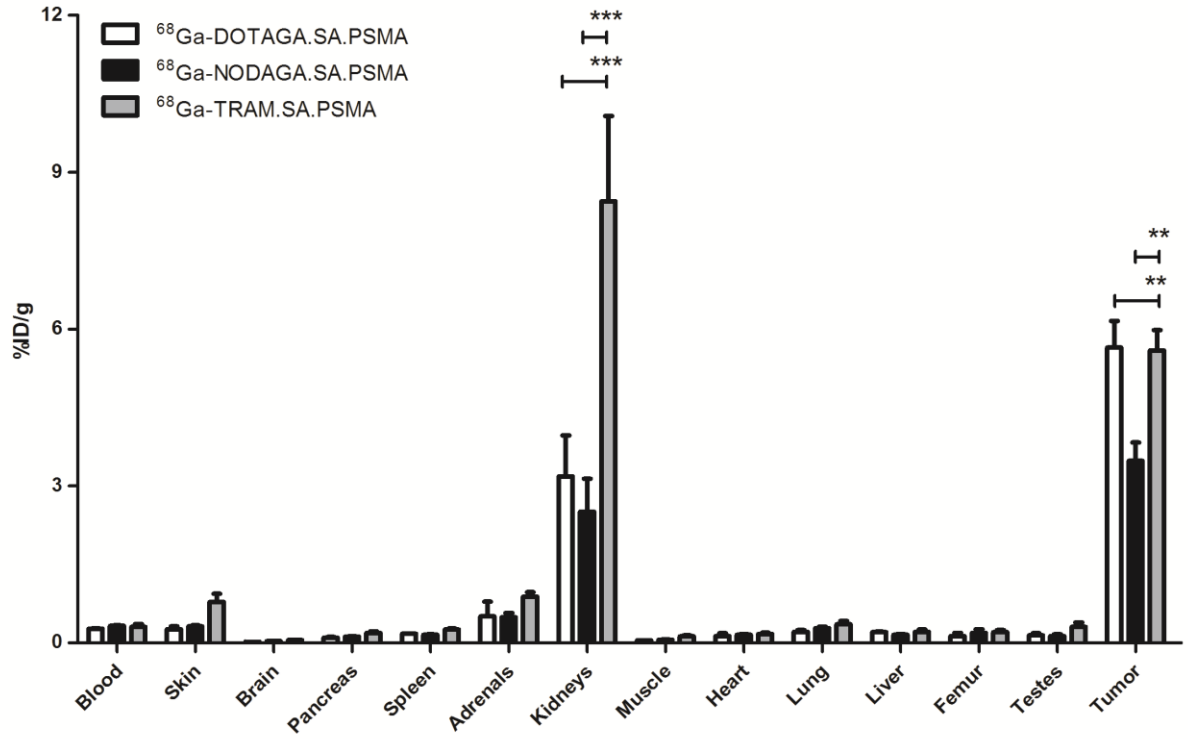

Figure 13: *ex vivo* biodistribution of the three SA.PSMA derivatives. The highest accumulation is found in the kidneys and the tumor. [^{68}Ga]Ga-DOTAGA.SA.PSMA and [^{68}Ga]Ga-TRAP.SA.PSMA have nearly same values with 5.64 %ID/g and 5.59 %ID/g, respectively. Both values are significantly higher than the ones for [^{68}Ga]Ga-NODAGA.SA.PSMA. [^{68}Ga]Ga-TRAP.SA.PSMA shows as only one significantly higher uptake in the kidneys. Statistics are calculated with Student's t-test by GraphPad Prism 5. Significances are defined as **: P<0.01 and ***: P<0.001. Other, non-significant result are not labelled.

Considering the results from the *ex vivo* studies, [^{68}Ga]Ga-DOTAGA.SA.PSMA with its high %ID/g value for accumulation in LNCaP tumor models and its very low off-target accumulation in the kidneys appears to be the most promising tracer labeled with ^{68}Ga. For this reason, this tracer was investigated in further test series. *In vivo* data were recorded and corresponding blocking studies with 2-PMPA were measured. Secondly, this tracer was compared *in vivo* and *ex vivo* with the two common tracers [^{68}Ga]Ga-PSMA-11 and [^{68}Ga]Ga-PSMA-617.

Comparative biodistribution and µPET studies of [^{68}Ga]Ga-DOTAGA.SA.PSMA, [^{68}Ga]Ga-PSMA-617 and [^{68}Ga]Ga-PSMA-11 in LNCaP tumor-bearing mice

ex vivo-comparison of [^{68}Ga]Ga-DOTAGA.SA.PSMA with [^{68}Ga]Ga-PSMA-11 and [^{68}Ga]Ga-PSMA-617

In Fig. 14 %ID/g-values are given for [^{68}Ga]Ga-DOTAGA.SA.PSMA, [^{68}Ga]Ga-PSMA-617 and [^{68}Ga]Ga-PSMA-11 in LNCaP tumor bearing mice for time points of 60 minutes p.i.. As expected all three molecules show significant uptake in the tumor. Values for [^{68}Ga]Ga-PSMA-11 are highest among this series even tough values show no significance. Within the error range [^{68}Ga]Ga-DOTAGA.SA.PSMA and [^{68}Ga]Ga-PSMA-617 show comparable value with 5.6±0.3 %ID/g and 6.4±1.0 %ID/g, respectively. This supports the prediction from *ex vivo* data, that [^{68}Ga]Ga-DOTAGA.SA.PSMA can be compared with clinicaly used PSMA inhibitors.

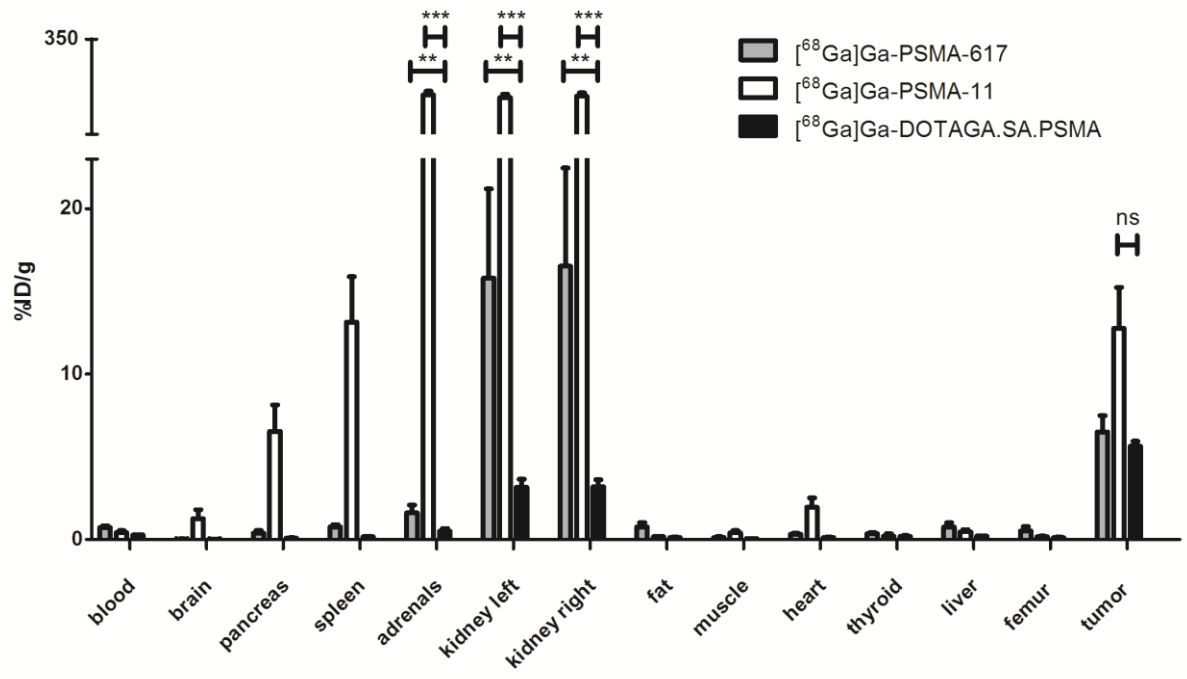

Figure 14: *ex vivo* biodistribution of [^{68}Ga]Ga-PSMA-617, [^{68}Ga]Ga-PSMA-11 and [^{68}Ga]Ga-DOTAGA.SA.PSMA. As expected, [^{68}Ga]Ga-PSMA-11 shows the highest value in the tumor. [^{68}Ga]Ga-DOTAGA.SA.PSMA shows nearly the same value as [^{68}Ga]Ga-PSMA-617 with a value of 5.6±0.3 %ID/g compared to [^{68}Ga]Ga-PSMA-617 with 6.4±1.0 %ID/g. There is no significance observed here. However, the uptake in the kidneys shows a great difference. Here, the [^{68}Ga]Ga-DOTAGA.SA.PSMA shows a significant lower value then both of the other tracers. Statistics are calculated with Student's t-test by GraphPad Prism 5. Significances are defined as **: P<0.01 and ***: P<0.001. Other, non-significant result are not labelled.

Off target enrichment is only observed in the kidneys. Only for [^{68}Ga]Ga-PSMA-11 there is an additional significant uptake in pancreas, spleen, adrenals and in the heart. Especially the values in the adrenals and in the kidneys are significantly higher compared to [^{68}Ga]Ga-PSMA-617 and [^{68}Ga]Ga-DOTA.SA.PSMA. This fact is as expected from literature for [^{68}Ga]Ga-PSMA-11 although the kidney value is surprisingly high (*31*). In comparison with [^{68}Ga]Ga-PSMA-617, the [^{68}Ga]Ga-DOTAGA.SA.PSMA indicates a significantly lower accumulation in the kidneys and adrenal glands. The superiority of the tracer in terms of the unwanted accumulation in the kidneys is shown in Fig. 15. Again, [^{68}Ga]Ga-DOTAGA.SA.PSMA got the potential to be promising radiopharmaceutical for diagnosis and therapy in comparison with the other two derivatives. On the one hand it demonstrates a good accumulation in the tumor, which is in the range of [^{68}Ga]Ga-PSMA-617; and on the other hand the accumulation in other organs is significantly reduced. This may result in a better imaging quality, as less superposition by other organs occurs. The very high accumulation in the kidneys for the other tracers is particularly noteworthy here. The therapeutic use of e.g [^{177}Lu]Lu-DOTAGA.SA.PSMA would significantly reduce radiation exposure for the patient in unaffected regions during treatment.

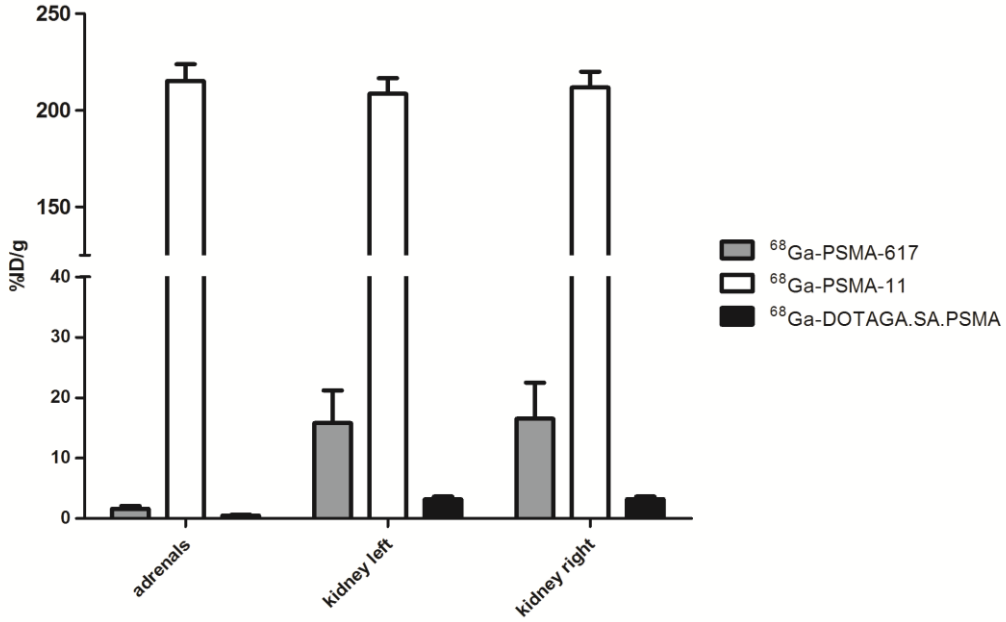

Figure 15: *ex vivo* biodistribution of [^{68}Ga]Ga-PSMA-617, [^{68}Ga]Ga-PSMA-11 and [^{68}Ga]Ga-DOTAGA.SA.PSMA, comparison of the %ID/g-values in the kidneys and adrenals. This diagram demonstrates that accumulation in all regions is significantly lowest in the [^{68}Ga]Ga-DOTAGA.SA.PSMA. Statistics are calculated with Student's t-test by GraphPad Prism 5. Significances are defined as **: P<0.01 and ***: P<0.001. Other, non-significant result are not labelled.

ex vivo and in vivo-blocking studies of [^{68}Ga]Ga-DOTAGA.SA.PSMA

To ensure the functionality of [^{68}Ga]Ga-DOTAGA.SA.PSMA additional blocking studies were conducted with 2-PMPA. This is a very affine inhibitor for the glutamate carboxypeptidase II, which is injected in a thousand-fold excess in addition to the tracer. Fig. 16 shows the results obtained from the *ex vivo* data. It is obvious that no enrichment of the tracer can be observed in the tumor under blocking conditions. Fig. 17 shows distinct and in accordance with the *ex vivo* dats that the uptake in the tumor region is significantly lower in the right image representing the blocking experiments. Additionally, uptake in the kidneys is reduced as well, which is also in accordance with *ex vivo* data. This result can be explained because 2-PMPA is known to accumulate in the kidneys preferring renal excretion. Even though the contrast of the bladder is very high, these images are quite conclusive about the functionality of [^{68}Ga]Ga-DOTAGA.SA.PSMA.

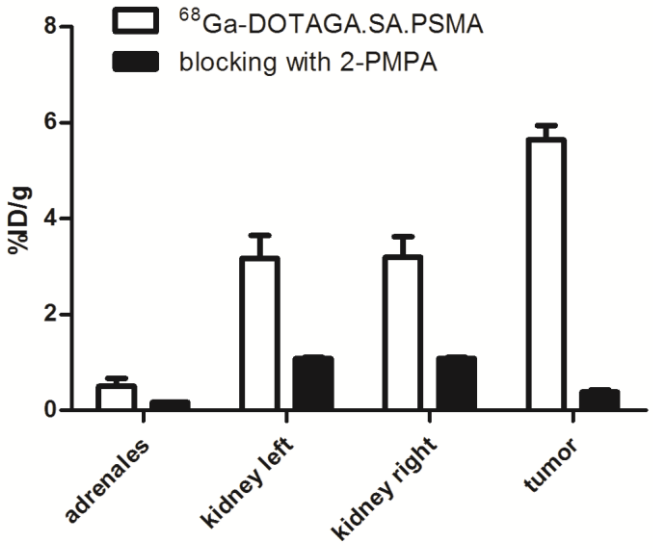

Fig 16: *ex vivo* data for the blocking studies of [^{68}Ga]Ga-DOTAGA.SA.PSMA. Blocking was performed using 2-PMPA. The graph clearly shows that the [^{68}Ga]Ga-DOTAGA.SA.PSMA can be actively blocked out of the active center of PSMA. Uptake in tumor and kidneys is significantly lower for the unblocked experiments

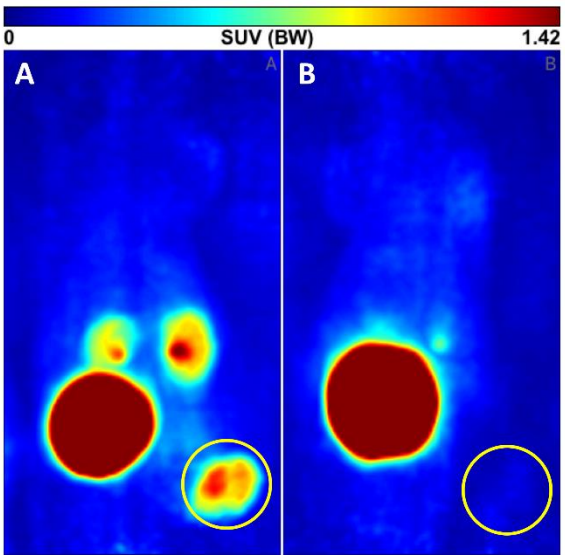

Fig. 17: Maximum intensity projections (midframe time 45 min p.i.) of PET studies with [^{68}Ga]Ga-DOTAGA.SA.PSMA in Rj:NMRI-*Foxn1*$^{nu/nu}$ mice with LNCaP tumors (yellow circle). (A) control unblocked; (B) complete uptake blocked by co-injection of 2-PMPA (10 mg/kg body weight).

in vivo-comparisson studies of [^{68}Ga]Ga-DOTAGA.SA.PSMA, [^{68}Ga]Ga-PSMA-11 and [^{68}Ga]Ga-PSMA-617

PET images of all three derivatives are shown in Fig. 18. They demonstrate that the SA-based KuE-tracer accumulates significantly in the tumor. From the *in vivo* PET data, an SUV value of 1.6 was obtained for this tracer in the tumor, which is comparable to data reported for e.g. ^{68}Ga-PSMA-617 in the literature (*32*). However, the significantly lower off-target enrichment is easy to detect from the images. As already proven from *ex vivo* data, the [^{68}Ga]Ga-DOTAGA.SA.PSMA derivative shows a reduced uptake in the kidneys. The SUV´s determined from the images show a significantly lower uptake for the SA-derivative in the kidneys compared to the [^{68}Ga]Ga-PSMA-617. The SUV for [^{68}Ga]Ga-PSMA-11 and the SA-derivative show nearly the same value, even if the SUV is quite difficult to use as a reference here, since the strong accumulation of activity in the bladder outshines the entire picture. It can be generalized that [^{68}Ga]Ga-DOTAGA.SA.PSMA produces an image quality comparable to [^{68}Ga]Ga-PSMA-617. Both compounds are clearly superior in relation to the off target accumulation to the [^{68}Ga]Ga-PSMA-11. In addition, radiation exposure in all organs is reduced, which is in line with the *ex vivo* data.

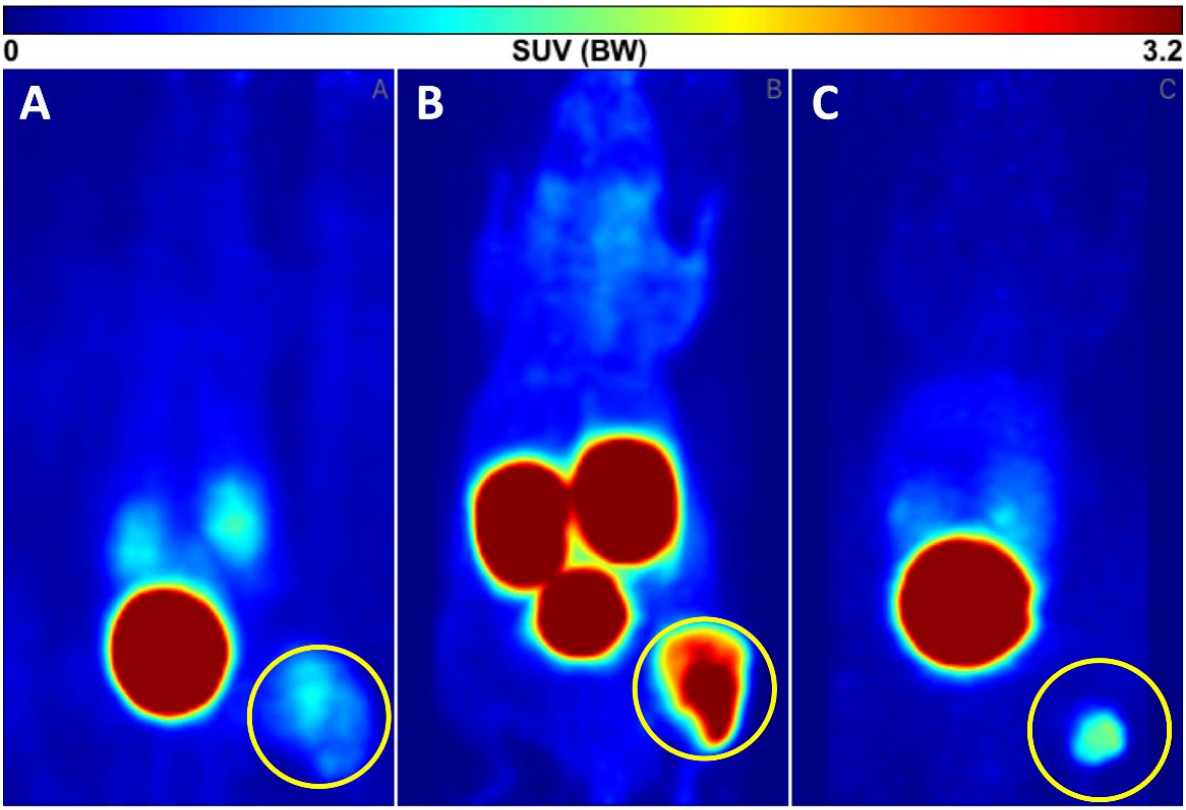

Fig. 18: Maximum intensity projections (midframe time 45 min p.i.) of PET studies with [^{68}Ga]Ga-DOTAGA.SA.PSMA, [^{68}Ga]Ga-PSMA-11 (B), [^{68}Ga]Ga-PSMA-617(C) in Rj:NMRI-*Foxn1*$^{nu/nu}$ mice with LNCaP tumors (yellow circle).

Discussion

Three novel SA-conjugates of the PSMA inhibitor KuE have been synthesized. Preparative organic synthesis proofed the advantage of the squaric acid chemistry.

Synthesis of the new tracers were carried out in an easy straight forward reaction with good yields and easy work up. The strategy of SADE is easy to use and transferable to any system. Additionally the synthesis of the targeting molecule was shortened by using three steps less compared to the established procedure for PSMA-617 resulting in an easier synthesis with more gentle conditions (*33*).

Radiolabeling with ^{68}Ga was completed quantitatively at 95° C for all tracers. Only the labeling of NODAGA.SA.PSMA and PSMA-11 were possible at lower temperatures. All complexes were furthermore stable in HS and PBS over a period of 2 h which enables them for *in vivo* studies.

Further *in vivo* and *ex vivo* studies were evaluation were carried out with LNCaP tumor bearing mice. All three newly designed tracers showed good tumor uptake in LNCaP tumor bearing mice in the *ex vivo* studies with 3.48±0.35, 5.64±0.29 and 5.59±.039 %ID/g for [^{68}Ga]Ga-NODAGA.SA.PSMA, [^{68}Ga]Ga-DOTAGA.SA.PSMA and [^{68}Ga]Ga-TRAM.SA.PSMA. In contrast to that [^{68}Ga]Ga-PSMA-11 and [^{68}Ga]Ga-PSMA-617 reached values of 12.75±2.49 and 6.51±0.98 %ID/G, respectively. Comparing the values it shows that the DOTAGA as well as the TRAM derivative appear to be in the same region as the PSMA-617 indicating that the SA unit not only works as a coupling species but also serves as a pharmacophore part of the molecule. Looking at the accumulations of the *ex vivo* studies in other organs, it can be seen that not only good values in the tumor can be observed, but also significantly lower accumulations in the kidneys and in the adrenals 1 hour after injection. This fact is very interesting especially with regard to a theranostic application because the corresponding [^{68}Ga]Ga-DOTAGA.SA derivative can also be labeled with ^{177}Lu or other therapeutic nuclides.

In particular [^{68}Ga]Ga-DOTAGA.SA.PSMA, the most potent designed molecule, was compared to state of the art tracer [^{68}Ga]Ga-PSMA-11 and [^{68}Ga]Ga-PSMA-617 in *in vivo* and *ex vivo* studies.

Therefore in addition to the *ex vivo* studies small animal PET studies were performed comparing [^{68}Ga]Ga-PSMA-11 and [^{68}Ga]Ga-PSMA-617 to the most promising candidate [^{68}Ga]Ga-DOTAGA.SA.PSMA. The uptake in the tumors was specific, reaching comparable values and following similar kinetics for all of the three tracers. The tumor uptake of [^{68}Ga]Ga DOTAGA.SA.PSMA was additionally blocked by 2-PMPA demonstrating specific binding of the tracer. Even though the µPET data for [^{68}Ga]Ga-DOTAGA.SA.PSMA and [^{68}Ga]Ga-PSMA-617 show very similar results for SUV´s, the *ex vivo* data shows superiority of [^{68}Ga]Ga-DOTAGA.SA.PSMA compared to [^{68}Ga]Ga-PSMA-617 for all other interesting organs. This can be seen in particular in the kidneys. The [^{68}Ga]Ga-DOTAGA.SA.PSMA derivative has a value of 3.18±0.45 %ID/g, the [^{68}Ga]Ga-PSMA-617 has a value of 16.2±5.7%ID/g and the [^{68}Ga]Ga-PSMA-11 even has a value of 210.8±8.1%ID/g. This effect can also be observed in the liver. Here, the *ex vivo* data show higher values for [^{68}Ga]Ga-PSMA-617 and [^{68}Ga]Ga-PSMA-11. This fact is also confirmed by the *in vivo* images resulting in a better imaging contrast for the [^{68}Ga]Ga-DOTAGA.SA.PSMA derivative.

Conclusion

It has been shown that all three new squaric acid-conjugated KuE derivatives can be synthesized in easy, straight forward synthesis without any difficulties. In addition, for all these chelators employed, all derivatives were labeled with ^{68}Ga under common conditions. The SA.PSMA compounds all demonstrated good stability in PBS and HS.

The small animal studies showed that [^{68}Ga]Ga-DOTAGA.SA.PSMA is comparable and in some perspective superior to[^{68}Ga]Ga-PSMA-617 and [^{68}Ga]Ga-PSMA-11 for the visualization of prostate cancer. Furthermore, the [^{68}Ga]Ga-DOTAGA.SA.PSMA represents a promising molecule for visualization and treatment of prostate cancer. From chemistry point of view this study highlights the potential that squaric acid has, combing the easy synthesis and improved pharmacology. Accordingly, we will continue to apply the SA.PSMA constructs to different chelates and to different nuclides and try to apply the SA strategy to different applications.

Experimental

L-lysin-urea-L-glutamate (KuE)

H-Glu(*t*Bu)-O*t*Bu (0.9 g; 3 mmol; 10 eq.) was dissolved with DIPEA (1.5 g; 2 mL; 12 mmol; 40 eq.) in dry DCM (200 mL). Triphosgene (300 mg; 1 mmol; 3.3 eq.) was then added dropwise to this solution in dry DCM (10 mL) at 0°C for 4 hours. After addition, the solution was stirred for 1 h at RT. The solid phase (H-Lys(*t*Boc)-2CT polystyrene; 0.78 mmol/g; 390 mg; 0.3 mmol; 1 eq.) was allowed to react with DCM (4 mL) for 45 min and then added to the reaction solution. The mixture was then stirred for 16 h at RT. The solid phase was then separated from the solution by filtration and washed with DCM. The raw product was then separated from the solid phase with TFA (3×7 mL, 10 min, RT). After removing the solvents in a vacuum, the raw product was purified using semi-preparative HPLC (column: Phenomenex Luna C18 (250 x 10 mm) 10 µm; flow rate: 5 mL/min; solvent: H_2O/MeCN +0.1 % TFA; gradient: 0-5 % MeCN in 20 min; Rt = 8.8 min). After lyophilisation, the product KuE (79 mg; 248 µmol; 83 %) was obtained as colourless oil.

MS (ESI positiv): m/z (%): 320.2 $[M+H]^+$; 639.3 $[2M+H]^+$; [M] calculated: 319.14.
UPLC (Gradient: 0-30 % B in 4 min): Rt = 0.47 min.
^{1}H-NMR (300 MHz, D_2O): δ (ppm) = 1.37-1.52 (m: 2H; NH2-CH2-CH2-C*H2*); 1.59-1.78 (m: 3H; NH2-CH2-C*H2*-CH2-C*H*H‘); 1.80-2.03 (m: 2H; NH2-CH2-CH2-CH2-CH*H*‘, HOOC-CH2-C*H*H‘); 2.09-2.23 (m: 1H; HOOC-CH2-CH*H*‘); 2.50 (t: 2H; J3HH = 7.3 Hz; C*H2*-COOH); 2.98 (t: 2H; J3HH = 7.5 Hz; C*H2*-NH2); 4.14-4.28 (m: 2H; C*H*).

2,2',2''-(10-(1-Carboxy-4-(2-(2-ethoxy-3,4-dioxocyclobut-1-enylamino)ethylamino)-4-oxobutyl)-1,4,7,10-tetraazacyclododecane-1,4,7-triacetic acid (DOTAGA.SA)

NH_2-DOTAGA (30 mg; 58 µmol; 1 eq.) and square acid diethyl ester (26 µL; 30 mg 176 µmol; 3 eq.) were dissolved in phosphate buffer (0.5 M; pH 7; 0.5 mL) and stirred for 2 h at RT. The pH value of the reaction was controlled and, if necessary, adjusted to pH 7-7.5 with sodium hydroxide solution (1 M). The product DOTAGA.SA (28 mg; 43.5 µmol; 75 %) was isolated by semi-preparative HPLC (column: Phenomenex Luna C18 (250 x 10 mm) 10 µm; flow rate: 5 mL/min; solvent: H_2O/MeCN +0.1 % TFA; gradient: 0-18 % MeCN in 15 min; Rt = 13 min) and obtained as a colorless solid after lyophilization.

MS (ESI positiv): m/z (%): 322.2 $[M+2H]^{2+}$; 643,3 $[M+H]^{+}$; [M] calculated: 642.29;
UPLC (Gradient: 0-100 % B in 15 min): [M] Rt = 3.01 min.
^{1}H-NMR (600 MHz, D_2O): δ (ppm) = 1.30 (dt: 3H, J3HH = 7.1 Hz; J = 12 Hz; C*H3*); 1.81 (br: 2H; C*H2*); 2.37 (br: 2H; C*H2*); 2.77-3.99 (m: 27H); 4.58 (dq: 2H; J3HH = 7.1 Hz; J = 21 Hz; C*H2*-CH3). ^{13}C-NMR (151 MHz, D_2O): δ (ppm) = 15,01 (*C*H3); 33,04 (*C*H2-*C*H2); 39,45 (*C*H2-*C*H2); 39,45 (*C*H2-*C*H2); 39,75 (*C*H2-*C*H2); 43,62 (*C*H2-*C*H2); 43,80 (*C*H2-*C*H2); 55,05 (*C*H2); (70,64 (*C*H2-CH3); 113,32 (*C*OOH); 115,26 (*C*OOH); 117,19 (*C*OOH); 119,12 (*C*OOH); 162,54 (*C*H2); 162,78 (*C*H2); 163,25 (*C*H2); 173,74 (*C*O-NH); 176,75 (*C*QS); 177,22 (*C*QS); 183,34 (*C*QS); 188,72 (*C*QS).

2,2',2''-(10-(1-Carboxy-4-(2-(L-Lysin-Urea-L-Glutamin)3,4-dioxocyclobut-1-enylamino)ethylamino)-4-oxobutyl)-1,4,7,10-tetraazacyclododecane-1,4,7- triacetic acid (DOTAGA.SA.PSMA)

DOTAGA.SA (20 mg; 31 µmol; 1 eq.) was dissolved with KuE (10 mg; 31 µmol; 1 eq.) in phosphate buffer (0.5 M; pH 9; 1 mL) and stirred for 24 h. The pH value of the reaction was controlled and, if necessary, adjusted to pH 9-9.5 with sodium hydroxide solution (1 M). The product DOTAGA.SA.PSMA (11.2 mg; 12.2 µmol; 39 %) was isolated using semi-preparative HPLC (column: Phenomenex Luna C18 (250 x 10 mm) 10 µm; flow rate: 5 mL/min; solvent: H_2O/MeCN +0.2 % TFA; isocratic: 8 % MeCN; Rt = 14.5 min) and obtained as a colorless solid after lyophilization.

MS (ESI positiv): m/z (%): 458.7 (45) $[M+2H]^{2+}$; 916.2 (100) $[M+H]^{2+}$; [M] calculated: 915.38;
UPLC (Gradient: 0-100 % B in 15 min): [M] Rt = 3.24 min.
^{1}H-NMR (300 MHz, D_2O): δ (ppm) = 1.36-1.51 (m: 2H; NH-CH2-CH2-C*H2*); 1.56-1.68 (m: 2H; NH-CH2-C*H2*-CH2); 1.69-1.83 (m: 1H; NH2-CH2-CH2-CH2-C*H*H‘); 1.84-2.02 (m: 4H; NH2-CH2-CH2-CH2-CH*H*‘, HOOC-CH2-C*H*H‘,C*H2*); 2.08-2.24 (m: 1H; HOOC-CH2-CH*H*‘); 2.38-2.54 (m: 4H; C*H2*); 2.84-4.09 (m: 29H); 4.14-4.28 (m: 2H; C*H*).

1,4,7-Triazacyclononan-1,4,7-tris(methyl(1-(2-ethoxy-3,4-dioxocyclobut-1-enylamino)-15-oxo-4,7,10-trioxa-14-azaheptadecan-17-yl)-phosphinic acid) (TRAM.SA)

TRAM (38 mg; 32 µmol; 1 eq.) and square acid diethyl ester (43 µL; 49.5 mg 290 µmol; 9 eq.) were dissolved in phosphate buffer (0.5 M; pH 7; 0.5 mL) and stirred for 36 h at RT. The pH value of the reaction was controlled and, if necessary, adjusted to pH 7-7.5 with sodium hydroxide solution (1 M). By semi-preparative HPLC (column: Phenomenex Luna C18 (250 x 10 mm) 10 µm; flow rate: 5 mL/min; solvent: H_2O/MeCN +0.1 % TFA; gradient: 27-30 % MeCN in 14 min; Rt = 11 min) the product TRAM.SA (10 mg; 6.5 µmol; 20 %) was isolated and after lyophilization obtained as colourless oil.

MS (ESI positiv): m/z (%): 520.4 (25) $[M+3H]^{3+}$; 779.8 (100) $[M+2H]^{2+}$; 1559.5 (10) $[M+H]^{+}$; [M] calculated: 1558.58;

UPLC (Gradient: 0-100 % B in 15 min): [M] Rt = 6.50 min

^{1}H-NMR (600 MHz, D_2O): δ (ppm) = 1.31 (dt: 9H; J3HH = 7 Hz; J = 13.6 Hz; C*H3*); 1.65 (dt: 6H; J3HH = 6.54 Hz; J = 13.2 Hz; CH2-C*H2*-CH2); 1.76 (dt: 6H; J3HH = 6.54 Hz; J = 13.2 Hz; CH2-C*H2*-CH2); 1.79-1,87 (m: 6H; C*H2*-CO); 2.33 (dt: 6H; J3HH = 10 Hz; J2PH = 6.6 Hz; P-C*H2*-CH2); 3.11 (t: 6H; J3HH = 6.54 Hz; CO-NH-C*H2*); 3.21 (d: 6H; J2PH = 5 Hz; N-C*H2*-P); 3.34 (s: 12H; ring-C*H2*); 3.41-3.56 (m: 42H); 4.59 (dq: 2H; J3HH = 7.1 Hz; J = 24.6 Hz; C*H2*-CH3).

^{13}C-NMR (151 MHz, D_2O): δ (ppm) = 15.03 (*C*H3); 25.67 (*C*H2-CO); 28.17 (P-*C*H2-CH2); 29.49 (CH2-*C*H2-CH2); 36.41 (CO-NH-*C*H2); 41.69 (CH2-*C*H2-NH); 51.29 (ring- *C*H2); 54.01 (N-*C*H2-P); 68.23 (*C*H2-*C*H2-O); 69.28 (*C*H2-*C*H2-O); 69.54 (*C*H2-*C*H2-O); 70.47 (*C*H2-CH3); 173.22 (*C*O-NH); 174.59 (*C*QS); 177.01 (*C*QS); 182.93 (*C*QS); 188.79 (*C*QS).

2,2'-(7-(1-Carboxy-4-(2-(2-ethoxy-3,4-dioxocyclobut-1-enylamino)ethylamino)-4-oxobutyl)-1,4,7-triazacyclononane-1,4-diacetic acid (NODAGA.SA)

NH_2-NODAGA (5 mg; 12 µmol; 1 eq.) and squaric acid diethyl ester (9 µL; 10 mg 60 µmol; 5 eq.) were dissolved in phosphate buffer (0.5 M; pH 7; 0.5 mL) and stirred for 2 h at RT. The pH value of the reaction was controlled and, if necessary, adjusted to pH 7-7.5 with sodium hydroxide solution (1 M). The product NODAGA.SA (6 mg; 11 µmol; 93 %) was isolated by semi-preparative HPLC (column: Phenomenex Luna C18 (250 x 10 mm) 10 µm; flow rate: 5 mL/min; solvent: H_2O/MeCN +0.1 % TFA; gradient: 0-30 % MeCN in 20 min; Rt = 13.1 min) and obtained as a colorless solid after lyophilization.

MS (ESI positiv): m/z (%): 542.2 $[M+H]^+$; 1084.3 $[2M+H]^+$; [M] calculated: 541,24;
UPLC (Gradient: 0-100 % B in 15 min): [M] Rt = 3.38 min
^{1}H-NMR (300 MHz, D_2O): δ (ppm) = 1.32 (dt: 3H, J3HH = 7 Hz; J = 7 Hz; C*H3*), 1.77-2.02 (m: 2H; C*H2*); 2.29 (dt; 2H; J3HH = 7.5 Hz; J3HH = 6.6 Hz; CH-C*H2*-CH2); 2.85-3.01 (m: 4H; cyclic-C*H2*); 3.02-3.22 (m: 8H; cyclic-C*H2*); 3.25-3.35 (m: 2H; C*H2*); 3.40-3.53 (m: 2H; C*H2*); 3.57-3.63 (m: 1H; C*H*); 3.78 (br: 4H; C*H2*-COOH); 4.61 (dq: 2H; J3HH = 7.1 Hz; J = 13 Hz; C*H2*-CH3).

1,4,7-Triazacyclononan-1,4,7-tris(methyl(1-(L-lysine-urea-L-glutamine-3,4-dioxocyclobut-1-enylamino)- 15-oxo-4,7,10-trioxa-14-azaheptadecan-17-yl)-phosphinic acid) (TRAM.SA.PSMA)

TRAM.SA (10 mg; 6.4 µmol; 1 eq.) was dissolved with KuE (6 mg; 19 µmol; 3 eq.) in phosphate buffer (0.5 M; pH 9; 1 mL) and stirred for 36 h. The pH value of the reaction was controlled and, if necessary, adjusted to pH 9-9.5 with sodium hydroxide solution (1 M). Using semi-preparative HPLC (column: Phenomenex Luna C18 (250 x 10 mm) 10 µm; flow rate: 5 mL/min; solvent: H_2O/MeCN +0.1 % TFA; gradient: 15-25 % MeCN in 20 min; Rt = 16.6 min) the product TRAM.SA.PSMA (3 mg; 1.3 µmol; 20 %) was isolated and obtained as a colourless solid after lyophilization.

MS (ESI positiv): m/z (%): 793.5 (70) $[M+3H]^{3+}$; 1189.9 (100) $[M+2H]^{2+}$; [M] calculated: 2376.99;

UPLC (Gradient: 0-100 % B in 15 min): [M] Rt = 5.25 min

((5-((2-((2-(4-(4,7-bis(carboxymethyl)-1,4,7-triazonan-1-yl)-4-carboxybutanamido)ethyl)amino)-3,4-dioxocyclobut-1-en-1-yl)amino)-1-carboxypentyl)carbamoyl)glutamic acid (NODAGA.SA.PSMA)

NODAGA.SA (6 mg; 1.1 µmol; 1 eq.) was dissolved with KuE (2 mg; 6.3 µmol; 1 eq.) in phosphate buffer (0.5 M; pH 9; 1 mL) and stirred for 36 h. The pH value of the reaction was controlled and, if necessary, adjusted to pH 9-9.5 with sodium hydroxide solution (1 M). Using semi-preparative HPLC (column: Phenomenex Luna C18 (250 x 10 mm) 10 µm; flow rate: 5 mL/min; solvent: H2O/MeCN +0.1 % TFA; gradient: 15-25 % MeCN in 20 min; Rt = 12.2 min) the product NODAGA.SA.PSMA (0.3 mg; 0.4 µmol; 27 %) was isolated and obtained as a colourless solid after lyophilization.

MS (ESI positiv): m/z (%): 758.3 $[M+H]^{+}$; [M] calculated:757.28;

UPLC (Gradient: 0-100 % B in 15 min): [M] Rt = 4.37 min.

References

1. Torre LA, Bray F, Siegel RL, Ferlay J, Lortet-Tieulent J, Jemal A. Global cancer statistics, 2012. *CA Cancer J Clin*. 2015;65:87-108.
2. Afshar-Oromieh A, Malcher A, Eder M, et al. PET imaging with a [^{68}Ga]gallium-labelled PSMA ligand for the diagnosis of prostate cancer: biodistribution in humans and first evaluation of tumour lesions. *Eur J Nucl Med Mol Imaging*. 2013;40:486-495..
3. Davidson PJ, van den Ouden D, Schroeder FH. Radical prostatectomy: prospective assessment of mortality and morbidity. *Eur Urol*. 1996;29:168-173.
4. Pillai MRA, Nanabala R, Joy A, Sasikumar A, Russ Knapp FF. Radiolabeled enzyme inhibitors and binding agents targeting PSMA: Effective theranostic tools for imaging and therapy of prostate cancer. *Nucl Med Biol*. 2016;43:692-720.
5. Silver DA, Pellicer I, Fair WR, Heston WD, Cordon-Cardo C. Prostate-specific membrane antigen expression in normal and malignant human tissues. *Clin Cancer Res*. 1997;3:81-85.
6. Perner S, Hofer MD, Kim R, et al. Prostate-specific membrane antigen expression as a predictor of prostate cancer progression. *Hum Pathol*. 2007;38:696-701.
7. Mosquera J-M, Perner S, Demichelis F, et al. Morphological features of TMPRSS2-ERG gene fusion prostate cancer. *J Pathol*. 2007;212:91-101.
8. Bařinka C, Rojas C, Slusher B, Pomper M. Glutamate carboxypeptidase II in diagnosis and treatment of neurologic disorders and prostate cancer. *Curr Med Chem*. 2012;19:856-870.
9. Wüstemann T, Bauder-Wüst U, Schäfer M, et al. Design of Internalizing PSMA-specific Glu-ureido-based Radiotherapeuticals. *Theranostics*. 2016;6:1085-1095.
10. Zhang AX, Murelli RP, Barinka C, et al. A remote arene-binding site on prostate specific membrane antigen revealed by antibody-recruiting small molecules. *J Am Chem Soc*. 2010;132:12711-12716.
11. Lütje S, Heskamp S, Cornelissen AS, et al. PSMA Ligands for Radionuclide Imaging and Therapy of Prostate Cancer: Clinical Status. *Theranostics*. 2015;5:1388-1401.
12. Witkowska-Patena E, Mazurek A, Dziuk M. ^{68}Ga-PSMA PET/CT imaging in recurrent prostate cancer: Where are we now? *Cent European J Urol*. 2017;70:37-43.
13. Kozikowski AP, Zhang J, Nan F, et al. Synthesis of urea-based inhibitors as active site probes of glutamate carboxypeptidase II: efficacy as analgesic agents. *J Med Chem*. 2004;47:1729-1738.
14. Eder M, Schäfer M, Bauder-Wüst U, et al. ^{68}Ga-Complex Lipophilicity and the Targeting Property of a Urea-Based PSMA Inhibitor for PET Imaging. *Bioconjugate Chem.* 2012;23:688-697.
15. Ian Storer R, Aciro C, Jones LH. Squaramides: physical properties, synthesis and applications. *Chem. Soc. Rev.* 2011;40:2330.
16. Neuse E, Green B. Amidierung von Quadratsäure-estern. *Justus Liebigs Ann. Chem.* 1973;1973:619-632.
17. Wurm FR, Klok H-A. Be squared: expanding the horizon of squaric acid-mediated conjugations. *Chem Soc Rev*. 2013;42:8220-8236.

18. Tietze LF, Arlt M, Beller M, Gl üsenkamp K-H, Jähde E, Rajewsky MF. Anticancer Agents, 15. Squaric Acid Diethyl Ester: A New Coupling Reagent for the Formation of Drug Biopolymer Conjugates. Synthesis of Squaric Acid Ester Amides and Diamides. *Chem. Ber.* 1991;124:1215-1221.
19. Quiñonero D, Frontera A, Ballester P, Deyà PM. A theoretical study of aromaticity in squaramide and oxocarbons. *Tetrahedron Letters*. 2000;41:2001-2005.
20. G. Davis B. Recent developments in glycoconjugates. *J. Chem. Soc., Perkin Trans. 1*. 1999:3215.
21. Gamblin DP, Scanlan EM, Davis BG. Glycoprotein synthesis: an update. *Chem Rev*. 2009;109:131-163.
22. Rudd SE, Roselt P, Cullinane C, Hicks RJ, Donnelly PS. A desferrioxamine B squaramide ester for the incorporation of zirconium-89 into antibodies. *Chem. Commun.* 2016;52:11889-11892.
23. Yoganathan S, Sit CS, Vederas JC. Chemical synthesis and biological evaluation of gallidermin-siderophore conjugates. *Org. Biomol. Chem.* 2011;9:2133.
24. Sato K, Seio K, Sekine M. Squaryl group as a new mimic of phosphate group in modified oligodeoxynucleotides: synthesis and properties of new oligodeoxynucleotide analogues containing an internucleotidic squaryldiamide linkage. *J Am Chem Soc*. 2002;124:12715-12724.
25. Rostami A, Colin A, Li XY, Chudzinski MG, Lough AJ, Taylor MS. N , N' -Diarylsquaramides: General, High-Yielding Synthesis and Applications in Colorimetric Anion Sensing. *J. Org. Chem.* 2010;75:3983-3992.
26. Lee C-W, Cao H, Ichiyama K, Rana TM. Design and synthesis of a novel peptidomimetic inhibitor of HIV-1 Tat–TAR interactions: Squaryldiamide as a new potential bioisostere of unsubstituted guanidine. *Bioorganic & Medicinal Chemistry Letters*. 2005;15:4243-4246.
27. Gauger J, Manecke G. Kondensationsprodukte der Quadratsäure mit primären und sekundären Aminen, II. *Chem. Ber.* 1970;103:3553-3562. d
28. Eder M, Schäfer M, Bauder-Wüst U. ^{68}Ga-complex lipophilicity and the targeting property of a urea-based PSMA inhibitor for PET imaging. *Bioconjug Chem*. 2012;23:688-697.
29. Cardinale J, Schäfer M, Benešová M, et al. Preclinical Evaluation of ^{18}F-PSMA-1007, a New Prostate-Specific Membrane Antigen Ligand for Prostate Cancer Imaging. *J Nucl Med*. 2017;58:425-431.
30. Benešová M, Schäfer M, Bauder-Wüst U, et al. Preclinical Evaluation of a Tailor-Made DOTA-Conjugated PSMA Inhibitor with Optimized Linker Moiety for Imaging and Endoradiotherapy of Prostate Cancer. *J Nucl Med*. 2015;56:914-920.
31. Afshar-Oromieh A, Malcher A, Eder M, et al. PET imaging with a [^{68}Ga]gallium-labelled PSMA ligand for the diagnosis of prostate cancer: biodistribution in humans and first evaluation of tumour lesions. *Eur J Nucl Med Mol Imaging*. 2013;40:486-495.
32. Benešová M, Bauder-Wüst U, Schäfer M, et al. Linker Modification Strategies To Control the Prostate-Specific Membrane Antigen (PSMA)-Targeting and Pharmacokinetic Properties of DOTA-Conjugated PSMA Inhibitors. *J Med Chem*. 2016;59:1761-1775.

33. Benešová M, Schäfer M, Bauder-Wüst U, et al. Preclinical Evaluation of a Tailor-Made DOTA-Conjugated PSMA Inhibitor with Optimized Linker Moiety for Imaging and Endoradiotherapy of Prostate Cancer. *J Nucl Med*. 2015;56:914-920.

Synthesis and labeling of a squaric acid containing PSMA-inhibitor coupled to AAZTA^{5} for versatile labeling with ^{68}Ga, ^{44}Sc, ^{177}Lu and ^{64}Cu

Lukas Greifenstein

Submitted to Applied Radiation and Isotopes, May 13, 2019

Abstract

Inhibitors of the PSMA became increasingly important over the last decades in nuclear medicine due to application for diagnosis and therapy of prostate cancer. Even if PSMA-11 and PSMA-617, the most prominent ones, are already used in clinical routine there is still a huge need for new, beneficial tracers making the molecules more accessible and easy to label for application as a kit. Most promising derivatives for an easy, straight forward room temperature labeling are hybrid chelates (DATA, AAZTA). Derivatives of those chelates were already used for different clinical applications and showed a good tolerance to a variety of nuclides. Combination of these molecules with a PSMA inhibitor would therefore be highly desirable. Herein the synthesis and the radiolabeling of hybrid coupled PSMA-inhibitor, AAZTA.SA.PSMA, is presented. Synthesis was performed in the already established way, additionally using squaric acid as connection motif on the chelate. This enables the chelate for a mild and efficient coupling. Radiolabeling was performed with ^{44}Sc, ^{64}Cu, ^{68}Ga and ^{177}Lu all producing excellent yield.

Introduction

Over the last few years, inhibitors of the prostate-specific membrane antigen (PSMA) have developed into one of the most important substance classes in nuclear medicine. PSMA, also known as glutamate carboxypeptidase II, is an enzyme that catalyzes the hydrolysis of N-acetylaspartyl glutamate to N-acetylaspertate. PSMA is well suited as a target because it is barely found in healthy tissue but shows overexpression in prostate cancer cells [1,2].This information has been used to develop a variety of radiopharmaceutical drugs over the last decade. Besides larger peptides and antibodies targeting PSMA, small molecules were successfully utilized for the diagnosis and treatment of prostate cancer. Those molecules typical have comparable structures to N-acetylaspartyl glutamate having a C-terminal glutamate for addressing the glutamate recognition area of PSMA [3-6]. Furthermore the glutamate has to be attached to a group, which is not cleavable by PSMA to ensure an intact molecule *in vivo*. These characteristics led to a large group of clinically relevant urea-based PSMA inhibitors. Most prominent examples of urea-based PSMA radiopharmaceuticals are PSMA-11 and PSMA-617 (see figure 1)[6,7]. The lead structure of these molecules is a glutamate-urea-lysine (KuE) motif that resembles the structure of N-acetylaspartyl glutamate. The further part of the molecule has variable parts. However, both molecules have a linker through, which a chelator is attached. It is noteworthy that both molecules contain aromatic groups, which have been proven to be beneficial regarding affinity. This is due to an additional pocket in the entrance funnel of the PSMA, which favors aromatic units [8]. The two PSMA molecules can be combined in a THERANOSTIC approach. For PET diagnosis of prostate cancer PSMA-11 can be labeled with ^{68}Ga. The containing HBED chelator can easily be labeled easily in a kit-type fashion at substance quantities of less than 1 nmol at room temperature. However, HBED can not complex therapeutic nuclides such as ^{177}Lu and is therefore not suitable for therapy. The PSMA-617 derivative carries a DOTA ligand and is used for this purpose. PSMA-617 can be labeled with therapeutic nuclides at elevated temperatures. It is also possible to label PSMA-617 with ^{68}Ga, but again elevated temperature is necessary and therefore no kit labeling is possible. Thus two molecules are necessary for efficient diagnostic and therapeutic use, whereby PSMA-11 is limited to ^{68}Ga use only. In addition, the synthesis of both derivatives is complex as both molecules have to be synthesized by multi-stage peptide synthesis. Ideal would be a derivative that has a

simple synthesis, the ability to complex a large number of nuclides under mild conditions and still offering comparable affinities.

An interesting attempt in this context are hybrid like chelators. In recent years, many chelators have been designed that combine the favorable properties of cyclic and acyclic chelators. Acyclic chelators are generally considered to be particularly fast in their kinetics for radio labeling and labeling is mostly temperature-independent. Negative properties are the low kinetic stability, which can be for example observed with EDTA or DTPA. In contrast to that macrocyclic chelators are particularly stable (compare DOTA), but require higher labeling temperatures and show slower kinetics. The hybrid chelators should now combine the positive properties in one structure [9]. In addition, some of them also show the properties to complex a variety of different radiometals.

One of the most promising approaches in this concept is the use of a diazepine backbone, which contributes two endocyclic amines to complexation. Introduction of another exocyclic amine provides a third coordination unit. A additional alkylation of these amines with carboxylic acid, three or four further donor units can be introduced and either the so-called DATA (6-amino-1,4-diazepine-triacetic acid) or AAZTA (6-amino-1,4-diazepine tetracetic acid) is obtained [10-12]. So far it is known that AAZTA has excellent properties for nuclides like scandium, gallium and lutetium but may also complex copper [11,13,14]. Both chelator classes complex the corresponding metals at room temperature and show very good stability.

Ligation chemistry of AAZTA is normally performed by attaching an amine to the carboxylic acid at the side arm via a typical peptide coupling reaction. Squaric acid diethyl ester (SADE) was additionally used in this study to simplify the synthesis and make possible intermediate products more stable.

Coupling by SADE makes synthetic procedures very easy. For instance, challenging protection group chemistry when coupling with other coupling reagents is not necessary. Furthermore, SADE offers the possibility of selective coupling of two amines. This is done by a stepwise, pH-dependent, asymmetric amidation of the diester under mild conditions, both in aqueous buffers or in organic solvents [15]. This stepwise pH-dependent course of the reaction is possible because of the change of the grade of aromaticity during the reaction.

This selectivity results in an enormous advantage of coupling by means of SADE. In contrast to alkynes and azides for azide-alkyne cycloaddition reactions, amines are present in many biomolecules and do not have to be introduced into the molecule with synthetic effort (see KuE).

Another positive property is that the monoamine intermediate is stable and can be isolated. This results in a squaric acid monoester (SAME), which can bind to amines. Furthermore, SAMEs are stable in solution at pH 9 for several days in contrast to e.g. N-hydroxy succinimide (NHS). NHS esters hydrolyse already after minutes under the same conditions. These positive properties are used in several fields of organic chemistry for example to couple carbohydrates to proteins[16,17] but interestingly, despite the well-known properties of squaric acid (SA) the use of this strategy in radiopharmaceutical chemistry is still limited. Only few examples of using SA to connect bioactive molecules to chelators for the use in nuclear imaging are known. However, the ones reported used SA to link proteins or antibodies to the chelator desferrioxamine (DFO), which has a peptide like structure [18,19].

In this study, we present a potential PSMA inhibitor (KuE) coupled to an AAZTA ligand with a squaric acid motif, which enables very mild and simple synthesis as well as labeling.
Additional, SA is an aromatic moiety and may have positive impact regarding the affinity by binding to the arene-binding side of PSMA. Radiochemical experiments were conducted with ^{68}Ga, ^{44}Sc, ^{64}Cu and ^{177}Lu.

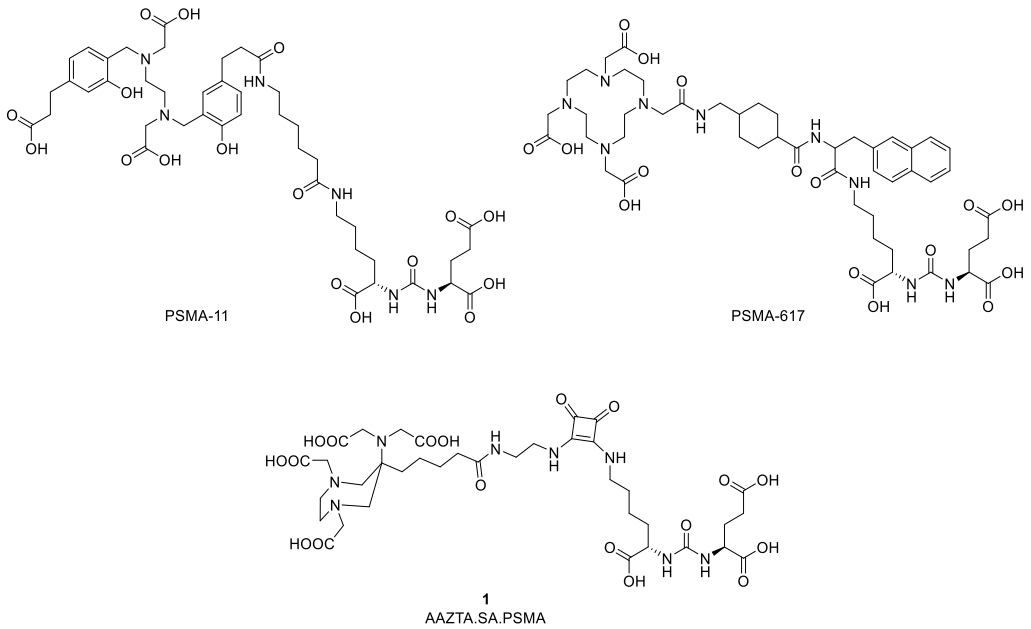

Figure 1: Schematic representation of different PSMA inhibitors for nuclear medicine applications. Top: The two standardly used derivatives PSMA-11 and PSMA-617. PSMA-11 contains a HBED ligand which is excellent for complexation of ^{68}Ga, but cannot complex further metals. PSMA-617 on the other hand has a DOTA ligand which is very versatile, but requires increased temperatures for labeling. Bottom: AAZTA.SA.PSMA, square acid mediated PSMA inhibitor using AAZTA as ligand. This ligand is very versatile and can label a variety of different metals at ambient temperatures.

Materials and Methodes

Synthetic part

Synthesis of the AAZTA.SA.PSMA

One of the interesting benefits of using SADE is the simplification of synthesis strategy. Application to any conceivable system is feasible in two steps without further complications. SADE has the ability to react selectively with amines. Thus, no sophisticated protective group chemistry is required for coupling. Furthermore, the coupling of the chelating component and the PSMA component is pH-controlled. A one-step synthesis of the KuE precursors is carried out.

The PSMA inhibitor lysine-urea-glutamic acid (KuE) is synthesized via solid phase peptide synthesis methods according to literature [20,21]. Since the linker function of the final compound is located on the chelator and no further reactions at the side chain of the lysine at the solid phase have to be carried out, the amino acids are not protected as usual with an orthogonal protective group, but with an acid-labile tert-butyl ester. This is an advantage compared to the standard protocol.

For the synthesis the protected glutamic acid (2) is reacted with triphosgene in the presence of *N,N*-Diisopropylethylamine (DIPEA) in dry dichloromethane (DCM) yielding the isocyanate. This is coupled to the solid phase bound lysine (3) yielding the urea containing motif. The product is cleaved from the solid phase and simultaneously completely deprotected in one step with trifluoroacetic acid (TFA). After removal of the TFA the product is separated from remaining free lysine using semi-preparative HPLC yielding KuE. Several things have to be considered during this synthesis in order to achieve good yields. On the one hand, the reaction must be kept at 0°C during the entire reaction time. Even a few degrees above can significantly reduce the yield. On the other hand, the drop speed of the triphosgene has to be very slow. If the triphosgene is added too quickly, the yield can be reduced by up to 80 %. KuE was then coupled to SADE in 0.5 M phosphate buffer at pH 7 yielding KuE.SA (6).

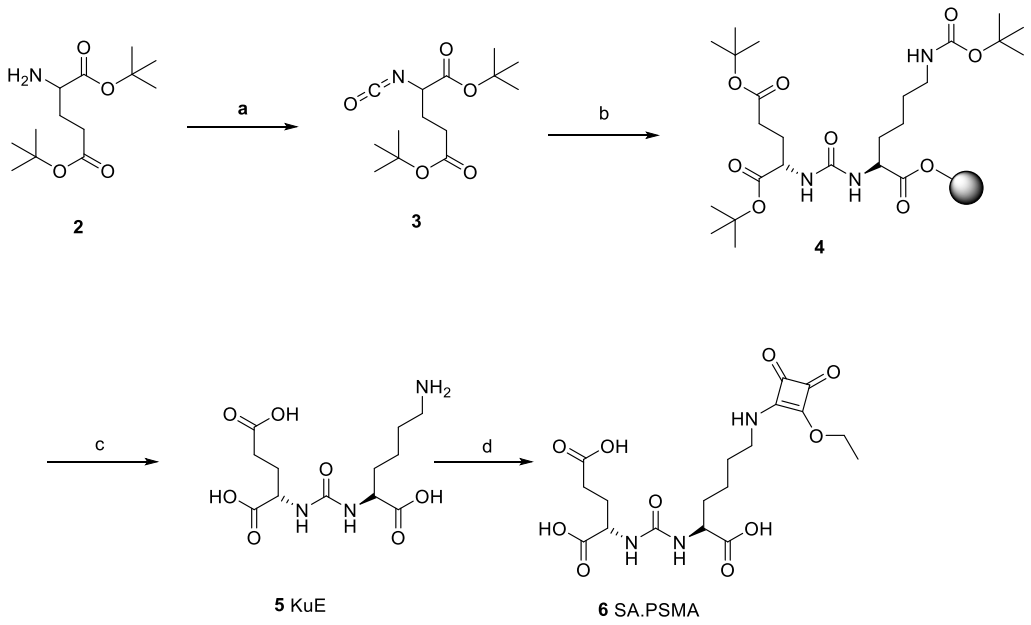

Figure 2: Solid phase synthesis of the PSMA inhibitor. a) DIPEA, triphosgene, DCM, 0°C, 4 h; b) H-Lys(tBoc)-2CT polystyrene Solid phase, DCM, RT, 16 h; c) TFA, RT, 71 %; d) 0.5 M phosphate buffer pH 7, RT, 16 h, 23 %.

For the synthesis of AAZTA.SA.PSMA, AAZTA^5(*t*Bu)$_4$ was prepared according to the sequence shown in figure 3. *N,N'*-dibenzylethylenediamine was used as starting reagent. The amine was alkylated twice with *tert*-butyl bromoacetate. The resulting product was then reduced with palladium on activated carbon and hydrogen to product (8) to remove the benzyl groups of the protected amino groups.

A double Nitro-Mannich reaction with paraformaldehyde and 2-nitrocyclohexanone led to ring closure and formation of diazepane (9). The added anion exchanger Amberlyst® A21 initiated the *in situ* ring cleavage of the 2-nitrocyclohexanone, whereupon the Nitro-Mannich reaction could proceed.

After reducing the nitro group with Raney® nickel and hydrogen, the resulting amine was converted to product (10) with *tert*-butyl bromoacetate. In order to functionalize AAZTA^5, the methyl ester was cleaved with LiOH. The resulting AAZTA^5(*t*Bu)$_4$ could be synthesized in a total yield of 16 % by 6-stage synthesis. Since the acid group of AAZTA^5(tBu)$_4$ can not be coupled directly to squaric acid diethyl ester, a linker had to be introduced, which provides a terminal amino group for coupling with squaric acid. This was done via *tert* butyl(2-aminoethyl)carbamate, DIPEA as base and HATU as coupling reagent resulting in product

(11). After deptotection using TFA (product 12), the squaric acid coupled target vector KuE.SA (6) was attached to the diaminoethylene linker via asymmetric amidation. The coupling is carried out in phosphate buffer at pH 9 to yield the final product (1). It is noteworthy that in contrast to typical synthesis for chelators containing molecules, no final deprotection with TFA or other reactive deprotection reagents is necessary.

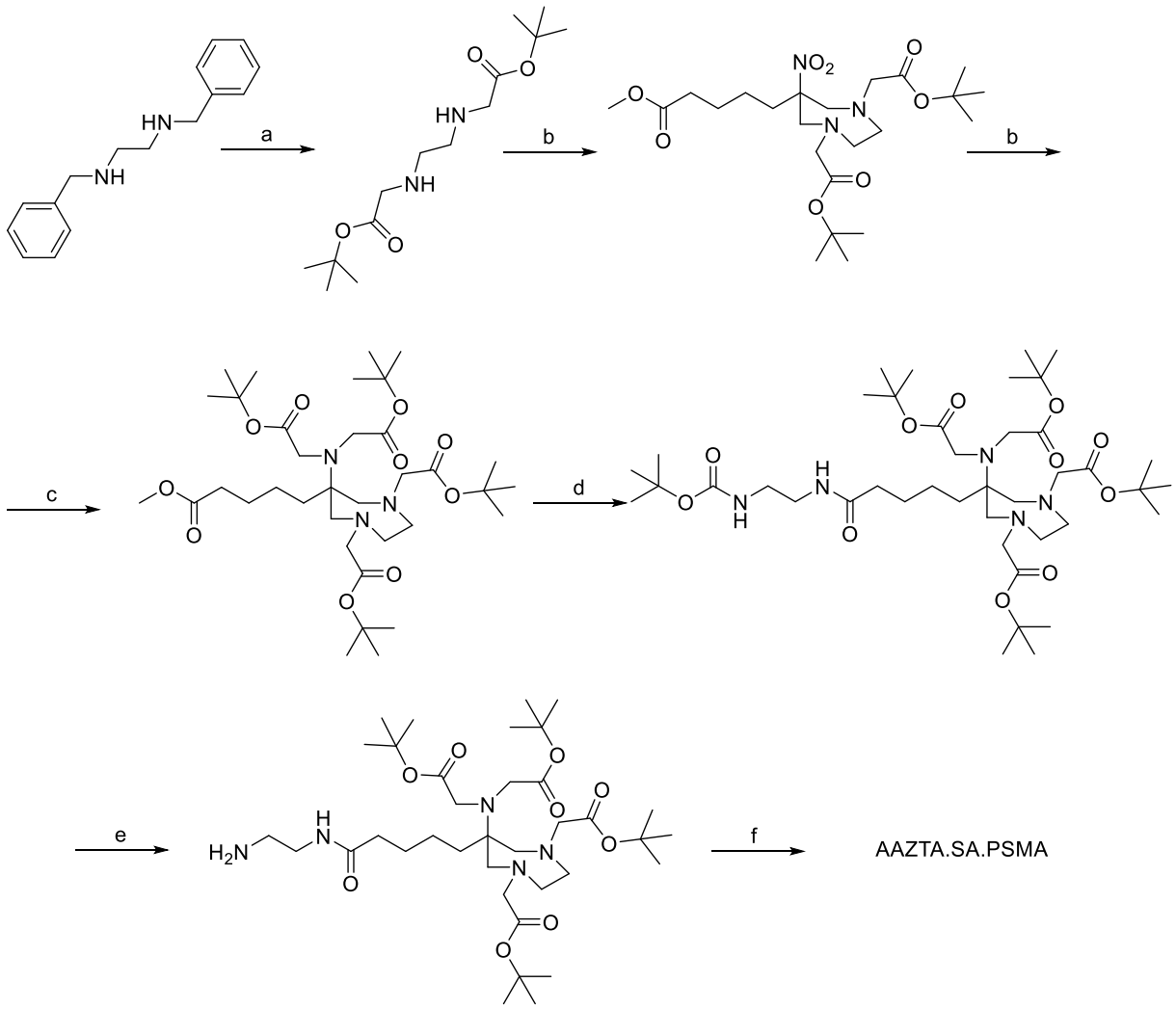

Figure 3: Synthesis of AAZTA^5(tBu)$_4$. a) i) *tert*-butyl bromoacetate, Na_2CO_3, MeCN, 90 °C, 16 h, 96 %; ii) Pd/C, H_2, formic acid, EtOH, RT, 1 d, 98 %; b) 2-Nitrocyclohexanone, Amberlyst® A21, paraformaldeyde, MeOH, 90 °C, 16 h, 77 %; c) i) Raney®-nickel, H_2, EtOH, 40 °C, 4 d, 72 %; ii) tert-butyl bromoacetate, DIPEA, MeCN, RT, 7 d, 36 %; d) i) LiOH, dioxane/water, RT, 6 h, 82 %; ii) *tert*-butyl(2-aminoethyl)carbamate, HATU, DIPEA, MeCN, RT, 1h, 64 %; e) TFA/DCM, RT, 24 h; 98 % f) 6,0.5 M phosphate buffer pH 9, RT, 16h, 29%. It is noteworthy that molecule 12 was never isolated but only appeared as an intermediate product.

Radiolabeling

For radiochemical evaluation with ^{68}Ga, a ^{68}Ge/^{68}Ga generator (TiO_2-based matrix, Cyclotron Co. Obninsk, Russia) was used with ongoing acetone post-processing separating iron and zinc impurities as well as ^{68}Ge breakthrough [22,23]. Radiolabeling with ^{44}Sc was performed with a ^{44}Sc/^{44}Ti generator located at the Institute of Nuclear Chemistry in Mainz [24-26]. The ^{177}Lu was provided by ITG Munich following the carrier-free production pathway ^{176}Yb(n,γ)^{177}Yb → ^{177}Lu [27]. [^{64}Cu]$CuCl_2$ was purchased from Universitätsklinikum Tübingen and was supplied in 20-50 µL of 0.1 M HCl solution with 200-350 MBq activity. This solution was diluted with 0.1 M HCl to a total concentration of 2 MBq/µL.

Labeling was performed in 1 ml of 0.2 M ammonium acetate buffer pH 4.5 or in 0.5 M HEPES buffer pH 4.5. Reactions were carried out at room temperature 25 °C. Labeling kinetics were recorded with precursor amounts of 10, 15 and/or 20 nmol. Kinetic studies were done with 30 MBq of the corresponding nuclide. Aliquot were taken at different time points of 1, 3, 5, 10 and 15 minutes. The pH was controlled at start of labeling and after labeling was finished. For reaction control TLC with 0.1 M citrate buffer, pH 4, as eluent and radio HPLC (Merck Chromolith® RP-18e-column, Water : MeCN with 0.1 % TFA, 5 to 95 % MeCN in 10 min) was used. TLC´s were measured in RITA TLC imager (Elysia Raytest). Radio HPLC was used to exclude the presence of colloidal radio metals not visible on TLC.

Stability studies

Stability studies were performed in HS and PBS solution (pH adjusted to 7 by PBS buffer) in triplicate. HS (human male AB plasma, USA origin) were bought from Sigma Aldrich, phosphate buffered saline (PBS) pH 7.4 was purchased from Sigma Aldrich as well. Final procedure used 50 - 70 µl of the labeling solution added to 1 ml of stability solution. The pH was controlled to ensure no influence of the labeling buffer on the stability solution.

Results

Synthesis of AAZTA.SA.PSMA

AAZTA[5] was synthesized according to literature [11]. Furthermore a successful transformation to a free amine for coupling with SADE was carried out using 2 more steps. Coupling of the SA.PSMA unit was carried out according to literature [28] achieving sufficient yields and easy purification via HPLC. For the last step it is noteworthy that recalibration of the pH needs to be watched very carefully because the buffer area of phosphate buffer is at a different pH than the reaction is performed. This is done with 0.1 M and 1 M NaOH depending on the pH drops. In total, synthesis of AAZTA.SA.PSMA was carried out in a 11 step synthesis with overall yield of 3 % afer efficient purification using HPLC.

Radiochemical Evaluation with ^{68}Ga

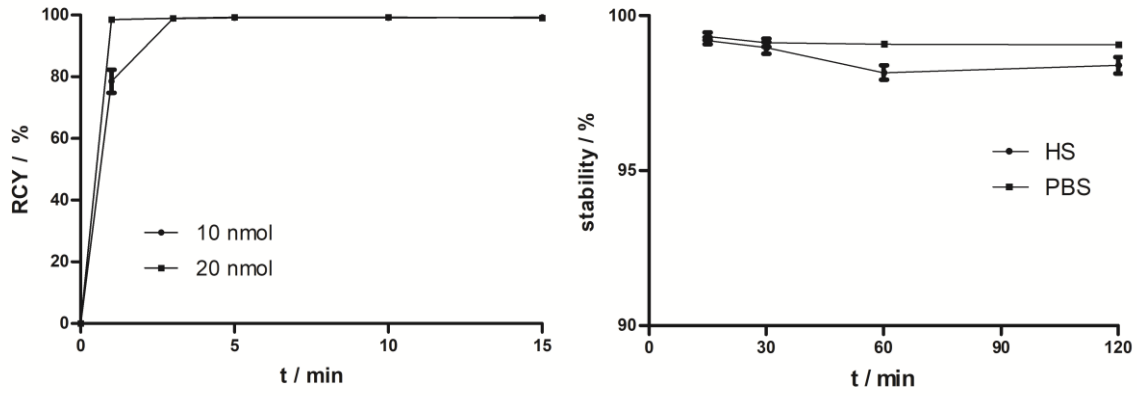

Figure 4: Labeling of AAZTA.SA.PSMA with ^{68}Ga. Left: Kinetic of different labeling amount labeled with 30 MBq ^{68}Ga in 0.2 M ammonium acetate buffer (pH 4.5). Both amounts show quantitative labeling after 3 minutes. Right: Stability studies in human serum and PBS buffer (pH = 7.4) at 37°C. The derivative shows more than 95% stability over a period of 2h.

The ^{68}Ga used for labeling was obtained using a ^{68}Ge/^{68}Ga-generator with subsequent post-processing. Labeling was performed in 0.2 M ammonium acetate buffer (pH 4.5) at room temperature for 15 minutes. For the ^{68}Ga-complex of (1) radiolabeling showed quantitative labeling yields of >95 % in less than 5 minutes for 10 nmol as well as for 20 nmol. At 20 nmol

the reactions reaches quantitative yields within 1 minute. For 10 nmol the reaction shows a slightly slower kinetic but reaches labeling yields of >95 % as well. Because both amounts yielded comparable yields after 15 min 10 nmol was chosen for subsequent stability studies.

Stabilities of [^{68}Ga]Ga-(1) were tested against PBS (pH 7.4) and HS at 37°C for 2 h. The derivative showed stabilities of more than 99 % in PBS buffer over 2 h. Stabilities in HS appeared to be slightly lower but still over 98 % after 2 h.

Radiochemical Evaluation with ^{44}Sc

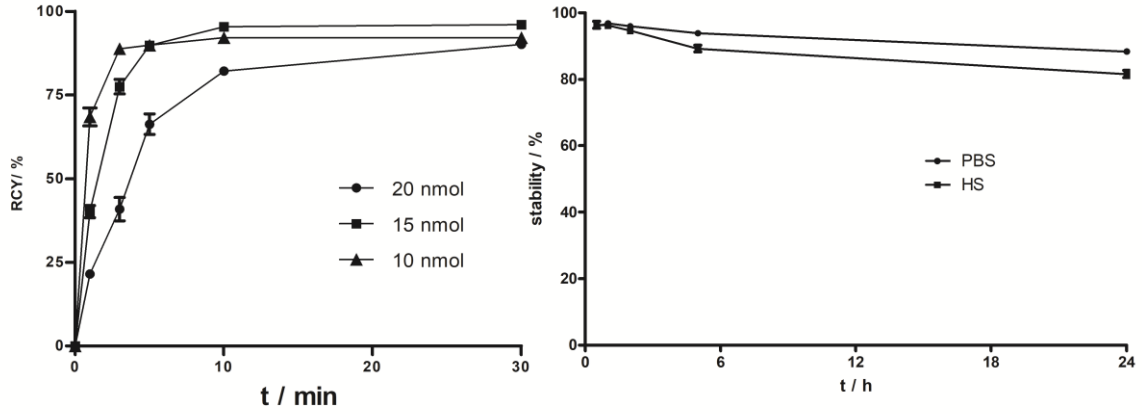

Figure 5: Labeling of AAZTA.SA.PSMA with ^{44}Sc. Left: Kinetic of different labeling amount labeled with 30 MBq ^{44}Sc in 0.25 M citric acid buffer (pH 4.0). All amounts show quantitative labeling after 30 minutes. Right: Stability studies in human serum and PBS buffer (pH = 7.4) at 37°C. The derivative shows more then 80% stability over a period of 2h.

The ^{44}Sc used for labeling was obtained using a ^{44}Ti/^{44}Sc generator with subsequent post-processing. Labeling was performed in 0.25 M sodium acetate buffer pH 4.0 at room temperature for 30 minutes. Labeling with 20 nmol, 15 nmol and 10 nmol was performed to investigate the influence of the chelator amount on the RCY. Approx. 30 MBq of activity were used for labeling experiments. Samples were taken after 1, 3, 5, 10 and 30 minutes to investigate the labeling kinetics (n=3). The radiochemical yield (RCY) was determined by radio TLC with citrate buffer (0.1 M, pH 4.0) as solvent. Figure 5 shows the labeling kinetics of [^{44}Sc]Sc AAZTA.SA.PSMA ([^{44}Sc]Sc-1).

Within the first 5 minutes reaction time it can be observed that the RCA is lower for larger amounts of substance compared to the use of smaller amounts of substance. After a reaction time of 30 minutes, all three substance amounts labelled with radiochemical yields of 90.1 % (20 nmol), 92.1 % (15 nmol) and 96.0 % (10 nmol) and were thus all in the range of > 90 %. Furthermore, the stability of [^{44}Sc]Sc-(1) in PBS buffer and human serum was investigated. To determine the *in vitro* stability, aliquots of the label solution were added to PBS buffer and human serum and incubated at 37 °C. Stabilities were measured after 30 min, 1 h, 2 h, 5 h and 24 h via radio-TLC. The results are shown in Figure 5. The results of the stability studies demonstrate that the [^{44}Sc]Sc-1 complex has stabilities of 90 % in both PBS

buffer and human serum five hours after reaction. After 24 hours, stability levels of 88.3 % in PBS buffer and 81.5 % in human serum could still be observed.

Radiochemical Evaluation with ^{64}Cu

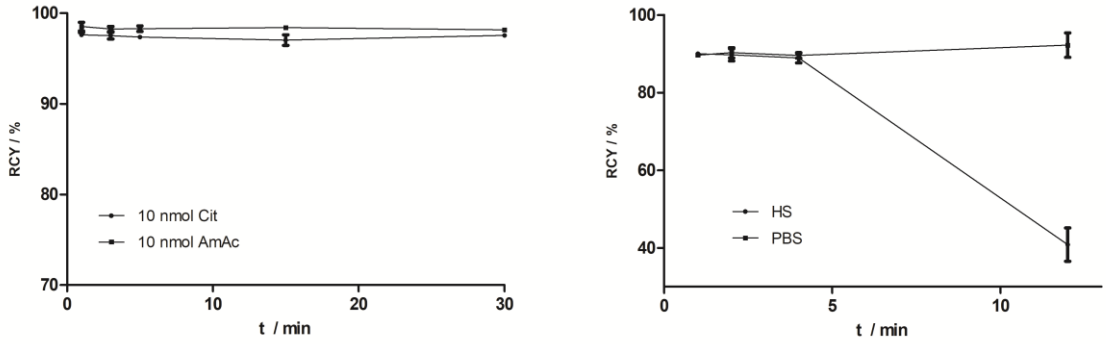

Figure 6: Labeling of AAZTA.SA.PSMA with ^{64}Cu. Left: Kinetic of 10 nmol labeled with 30 MBq ^{64}Cu in 0.2 M acetate buffer (pH 5.5). The derivative shows quantitative labeling after 1 minute under both TLC conditions (Citric acid buffer and ammonium acetate buffer). Right: Stability studies in human serum and PBS buffer (pH = 7.4) at 37°C. The derivative shows 90% stability in PBS over 12h. Stability in human serum decreases to 40%.

Labelling of (1) with ^{64}Cu was performed in 0.2 M sodium acetate buffer (pH 5.5) at room temperature for 30 minutes with 10 nmol precursor (n =3). Samples were taken after 1, 3, 5, 15 and 30 minutes to investigate the labeling kinetics. The radiochemical yield (RCY) was determined by radio TLC with citric acid buffer (0.1 M, pH 4.0) as mobile phase. Approx. 30 MBq activity were used. In order to investigate the behavior of free ^{64}Cu and the [^{64}Cu]Cu-1 complex on the TLC., the kinetics were additionally tested using radio-TLC with ammonium acetate buffer (0.25 M, pH = 4.5)/methanol (9:1) as solvent and the RCY was compared.

Comparison of the two radio TLCs shows that the citrate solvent system uncomplexed ^{64}Cu shows a R_f value of 1.0, whereas for the ammonium acetate buffer/methanol system the uncomplexed Cu retains at an R_f value of 0.0. Accordingly, the complex [^{64}Cu]Cu-1 behaves the other way round. In citrate buffer, the complex remains at R_f = 0.0 and in the ammonium acetate buffer/methanol system, it shows an R_f value of 0.58.

Investigation of the kinetics shows that the ^{64}Cu labels almost quantitatively after only one minute with radiochemical yields of over 95%. No better RCY could be achieved in the further period of the labeling and therefore the reaction was finished after one minute.

Aliquots of the labeled solution were added to PBS buffer (pH 7.4) and human serum and incubated at 37 °C to investigate *in vitro* stability. Stabilities were determined after 1 h, 2 h,

4 h and 12 h by radio-TLC. The test was performed in a triplicate and the results are shown in Figure 5. The *in vitro* stability experiment shows that the complex [^{64}Cu]Cu-1 is stable over a periode of 4 hours in both human serum and PBS with over 95 %. After 12 hours the complex in PBS is still very stable with almost 90 % remaining complex. In contrast, the stability in human serum decreased significantly after 12 hours. Here the RCY of the complex [^{64}Cu]Cu-1 was 40 % compared to free ^{64}Cu.

Radiochemical evaluation with ^{177}Lu

^{177}Lu was obtained from an (n,γ) reaction of [^{176}Yb]Yb_2O_3 and a subsequent β-emission. Experiments were performed in 0.25 M HEPES buffer (pH = 4.4) and different ratios for chelate to activity were investigated reaching from 15:1 to 2:1. Additionally reactions with 10 nmol precursor were performed. For all reaction 30 to 50 MBq of Lu were used. After successful synthesis, stability tests were performed in PBS buffer as well as in HS over a period of 2 days. All values were calculated from radio-TLCs and additionally radio-HPLC was performed to confirm the results.

RCYs for all reactions reached excellent values. For 10 nmol yields greater than 95 % were reached after 1 minute making a really fast labeling possible. Even for ratios of 15:1 (ligand/activity) more than 95 % RCY were reached after 5 minutes. Both, 10 nmol and 15:1 reached RCYs of more than 95 % after 30 minutes reaction time. RCYs for 5:1 and 2:1 kinetics were slightly slower but reached RCYs of more than 90 % and 85 % after 30 minutes, respectively. The results of all reactions were verified by radio-HPLC after 30 minutes confirming the results for the TLC.

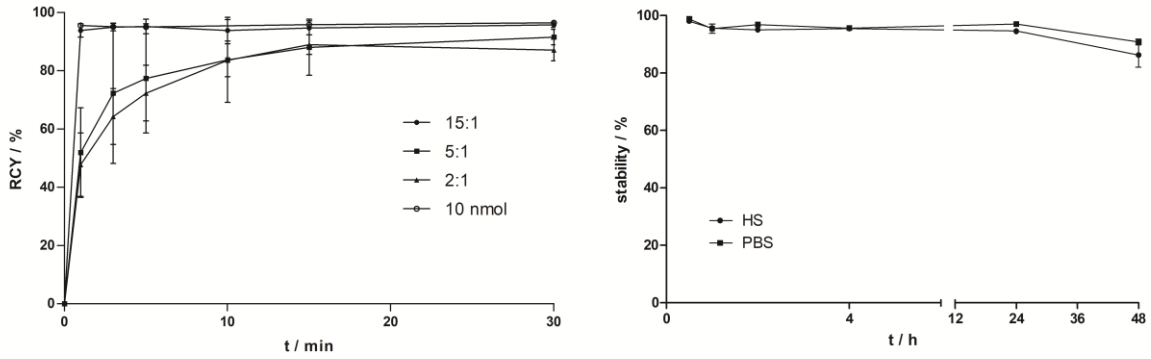

Figure 7: Labeling of AAZTA.SA.PSMA with ^{177}Lu. Left: RCYs of 10 nmol, 15:1, 5:1 and 2:1 (ligand/activity) labeled with 30-50 MBq ^{177}Lu in 0.25M HEPES buffer (pH = 4.4). The derivative shows quantitative labeling after 1 minute for 10 nmol chelate and after 3 minutes for 15:1. In total al tested ratios reach at least 85 % after 30 minutes reaction time Right: Stability studies in human serum and PBS buffer (pH = 7.4) at 37°C. The derivative shows 96% stability in PBS over 24h and 94% in HS. Stability increases slightly over 48 h to 90 % in PBS and 86 % in HS, respectively.

For investigation of *in* vitro stabilities, aliquots of the labeled solution were added to PBS buffer (pH 7.4) and human serum and incubated at 37 °C to investigate *in vitro* stability. Stabilities were determined after 1 h, 2 h, 4 h, 20 h, 24 h and 48 h by radio-TLC. The test was performed in a triplicate and the results are shown in Figure 6. The *in vitro* stability experiment shows that the complex [^{177}Lu]Lu-1 is stable over a periode of 24 hours in both human serum and PBS with over 95 %. After 48 hours stability decreases slightly but still remains at rations high as 90 % in PBS and 86 % in HS, respectively.

Discussion

With regard to synthesis, it was possible for the first time to present a potential PSMA inhibitor coupled to a hybrid ligand. The existing knowledge from previous DATA and AAZTA synthesis could be transferred to use squaric acid mediated coupling in this model complex [10,11,29]. The derivative could be obtained in good yield in a very easy and well applicable synthesis. Furthermore, the purification of the final product by HPLC was very efficient.

Labeling with ^{68}Ga is very efficient even at room temperature and precursor amounts as low as 10 nmol. Reactions reach more than 98 % RCY after 3 minutes at a pH of 4.5. The ability to label at room temperature makes AAZTA clearly superior to DOTA ligands. In addition, very small precursor quantities as low as 10 nmol can be used.

Stabilities of the compound reaching more than 95 % in HS and PBS over a periode of 2 h which is about two half-lives of ^{68}Ga. Therefore, AAZTA.SA.PSMA shows perfect properties for labeling with ^{68}Ga. AAZTA even shows slightly improved stability than already known in the literature. Different AAZTA derivatives tend to release up to 15 % of the gallium within the first 2 hours but the AAZTA.SA.PSMA shows a slightly increased stability [11,13].

Labeling of AAZTA is a rare discussed topic in literature so far. Only a few examples are known [14]. Nevertheless, this AAZTA.SA.PSMA derivative shows excellent properties for labeling with ^{44}Sc [12]. Quantitative labeling is possible at room temperature in a simple buffer system such as citric acid buffer at pH 4.0. [30,31]. This makes AAZTA superior to DOTA as it can not label ^{44}Sc without elevated temperatures [32,33]. In addition, very small amounts of substance can be labeled with 10 nmol within 30 minutes and larger amounts of substance (15 and 20 nmol) with RCY of more than 90 % each can be labeled within a maximum of 5 minutes. This enables very short reaction times.

Stabilities of the [^{44}Sc]Sc-AAZTA.SA.PSMA derivative are very good over the 24-hour period with 88 % in PBS and 81 % in HS. During one half-life period of the ^{44}Sc, the stability is even above 95 % and is therefore sufficiently stable in the same range of known derivatives.

The ability to label copper isotopes in addition to ^{44}Sc and ^{68}Ga is another feature that makes AAZTA.SA.PSMA a versatile tool for different applications. For example, a dual use as diagnostic and therapeutic agent would be possible for combinations of for example

^{68}Ga/^{177}Lu. Labeling properties are excellent with ^{64}Cu. Amounts as low as 10 nmol AAZTA.SA.PSMA can be labeled at room temperature in a conventional buffer. More than 95 % RCY is obtained within one minute. Since HPLC measurements for the [^{64}Cu]Cu-1 complex proved to more difficult than for the other complexes , two different TLC systems were used for the analysis to verify this result consistently. With regard to *in vitro* stability, the copper derivative has only moderate values. Although it shows a stability of > 89 % in PBS buffer over one half-life of ^{64}Cu, the stability after the same time in HS is only just over 40 %. This fact can be explained by an active transport of the copper from the chelator. This fact is known in literature and has been observed on a number of other copper labeling derivatives [34].

Labeling of AAZTA.SA.PSMA with ^{177}Lu shows good RCYs even with very low amounts of chelate and at room temperature. Furthermore stabilities for this combination are very good over a period of 24 hours 96 % stability in PBS and 94 % in HS are obtained. Even if stability increases slightly over 48 h to 90 % in PBS and 86 % in HS the values are still acceptable.

The most powerful property of the AAZTA.SA.PSMA is the ability to label ^{177}Lu in a fast and stable way. The fast labeling at very low amounts of chelate makes the AAZTA a perfect option for the use with different targeting vectors besides PSMA. Furthermore, the combination of ^{177}Lu with all the other introduced nuclides gives rise to a variety of theranostic pairs. A huge advantage in this context is the possible labeling at ambient temperature making AAZTA even more interesting in contrast to the comely used DOTA for the labeling of ^{177}Lu, which only can be used at elevated temperature. Low temperatures therefore enable the usage of AAZTA with fragile targeting vectors like larger peptides or anti-bodies. Furthermore the usage of the AAZTA.SA fragment allows for an easy and mild coupling reaction with those molecules.

Conclusion

It was shown that AAZTA.SA is an excellent building block for labeling with various radiolabels for diagnostic as well as therapy purposes. Labeling of AAZTA.SA.PSMA with ^{68}Ga, ^{44}Sc, ^{64}Cu and ^{177}Lu could be carried out with 10 nmol or less of the corresponding molecule at room temperature and moderate pH values (4.0-5.5) making AAZTA one of the most versatile and easy to label chelators described at the moment. Furthermore AAZTA.SA.PSMA may be used as a PSMA inhibitor in further experiments. We continue to investigate the *in vivo* properties in the future.

Experimental

All chemicals were purchased from Sigma-Aldrich, Merck, Fluka, AlfaAesar, VWR, AcrosOrganics, TCI, Iris Biotech and Fisher Scientific and used without purification. Dry solvents were obtained from Merck and VWR, deuterated solvents for NMR spectra from Deutero. Thin layer chromatography was performed with silica gel 60 F_{254} coated aluminum plates from Merck. Evaluation was carried out by fluorescence extinction at λ = 254 nm and staining with potassium permanganate. The radio DCs were evaluated using a CR-35 Bio test imager from Raytest and the AIDA (Raytest) software. The ^{1}H, ^{13}C, and ^{19}F NMR measurements were performed on an Avance III HD 300 spectrometer (300 MHz, 5 mm BBFO sample head with z-gradient and ATM and BACS 60 sample changer), an Avance II 400 spectrometer (400 MHz, 5 mm BBFO sample head with z-Gradient and ATM and SampleXPress 60 sample changer) and an Avance III 600 spectrometer (600 MHz, 5 mm TCI CryoProbe sample head with z-Gradient and ATM and SampleXPress Lite 16 sample changer) from Bruker. The LC/MS measurements were performed on an Agilent Technologies 1220 Infinity LC system coupled to an Agilent Technologies 6130B Single Quadrupole LC/MS system. Semi-preparative HPLC purification was performed on a 7000 series Hitachi LaChrom with a Phenomex Luna C18 (250 x 10 mm 10 µ) column.

L-Lysine-Urea-L-Glutamate (KuE / PSMA) (5)

H-Glu(*t*Bu)-O*t*Bu (0.9 g, 3 mmol) was dissolved together with DIPEA (2 mL, 12 mmol) in dry dichloromethane (150 mL). At 0 °C, triphosgene (300 mg, 1 mmol) was added dropwise over a period of 4 hours. The solution was then stirred for 1 h at room temperature. The H Lys(*t*Boc)-2CT polystyrene solid phase (0.78 mmol/g, 390 mg, 0.3 mmol) was allowed to stand in dichloromethane for 45 min, then added to the reaction solution and stirred for 16 h at room temperature. The solid phase was separated from the solution by filtration and washed with dichloromethane. The product was cleaved from the solid phase with TFA (3 x 7 mL, 10 min, RT) and purified by semi-preparative HPLC (column: Phenomex Luna C18 (250 x 10 mm) 10 µ, flow rate: 5 mL/min, H2O/MeCN + 0.1 % TFA, 0-5 % MeCN in 20 min, Rt = 9.0 min). The product KuE 5 was obtained as colourless oil (67.9 mg, 0.213 mmol, 71 %).

^{1}H-NMR (300 MHz, D_2O): δ [ppm] = 4.28-4.14 (m, 2H), 2.98 (t, *J* = 7.5 Hz, 2H), 2.50 (t, *J* = 7.3 Hz, 2H), 2.23-2.09 (m, 1H), 2.03-1.80 (m, 2H,), 1.78-1.59 (m, 3H), 1.52-1.37 (m, 2H).
MS (ESI-Positiv): 320.1 $[M+H]^+$, calculated $C_{12}H_{21}N_3O_7$: 319.14 $[M]^+$.

PSMA.SA (6)

KuE (10 mg, 0.0313 mmol) was dissolved in 0,5 M phosphate buffer (pH 7; 250µL) and 3,4-diethoxycyclobut-3-ene-1,2-dione (squaric acid; 5.3 mg, 4.6 µL, 0.0313 mmol) was added. The pH value was adjusted to pH 7 with 1 M NaOH solution and the reaction solution was shaken overnight. The product 2 (27.8 mg, 0.063 mmol, 23 %) was obtained as colourless solid after HPLC purification (column: Phenomex Luna C18 semi-preparative (250 x 10 mm) 10 µ, flow rate: 5 mL/min, H2O/MeCN + 0.1 % TFA, 12-30 % MeCN in 20 min, R_t = 10.0 min).

^{1}H-NMR (300 MHz, D_2O): δ [ppm] = 4.75-4.65 (m, 2H), 4.30-4.12 (m, 2H), 3.59 (dt, *J* = 23.5 Hz, 6.6 Hz, 1H), 3.48 (t, J = 6.6 Hz, 1H) 2.49 (t, *J* = 7.3 Hz, 2H), 2.16 (dtd, *J* = 15.3 Hz, 7.4 Hz, 5.2 Hz,1H), 2.04-1.90 (m, 1H) 1.86-1.75 (m, 2H, 1-H), 1.73-1.46 (m, 3H, 5-H), 1.41 (dt, *J* = 7.1 Hz, 3.6 Hz, 5H, 6-H). ^{13}C-NMR (300 MHz, D_2O): δ [ppm] = 188.86, 182.94, 177.13, 176.95, 176.05, 173.15, 159.08, 70.41, 52.91, 52.48, 30.26, 29.9, 28.86, 26.15, 21.59, 14.95.
MS (ESI-Positiv): 444.2 $[M+H]^+$, calculated $C_{18}H_{25}N_3O_{10}$: 443.15 $[M]^+$.

_N,N'_-Dibenzyl-_N,N'_-di-(tert-butylacetate)-ethylendiamine (8a)

_N,N'_-dibenzylethylenediamine (2.92 mL, 3.00 g, 12.48 mmol) and sodium carbonate (5.12 g, 48.67 mmol) were stirred in dry acetonitrile (50 mL) for 30 minutes at room temperature. _Tert_ butyl bromoacetate (3.60 mL, 4.64 g, 72 mmol) was added to acetonitrile (10 mL) at room temperature within 30 minutes. The reaction solution was stirred overnight at 90 °C, filtered and the solvent was removed at reduced pressure. The product was obtained by column chromatography (hexane/ethyl acetate; 6:1; R_f = 0.37) as a colourless solid (5.73 g, 12.2 mmol, 96 %).

^{1}H-NMR (400 MHz, $CDCl_3$): δ [ppm] = 7.34-7.21 (m, 10H), 3.78 (s, 4H), 3.26 (s, 4H), 2.82 (s, 4H), 1.44 (s, 18H). ^{13}C-NMR (400 MHz, $CDCl_3$): δ [ppm] = 171.03, 139.18, 129.05, 128.30, 127.10, 80.86, 58.39, 55.27, 51.73, 28.24.
MS (ESI-Positiv): 469.4 $[M+H]^+$, calculated $C_{28}H_{40}N_2O_4$: 468.30 $[M]^+$.

_N,N'_-di-(_tert_-butylacetate)-ethylendiamine (8)

Product 8a (2.26 g, 5.60 mmol) was dissolved in abs. ethanol (15 mL) and formic acid (427 µL, 0.52 g, 11.2 mmol). Palladium on activated carbon (416 mg, 16 %wt) was added and stirred under hydrogen for 24 hours. The palladium was filtered off via Celite and the solvent was removed under reduced pressure. The product (1.58 mg, 5.50 mmol, 98 %) was used without further purification.

MS (ESI-Positiv): 289.3 $[M+H]^+$, calculated $C_{14}H_{28}N_2O_4$: 288.36 $[M]^+$.

1,4-Di(*tert*-butylacetate)-6-methylpentanoate-6-nitroperhydro-1,4-diazepane (9)

2-nitrocyclohexanone (1.73 g, 12.08 mmol) and Amberlyst® A21 (7 g, 2 mass equivalents) were dissolved in dry methanol (30 mL) and stirred for one hour at 90 °C. Product 8 (3.48 g, 12.08 mmol) and paraformaldehyde (1.27 g, 42.28 mmol) were added and the reaction solution was heated overnight under reflux. The reaction solution was filtered and the solvent was removed under reduced pressure. The product was obtained by column chromatography (hexane/ethyl acetate; 2:1; R_f = 0.33) as yellowish oil (4.52 g, 9.28 mmol, 77 %).

^{1}H-NMR (400 MHz, $CDCl_3$): δ [ppm] = 3.65 (s, 3H), 3.60 (d, *J* = 14.6 Hz), 3.45 (d, *J* = 17.3 Hz, 2H), 3.30 (d, J = 17.3 Hz, 2H), 3.12 (d, *J* = 14.6 Hz, 2H), 2.84 (m, 4 H), 2.27 (t, 2H), 1.83 (m, 2H), 1.57 (m, 2H), 1.46 (s, 18H), 1.18 (m, 2H). ^{13}C-NMR (400 MHz, $CDCl_3$): δ [ppm] = 173.73, 170.92, 95.12, 81.31, 61.57, 61.18, 56.87, 51.68, 37.27, 33.71, 28.35, 24.82, 22.99.
MS (ESI-Positiv): 488.3 $[M+H]^+$, calculated $C_{23}H_{41}N_3O_8$: 487.29 $[M]^+$.

1,4-Di(*tert*-Butylacetat)-6-Methylpentanoat-6-Amino-perhydro-1,4-diazepane 10a

Product 9 (4.52 g, 9.28 mmol) was dissolved in absolute ethanol (40 mL). Raney® nickel was washed 5 times with abs. ethanol, added to the reaction solution and stirred with hydrogen at 40 °C for four days. The nickel was filtered off via Celite and the solvent was removed under reduced pressure. Product 10a (3.92 g, 8.60 mmol, 72 %) was obtained as greenish oil and used without further processing.

MS (ESI-Positiv): 458.3 $[M+H]^+$, calculated $C_{23}H_{43}N_3O_6$: 457.32 $[M]^+$.

1,4-Di(*tert*-butylacetate)-6-methylpentanoate-6-amino-di(*tert*-butylacetate)-perhydro-1,4-diazepane 10

Product 10a (1 g, 2,20 mmol) and diisopropylethylamine (372 µL, 283 mg, 2.20 mmol) were dissolved in acetonitrile (10 mL) and stirred under nitrogen for 30 minutes. *Tert*-butyl bromoacetate (747 µL, 987 mg, 5.06 mmol) in acetonitrile (2 mL) was added and stirred for 3 days at room temperature. The reaction solution was concentrated under reduced pressure

and purified by column chromatography (hexane/ethyl acetate; 5:1; R_f = 0.33). The product 10b (546.2 mg, 0.80 mmol, 36 %) was obtained as yellowish oil.

^{1}H-NMR (400 MHz, $CDCl_3$): δ [ppm] = 3.65 (s, 3H), 3.61 (s, 4H), 3.22 (s, 4H), 2.99 (d, *J* = 14.1 Hz, 2H), 2.85-2.65 (m, 4H), 2.63 (d, *J* = 14.1 Hz, 2H), 2.31 (t, *J* = 7.4 Hz, 2H), 1.62-1.52 (m, 4H), 1.44 (s, 18H), 1.43 (s, 18H), 1.25 (m, 2H). ^{13}C-NMR (400 MHz, $CDCl_3$): δ [ppm] = 174.37, 172.89, 170.94, 80.86, 80.38, 65.29, 63.17, 62.61, 59.39, 52.09, 51.56, 37.34, 34.26, 28.31, 28.25, 25.89, 21.83.
MS (ESI-Positiv): 686.5 $[M+H]^+$, calculated $C_{35}H_{63}N_3O_{10}$: 685.45 $[M]^+$.

1,4-Di(*tert*-butylacetat)-6-pentansäure-6-(amino-di(*tert*-butylacetat))-perhydro-1,4-diazepan 11a

Product 10 (546 mg, 0.80 mmol) was dissolved in a mixture of 1,4-dioxane and water (2:1, 14 mL) and 1 M LiOH and stirred at room temperature for 6 hours. The solvent was removed under reduced pressure. The residue was washed with sodium hydrogen carbonate solution (1 M, 20 mL) and chloroform (20 mL). The organic phase was dried over sodium sulfate and filtered. The chloroform was removed under reduced pressure and the product 11a (431 mg, 0.64 mmol, 82 %) was used without further purification.
^{1}H-NMR (400 MHz, $CDCl_3$): δ [ppm] = 3.60 (s, 4H), 3.23 (s, 4H), 3.00-2.97 (d, *J* = 14.1 Hz, 2H), 2.88-2.60 (m, 6H), 2.36-2.32 (t, 2H, *J* = 7.90 Hz), 1.64-1.52 (m, 4H), 1.43 (s, 18H), 1.42 (s, 18H,), 1.24 (m, 2H).
^{13}C-NMR (400 MHz, $CDCl_3$): δ [ppm] = 178.92, 172.93, 170.87, 81.04, 80.54, 65.10, 63.10, 59.35, 52.16, 34.20, 29.82, 28.32, 28.22, 25.62, 22.81, 21.87.
MS (ESI-Positiv): 672.5 $[M+H]^+$, calculated $C_{34}H_{61}N_3O_{10}$: 671.44 $[M]^+$.

1,4-Di(tert-butylacetate)-6-methylpentanoate-6-amino-di(tert-butylacetate)-perhydro-1,4-diazepane 11

Product 11a (431 mg, 0.64 mmol), HATU (243 mg, 0.64 mmol) and DIPEA (335 µL, 248 mg, 1.92 mmol) were dissolved in dry acetonitrile (4 mL) and stirred for 15 minutes at room temperature. *Tert* butyl(2-aminoethyl)carbamate (163 µL, 165 mg, 1.03 mmol) was added and stirred for 1 hour at room temperature. The solvent was removed under reduced

pressure and after column chromatography (hexane/ethyl acetate; 2:1; R_f = 0.12) the product 11 (333 mg, 0.41 mmol, 64 %) was obtained as yellowish oil.

^{1}H-NMR (400 MHz, DMSO): δ [ppm] = 6.34 (br, 1H), 5.26 (br, 1H), 3.60 (s, 4H), 3.38-3.34 (m, 2H), 3.26-3.24 (m, 2H), 3.21 (s, 4H), 2.96 (d, *J* = 14.1 Hz, 2H), 2.75-2.63 (m, 2H), 2.66-2.63 (m, 2H), 2.59 (d, *J* = 14.1 Hz, 2H), 2.19 (t, 2H), 1.62-1.53 (m, 4H), 1.43 (s, 18H), 1.42 (s, 27H), 1.28-1.20 (m, 2H). ^{13}C-NMR (400 MHz, $CDCl_3$): δ [ppm] = 174.38, 173.31, 172.80, 165.88, 82.85, 82.77, 63.44, 62.48, 62.05, 55.48, 54.47, 47.11, 40.81, 39.87, 35.55, 29.82, 28.53, 28.32, 28.14, 27.91, 26.17, 23.41.
MS (ESI-Positiv): 814.5 $[M+H]^+$ 836.5 $[M+Na]^+$, calculated $C_{41}H_{75}N_5O_{11}$: 813.55 $[M]^+$.

AAZTA.SA.PSMA 1

Product 11 (10 mg, 0,012 mmol) was dissolved in a solution of dichloromethane and trifluoroacetic acid (1:1, 3 mL) and stirred overnight at room temperature. The solvent mixture was removed under reduced pressure and the residue was dissolved together with product 2 (5.5 mg, 0.012 mmol) in 0.5 M phosphate buffer pH 9 (400 µL). The pH was readjusted with 1M NaOH solution and shaken overnight at room temperature. The product 1 (AAZTA.SA.PSMA) (3.2 mg, 0.0036 mmol, 30 %) was obtained as a colorless solid after HPLC purification (column: Phenomex Luna C18 semi-preparative (250 x 10 mm) 10 µ, flow rate: 5 mL/min, H2O/MeCN + 0.1 % TFA, 5-40 % MeCN in 20 min, Rt = 9.0 min).

^{1}H-NMR (600 MHz, D_2O): δ [ppm] = 4.10 (m, 1H), 4.04 (m, 1H), 3.71-3.59 (m, 6 H), 3.56 (m, 2H), 3.50-3.43 (m, 4H), 3.27 (s, 2H), 2.35 (t, *J* = 7.3 Hz, 2H), 2.09-1.97 (m, 4H), 1.85-1.77 (m, 2H), 1.75-1.68 (m, 2H), 1.62-1.54 (m, 2H), 1.53-1.42 (m, 4H), 1.31 (m, 2H), 1.20-1.11 (m, 4H). ^{13}C-NMR (600 MHz, D_2O): δ [ppm] = 177.24, 174.56, 170.81, 159.16, 64.53, 59.06, 57.75, 54.20, 53.17, 52.55, 51.60, 43.70, 39.62, 35.28, 32.59, 30.44, 29.92, 26.18, 25.57, 22.28, 21.68.
MS (ESI-Positiv): 887.4 $[M+H]^+$ 444.3 $[1/2M]^+$, calculated $C_{36}H_{54}N_8O_{18}$: 886.36 $[M]^+$.

References

1. Silver, D. A., Pellicer, I., Fair, W. R., Heston, W. D., Cordon-Cardo, C.: Prostate-specific membrane antigen expression in normal and malignant human tissues. Clinical cancer research an official journal of the American Association for Cancer Research. **3**, 81–85 (1997).
2. Perner, S., Hofer, M. D., Kim, R., Shah, R. B., Li, H., Möller, P., Hautmann, R. E., Gschwend, J. E., Kuefer, R., Rubin, M. A.: Prostate-specific membrane antigen expression as a predictor of prostate cancer progression. Human pathology. **38**, 696–701 (2007).
3. Bařinka, C., Rojas, C., Slusher, B., Pomper, M.: Glutamate carboxypeptidase II in diagnosis and treatment of neurologic disorders and prostate cancer. Current medicinal chemistry. **19**, 856–870 (2012).
4. Wüstemann, T., Bauder-Wüst, U., Schäfer, M., Eder, M., Benesova, M., Leotta, K., Kratochwil, C., Haberkorn, U., Kopka, K., Mier, W.: Design of Internalizing PSMA-specific Glu-ureido-based Radiotherapeuticals. Theranostics. **6**, 1085–1095 (2016).
5. Zhang, A. X., Murelli, R. P., Barinka, C., Michel, J., Cocleaza, A., Jorgensen, W. L., Lubkowski, J., Spiegel, D. A.: A remote arene-binding site on prostate specific membrane antigen revealed by antibody-recruiting small molecules. Journal of the American Chemical Society. **132**, 12711–12716 (2010).
6. Pillai, M. R. A., Nanabala, R., Joy, A., Sasikumar, A., Russ Knapp, F. F.: Radiolabeled enzyme inhibitors and binding agents targeting PSMA: Effective theranostic tools for imaging and therapy of prostate cancer. Nuclear medicine and biology. **43**, 692–720 (2016).
7. Kozikowski, A. P., Zhang, J., Nan, F., Petukhov, P. A., Grajkowska, E., Wroblewski, J. T., Yamamoto, T., Bzdega, T., Wroblewska, B., Neale, J. H.: Synthesis of urea-based inhibitors as active site probes of glutamate carboxypeptidase II: efficacy as analgesic agents. Journal of Medicinal Chemistry. **47**, 1729–1738 (2004).
8. Eder, M., Schäfer, M., Bauder-Wüst, U., Hull, W.-E., Wängler, C., Mier, W., Haberkorn, U., Eisenhut, M.: 68 Ga-Complex Lipophilicity and the Targeting Property of a Urea-Based PSMA Inhibitor for PET Imaging. Bioconjugate Chem. **23**, 688–697 (2012).
9. Tsionou, M. I., Knapp, C. E., Foley, C. A., Munteanu, C. R., Cakebread, A., Imberti, C., Eykyn, T. R., Young, J. D., Paterson, B. M., Blower, P. J., Ma, M. T.: Comparison of macrocyclic and acyclic chelators for gallium-68 radiolabelling. RSC advances. **7**, 49586–49599 (2017).
10. Seemann, J., Waldron, B. P., Roesch, F., Parker, D.: Approaching 'Kit-Type' Labelling with (68)Ga: The DATA Chelators. ChemMedChem. **10**, 1019–1026 (2015).
11. Waldron, B. P., Parker, D., Burchardt, C., Yufit, D. S., Zimny, M., Roesch, F.: Structure and stability of hexadentate complexes of ligands based on AAZTA for efficient PET labelling with gallium-68. Chemical communications (Cambridge, England). **49**, 579–581 (2013).

12. Aime, S., Calabi, L., Cavallotti, C., Gianolio, E., Giovenzana, G. B., Losi, P., Maiocchi, A., Palmisano, G., Sisti, M.: Gd-AAZTA-: a new structural entry for an improved generation of MRI contrast agents. Inorg. Chem. **43**, 7588–7590 (2004).
13. Baranyai, Z., Uggeri, F., Maiocchi, A., Giovenzana, G. B., Cavallotti, C., Takács, A., Tóth, I., Bányai, I., Bényei, A., Brucher, E., Aime, S.: Equilibrium, Kinetic and Structural Studies of AAZTA Complexes with Ga 3+ In 3+ and Cu 2+. Eur. J. Inorg. Chem. **2013**, 147–162 (2013).
14. Nagy, G., Szikra, D., Trencsényi, G., Fekete, A., Garai, I., Giani, A. M., Negri, R., Masciocchi, N., Maiocchi, A., Uggeri, F., Tóth, I., Aime, S., Giovenzana, G. B., Baranyai, Z.: AAZTA: An Ideal Chelating Agent for the Development of 44 Sc PET Imaging Agents. Angewandte Chemie (International ed. in English). **56**, 2118–2122 (2017).
15. Tietze, L. F., Arlt, M., Beller, M., Gl üsenkamp, K.-H., Jähde, E., Rajewsky, M. F.: Anticancer Agents, 15. Squaric Acid Diethyl Ester: A New Coupling Reagent for the Formation of Drug Biopolymer Conjugates. Synthesis of Squaric Acid Ester Amides and Diamides. Chem. Ber. **124**, 1215–1221 (1991).
16. G. Davis, B.: Recent developments in glycoconjugates. J. Chem. Soc., Perkin Trans. 1, 3215 (1999).
17. Gamblin, D. P., Scanlan, E. M., Davis, B. G.: Glycoprotein synthesis: an update. Chemical reviews. **109**, 131–163 (2009).
18. Rudd, S. E., Roselt, P., Cullinane, C., Hicks, R. J., Donnelly, P. S.: A desferrioxamine B squaramide ester for the incorporation of zirconium-89 into antibodies. Chem. Commun. **52**, 11889–11892 (2016).
19. Yoganathan, S., Sit, C. S., Vederas, J. C.: Chemical synthesis and biological evaluation of gallidermin-siderophore conjugates. Org. Biomol. Chem. **9**, 2133 (2011).
20. Eder, M., Schäfer, M., Bauder-Wüst, U., Hull, W.-E., Wängler, C., Mier, W., Haberkorn, U., Eisenhut, M.: 68Ga-complex lipophilicity and the targeting property of a urea-based PSMA inhibitor for PET imaging. Bioconjugate chemistry. **23**, 688–697 (2012).
21. Cardinale, J., Schäfer, M., Benešová, M., Bauder-Wüst, U., Leotta, K., Eder, M., Neels, O. C., Haberkorn, U., Giesel, F. L., Kopka, K.: Preclinical Evaluation of 18F-PSMA-1007, a New Prostate-Specific Membrane Antigen Ligand for Prostate Cancer Imaging. Journal of nuclear medicine official publication, Society of Nuclear Medicine. **58**, 425–431 (2017).
22. Zhernosekov, K. P., Filosofov, D. V., Baum, R. P., Aschoff, P., Bihl, H., Razbash, A. A., Jahn, M., Jennewein, M., Rösch, F.: Processing of generator-produced 68Ga for medical application. Journal of nuclear medicine official publication, Society of Nuclear Medicine. **48**, 1741–1748 (2007).
23. Eppard, E., Wuttke, M., Nicodemus, P. L., Rösch, F.: Ethanol-Based Post-processing of Generator-Derived ^{68}Ga Toward Kit-Type Preparation of ^{68}Ga-Radiopharmaceuticals. Journal of nuclear medicine official publication, Society of Nuclear Medicine. **55**, 1023–1028 (2014).
24. Roesch, F.: Scandium-44: benefits of a long-lived PET radionuclide available from the (44)Ti/(44)Sc generator system. Current radiopharmaceuticals. **5**, 187–201 (2012).

25. Filosofov, D. V., Loktionova, N. S., Rösch, F.: A 44Ti/44Sc radionuclide generator for potential application of 44Sc-based PET-radiopharmaceuticals. Radiochimica Acta. **98**, 152 (2010).
26. Greene, M. W., Hillman, M.: A scandium generator. The International Journal of Applied Radiation and Isotopes. **18**, 540–541 (1967).
27. Lebedev, N. A., Novgorodov, A. F., Misiak, R., Brockmann, J., Rösch, F.: Radiochemical separation of no-carrier-added 177Lu as produced via the 176Yb(n,gamma)177Yb--177Lu process. Applied radiation and isotopes including data, instrumentation and methods for use in agriculture, industry and medicine. **53**, 421–425 (2000).
28. Wurm, F. R., Klok, H.-A.: Be squared: expanding the horizon of squaric acid-mediated conjugations. Chemical Society reviews. **42**, 8220–8236 (2013).
29. Seemann, J., Waldron, B., Parker, D., Roesch, F.: DATATOC: a novel conjugate for kit-type 68Ga labelling of TOC at ambient temperature. Ejnmmi Radiopharmacy and Chemistry. **1** (2016).
30. Ackova, D. G., Smilkov, K., Janevik-Ivanovska, E.: Physicochemical Evaluation of Lyophilized Formulation of p-SCN-Bn-DOTA- and p-SCN-Bn-DTPA-rituximab for NHL Radio Immunotherapy. Iranian journal of pharmaceutical research IJPR. **15**, 295–302 (2016).
31. Domnanich, K. A., Müller, C., Farkas, R., Schmid, R. M., Ponsard, B., Schibli, R., Türler, A., van der Meulen, N. P.: 44Sc for labeling of DOTA- and NODAGA-functionalized peptides: preclinical in vitro and in vivo investigations. Ejnmmi Radiopharmacy and Chemistry. **1**, 8 (2017).
32. Koumarianou, E., Loktionova, N. S., Fellner, M., Roesch, F., Thews, O., Pawlak, D., Archimandritis, S. C., Mikolajczak, R.: 44Sc-DOTA-BN2-14NH2 in comparison to 68Ga-DOTA-BN2-14NH2 in pre-clinical investigation. Is 44Sc a potential radionuclide for PET? Applied radiation and isotopes including data, instrumentation and methods for use in agriculture, industry and medicine. **70**, 2669–2676 (2012).
33. Pruszyński, M., Loktionova, N. S., Filosofov, D. V., Rösch, F.: Post-elution processing of (44)Ti/(44)Sc generator-derived (44)Sc for clinical application. Applied radiation and isotopes including data, instrumentation and methods for use in agriculture, industry and medicine. **68**, 1636–1641 (2010).
34. Bass, L. A., Wang, M., Welch, M. J., Anderson, C. J.: In vivo transchelation of copper-64 from TETA-octreotide to superoxide dismutase in rat liver. Bioconjugate chemistry. **11**, 527–532 (2000).

Conclusion

The aim to conduct a competitive study for the derivatives DOTAGA.SA.PSMA, TRAM.SA.PSMA and NODAGA.SA.PSMA in comparison to the clinically established tracers PSMA-11 and PSMA-617 was achieved. With the conducted experiment it was demonstrated that DOTAGA.SA.PSMA can keep up with PSMA-11 and PSMA-617 in terms of tumor enrichment, but clearly exceeds both derivatives when it comes to off-tray enrichment. Thus it was shown that with DOTAGA.SA.PSMA PET images can be obtained showing a substantially improved tumor-to-background ratio. In addition, [^{68}Ga]Ga-DOTAGA.SA.PSMA was shown to have a significantly reduced accumulation in kidneys and liver compared to PSMA-11 and PSMA-617, which considerably favors a therapeutic approach. In addition, it was confirmed that the TRAM.SA.PSMA derivative does not offer any advantages as previously assumed [109]. The investigation of the [^{68}Ga]Ga-NODAGA.SA.PSMA also showed that a changed charge distribution has disadvantages compared to the DOTA derivative. It was shown that the obtained images show a significantly poorer imaging and that the tracer has a lower accumulation in the tumor in *ex vivo* biodisrtibution studies. In general it can be said that the great potential of the [^{68}Ga]Ga-DOTAGA.SA.PSMA could be further improved. The superiority of this derivative over [^{68}Ga]Ga-PSMA-11 or [^{68}Ga]Ga-PSMA-617 in preclinical trials is extremely promising concluding that this molecule should be considered for clinical trials in the future.

Furthermore, in this thesis the new compound AAZTA.SA.PSMA was presented which contains a hybrid chelator which can be used for versatile labeling with both diagnostic and therapeutic nuclides. Examinations were performed with ^{44}Sc, ^{68}Ga, ^{64}Cu and ^{177}Lu and all

tests showed very good results including fast kinetics, excellent RCYs and good stabilities in HS and PBS. Only ^{64}Cu did not show sufficient stability with AAZTA.SA.PSMA and AAZTA^{5}OMe over longer periodes of time in HS, which could be explained by active tranchelation. In addition to synthesis and radiochemical evaluation, the first *in vivo* results with ^{177}Lu have been obtained. The SPECT images suggest that this derivative provides comparable good results as the corresponding DOTAGA derivative. It was shown that after 7 days the injected activity is mostly located in the LnCAP tumor which enables a therapeutic use. Nevertheless, these results need to be followed up and expanded. Extensive *in vitro* tests with different nuclides have to be performed as well as preclinical studies with other nuclides such as ^{68}Ga and ^{44}Sc. In addition, the obtained results should be compared with the corresponding DATA.SA.PSMA to show which derivative is superior to imaging.

Interesting results were obtained for the investigation of hybrid chelators with radioactive ^{64}Cu. The results obtained with inactive copper prove that this labeling is possible in principle and predict high stabilities for the coresponding complexes [113]. The radioactiv labeling itself could be carried out without any restrictions with excellent results. Stabilities reached more than 95% RCY for AAZTA^{5}OMe and DATA^{5m}OMe after 3 minutes making them interesting chelates for labeling with ^{64}Cu or even other copper isotopes. However, the *in vitro* studies revealed that, as with most typical chelators, sufficient stability in human serum cannot be maintained over a period of time longer than 4 hours. This is due to the fact that the copper is actively transported out of the complexes by the SOD.

Appendix

list of abbreviations

meaning	abbreviation
(4-amino-1-carboxybutyl)carbamoyl)glutamine	KuE
[*O*-(7-Azabenzotriazol-1-yl)-*N*,*N*,*N*',*N*'-tetramethyluronium-hexafluorphosphate]	HATU
1,2-[[6-carboxy-pyridin-2-yl]-methylamine]ethane	H_2dedpa
1,4,7,10-tetraazacyclododecane-1,4,7,10-tetraacetic acid	DOTA
1,4,7-triazacyclononane-1,4,7-tri(methylene phosphonic acid	NOTP
1,4,7-triaza-cyclo-nonane-1,4,7-triacetic acid	NOTA
1,4,7-triazacyclononononane-1,4,7-tris[methyl(2-carboxyethyl)phosphinic acid]	TRAP
1-hydroxybenzotriazole	HOBt
2-phosphonomethyl pentanedioic acid	2-PMPA
6-amino-1,4-diazepine tetracetic acid	AAZTA
6-amino-1,4-diazepine-triacetic acid	DATA
acetonitrile	ACN
alpha decay	α
ammonium acetate	AmOAc
angstroem	Å
atomic number	Z
average lifetime	τ
Bequerel	Bq
beta decay	β
bidentate ligand	L^L
bifunctional chelator	BFC
bifunctional chelator	BFC
bismuth germanate	BGO
carcinomaof the prostate	CaP
chemical shift	δ
chloroform	$CHCl_3$
computed tomography	CT
coordination number	CN
coupling constant	J
day	d
decay energy	Q
degree Celcius	°C
desferrioxamine	DFO
deuterochloroform	$CDCl_3$
dichloromethane	DCM
diethylenetriamine pentaacetate	DTPA
dublett	d
electron capture	EC
electron neutrino	ν_e
electron volt	eV
equilibrium constant	K

ethanol	EtOH
ethyl acetate	EA
ethylenediaminetetraacetate	EDTA
free energy	ΔG_b
gamma quantum	γ
gram	g
half-life	$t_{½}$
hard and soft acids and bases	HSAB
Hertz	Hz
hexane	H
high performance liquid chromatography	HPLC
hour	h
hydrochloric acid	HCl
hydrogen	H_2
kilodalton	kDa
line of response	LOR
linear energy transfer	LET
lithium hydroxide	LiOH
lithium orthosilicate	LOS
magnetic resonance imaging	MRI
mass spectrum	MS
maximum energy	E_{max}
methanol	MeOH
microlitre	µL
milligram	mg
minute	min
molar	M
monodentate ligand	L
multiplett	m
N,N-bis(2-hydroxybenzyl)ethylenediamine-N,N-diacetic acid	HBED
N-acetyl-aspartyl-glutamate	NAAG
neutron number	N
N-hydroxysuccinimide	NHS
non carrier added	n. c. a.
nuclear magnetic resonance spectroscopy	NMR
palladium on charcoal	Pd/C
parts per million	ppm
Positron emisson tomography	PET
post injection	p. i.
Prostate specific antigen	PSA
Prostate specific membrane antigen	PSMA
retention time	t_R
room temperature	RT
second	s
single photon emission computer tomography	SPECT
singulett	s
sodium acetate	NaOAc
sodium hydroxide	NaOH

speed of light	c
squaric acid	SA
squaric acid monoester	SAME
standard uptake value	SUV
thin layer chromatography	TLC
triethylamine	TEA
trifluoroacetic acid	TFA
triplett	t triplett
ultrasound	US

list of figures

list of tables